Trabajo Fin de Grado
Grado en Ingeniería Aeroespacial

Uncertainty Propagation in Low Earth Orbits

Autor: Manuel Ruiz Pérez

Tutor: Rafael Vázquez Valenzuela

Dpto. Ingeniería Aeroespacial y Mecánica de Fluidos
Escuela Técnica Superior de Ingeniería
Universidad de Sevilla

Sevilla, 2019

Trabajo Fin de Grado
Grado en Ingeniería Aeroespacial

Uncertainty Propagation in Low Earth Orbits

Autor:
Manuel Ruiz Pérez

Tutor:
Rafael Vázquez Valenzuela
Profesor Titular

Dpto. Ingeniería Aeroespacial y Mecánica de Fluidos
Escuela Técnica Superior de Ingeniería
Universidad de Sevilla

Sevilla, 2019

Trabajo Fin de Grado: Uncertainty Propagation in Low Earth Orbits

Autor: Manuel Ruiz Pérez
Tutor: Rafael Vázquez Valenzuela

El tribunal nombrado para juzgar el trabajo arriba indicado, compuesto por los siguientes profesores:

Presidente:

Vocal/es:

Secretario:

acuerdan otorgarle la calificación de:

El Secretario del Tribunal

Fecha:

Agradecimientos

Las personas amamos los grandes finales en que los protagonistas consiguen sobreponerse a multitud de adversidades aplicando para ello esfuerzo, paciencia y grandes dosis de pasión y ambición. Pero los protagonistas sólo lo consiguen por estar respaldados y ayudados por otros personajes "secundarios". Personas que ocupan un segundo plano pero que a la hora de la verdad son los que hacen reír y llorar, los que se sacrifican para ayudar al protagonista y que son los que suelen cautivar al espectador.

Este agradecimiento va a todos aquellos "personajes secundarios" que me ayudan a poner con éxito punto y final a esta extremadamente dura, pero también apasionante, etapa de mi vida.

A mis padres, Cati y Manolo. Con este trabajo pongo fin a mi carrera, pero en verdad no es mía, es nuestra. Decía Newton que llegó a ver más alto porque se subió a hombros de gigantes. Gracias por ser los gigantes sobre los que subirme, dejándome ver más allá y creer en mí cuando incluso yo no lo hago. Por ser un ejemplo vivo de amor, responsabilidad y respeto que algún día espero alcanzar. Por inculcar en mí el amor a las ciencias y en especial a la ingeniería, así como al trabajo bien hecho, la perseverancia, el esfuerzo y la pasión, la lectura, la cultura, la ambición y la bondad valores que gracias a vosotros, llevaré conmigo para siempre.

A mis hermanos, Juan y Ana, por darme todo su apoyo y su amor y por confiar siempre en mí. Dicen que el hogar está donde esté el corazón. Mi hogar estará donde estéis vosotros.

A todos mis familiares y en especial a mis abuelos, Juan, Plácida, Inocencio y Carmen. Este trabajo es el culmen de una vida de duro esfuerzo y sacrifico para conseguir lo mejor para vuestros hijos y nietos. Permitidme decir que lo habéis conseguido.

A todos mis amigos. A los de Córdoba, los que me dio Sevilla y los que me acompañaron en la Ruta Quetzal. Muchas gracias por hacerme ver que hay más vida más allá de los libros y apuntes. A los que me habéis aguantado a lo largo de estos años de carrera: a Peri, Juangra, Mogollo, Andrés, Chema, Manu y muchos otros nombres que me dejo en el tintero. Pero especialmente a Ignacio Bértiz, por haber sido compañero inquebrantable de sufrimientos, risas, prácticas y exámenes, por ayudarme en todo momento, animarme y sobre todo escucharme. Gracias a tí me siento menos mal si llego tarde a clase.

A todos los profesores que me marcaron tanto en lo académico como en lo personal, haciendo de mí una persona curiosa, trabajadora y motivada. Por enseñarme lo que soy capaz de ser y hacer.

Y por último gracias a mi tutor, Rafa, por aconsejarme y atenderme en todo momento y por haberme elegido para hacer este proyecto con él. Por hacerme dar lo mejor de mí y permitirme culminar la carrera alcanzando el espacio, la última frontera.

Manuel Ruiz Pérez
Sevilla, 2019

Resumen

Debido al efecto de las perturbaciones, el cual es difícil de modelar con precisión, siempre aparece un cierto grado de incertidumbre asociado a la órbita. Para modelar y trabajar con dicha incertidumbre se puede utilizar la teoría de la probabilidad. El objetivo de este proyecto es el de estudiar y analizar distintos métodos que permitiesen la propagación de la incertidumbre a lo largo de la órbita, tales como la linearización de la covarianza, caos polinomial, álgebra diferencial, el método de Monte Carlo o el PTM. Además, los modelos de las perturbaciones se desarrollarán y presentarán, analizando también su efecto en los elementos orbitales.

Abstract

Due to perturbation effects that are difficult to model with enough precision, there is always a degree of uncertainty associated with orbits. Probability theory can be used to model this uncertainty. The goal of this project is to explore several methods that propagate this uncertainty along the orbit, such as linearized covariance, polynomial chaos, differential algebra, or the Monte Carlo method. Moreover, perturbation models will be developed and attached and their effects in the orbital elements will be analyzed as well.

Contents

List of Figures

List of Tables

Notation

a	Semimajor axis
e	Eccentricity
ω	Argument of the perigee
Ω	RAAN
i	Inclination
M	Mean anomaly
θ	True anomaly
ϕ	Latitude
λ	Longitude
$\oplus$	Earth's astronomic symbol
$\odot$	Sun's astronomic symbol
t	Time
T_{sat}	Satellite's period
m_v	Vehicle's mass
ρ	Density
A	Area
c_D	Drag coefficient
r_p	Perigee radius
r_a	Apogee radius
p_{rad}	Solar radiation pressure
$R_\oplus$	Earth's radius
$\mu_\oplus$	Earth's gravitational parameter
N_{sat}	Number of revolutions
$J2$	J2 perturbation
$\omega_\oplus$	Earth's rotation velocity
n	Orbital mean velocity
$n_\odot$	Orbital mean velocity of the Sun
$\vec{r}$	Position vector
$\vec{v}$	Velocity vector
$\delta_\odot$	δ del sol
$AR_\odot$	Sun's rigth ascension
$\vec{h}$	Specific angular moment
$\vec{n}$	Nodal vector
$\vec{e}$	Eccentricity vector
LEO	Low Earth orbit
GEO	Geostationary orbit
DA	Differential Algebra
PTM	Probability transformation method
GPC	Generalized polynomial chaos
$LinCov$	Linearized covariance
σ	Standard deviation

1 Introduction

That's one small step for a man, one giant leap for mankind.

Neil Armstrong, 1969

Since the first humans walked on the Earth, we have observed the sky with curiosity but also fear. However, nowadays it has changed. A lot of companies firmly believe that space is a great opportunity, not only to profit, but also to improve our daily life. Because of this fact, engineers launch powerful rockets to space with the purpose to put in orbit satellites that could achieve this goal.

1.1 Motivation

Satellites orbit every day over us and, most of the time, we do not realize this fact. Nowadays they have an extremely important role in the development of technology and science. They are also crucial for navigation, communication or observation.

The first satellite, which was launched in 1957 by the URSS, was the "Sputnik 1." Although it only had to emit radio pulses in a certain frequency, it proved that we could send an object to orbit around the world and, with some accuracy, control it.

One month later the URSS launched the "Sputnik 2." In response to those launches, the United States of America sent to space the first scientific satellite: the "Explorer I". Since then, the space race began between the USA and the URSS. Both wanted to succeed in developing better vehicles that could last more time in space. As this "competition" was too expensive, they tried to obtain some economic and scientific benefits from them. Because of that the first communications satellites were launched: "Project Score" (1958), "Syncom 2" (1963) and "Syncom 3" (1964).

Nowadays, according to the United Nations, [12], until 2017 there were around 19,000 artificial objects presently being tracked in Earth orbit, but only 1,400 of them are functional satellites. The others are called "space waste". All of them are developing different missions. On the one hand there are vehicles that make scientific experiments related to microgravity. On the other hand, most of them observe the Earth to analyze and predict the weather, allow global communications or take photos of certain places in the world. Satellites could also be defined as a function of their altitude: LEO (Low Earth Orbits), MEO (Medium Earth orbits) and high altitude satellites (like GEO).

LEO are defined as satellites which have less than 2000 km altitude. However, as the Van Allen belt is located over 1000 km, a LEO's altitude is usually between 200 and 1000 km. On the other hand, a MEO's altitude is around 20000 km and a GEO's altitude is 36000km.

According to the UCS Satellite database, [22], until December 2018, there were 1,957 working satellites orbiting around the Earth. The same database exposes that 1,232 of all of those artificial objects are orbiting

in a LEO orbit. This fact shows this orbit's importance.

As Low Earth Orbits are closer to the Earth than any other orbits, they allow us to take better photographs. Moreover, if we use a constellation, it would be possible to cover the entire world. Additionally, the biggest LEO's advantage is the smaller cost of the missions, as the rockets need less fuel to reach the altitude. The orbits are closer to the Earth, which means that less energy is necessary to reach this altitude.

The equations of Orbital Mechanics, which will be introduced later, enable us to determine the velocity required to reach and stay in a certain orbit. Those mathematical equations show us that typical speeds for LEO are between 6 and 8 km per second. This extremely high velocity implies that an accurate method should be used to exactly determine the position of the body.

Taking into consideration the vast amount of vehicles in space, it is obvious that determining their exact position is crucial. On the one hand, navigation satellites need exceptionally accurate calculations, which could guess the body's position within a few meters. On the other hand, it allows us to point the antennas correctly, so that we can communicate. In addition, if we know where the vehicle is, we could avoid some risks, such being too close to the Earth, which could provoke a catastrophic unintended reentry.

Every space agency knows this fact and works hard to perfect methods to propagate the orbits in time making as fewer mistakes as possible. In these models it is vital to include perturbations. Perturbations affect the ideal behavior of the orbit. These phenomena introduce uncertainty in the orbit, as they are often complicated to model. They will be later described and developed. To succeed in propagating the orbit, it is extremely important to know which perturbations should be studied and how they affect the orbital elements. Moreover, scientists endeavor to develop accurate models for these perturbations, whose behavior is not always clear and obvious.

In addition, perturbation analysis can save a considerable amount of money, as one could determine which station keeping maneuvers are necessary and the amount of required fuel. In terms of security, an accurate propagation method is vital to predict and avoid a catastrophic reentry.

According to all of these facts, the importance of LEO, as well as the significance of an accurate propagation model, have been established. Due to this reason, the exploration of several methods, as well as their accuracy and efficiency, is required for the sake of success in propagating uncertainty along the orbit.

1.2 Aim of the project

The aim of this project is to analyze and explore several methods that propagate uncertainty along the orbit. This uncertainty is mainly caused by perturbations and inaccurate measurements.

To achieve this goal, some of the most important perturbations are considered. First at all, the nonspherical shape of the Earth is considered, hence J_2 and C_{22} perturbations are developed. Secondly, the effects of atmospheric drag and solar radiation pressure are examined. Finally, third body perturbations are also included.

However, if we propagate using models for such phenomena, it is required to guess some values and functions like the density or the effect of the Earth's shadow. Therefore, a few statistical distributions will be used to accurately model those parameters.

After this "perturbation analysis," the main goal of the project is developed.Different methods are explored and compared in order to determine their strengths and weaknesses.

On the other hand, the scope of the project is as follows. As it has been said, a perturbation analysis is carried out and thus their effects are studied. However, several simplifying hypotheses have been made and a deeper analysis of their outcomes is not considered. After this chapter, five uncertainty propagation methods are presented. Their characteristics, as well as their implementation, are described in detail. Two test cases are developed in each chapter: uncertainty in density and in the initial position. The examples

enable us to compare properly such techniques. Moreover, other cases are taken into consideration, in order to obtain aditional conclusions about them. Accuracy and precision are finally compared between all of these procedures. However, a deeper analysis considering unpredictability in more parameters (like the orbital elements) is not performed and it will be recommended for future works.

1.3 Structure

In this section, the structure of the project is defined:

Chapter 1: The cahpter starts with an introduction. the main motivation is presented to explain and show the relevance of the developments and calculations that are carried out in the project. The purpose, scope and structure are explained.

Chapter 2: The basics of orbital mechanics are introduced. The motion equation is defined, as well as the orbital elements' expressions. The reference systems that are considered in the project are defined as well.

Chapter 3: Next, a perturbation analysis is carried out. As it has been said, there are several phenomena which affect the ideal behavior of the orbit. Atmospheric drag, third body perturbations or the nonspherical model of the Earth are considered. Their effects in the orbital elements are showed and commented.

After the third chapter, the five methods are introduced. There is one chapter per technique and, in all of them, the same sections are considered. First at all, the method and its importance are introduced. Secondly, the mathematical equations and the implementation of the method are explained. Finally, results are presented. Three test cases are considered: uncertainty in initial position, uncertainty in density and one last case which is different in every chapter. The first and second cases allow us to compare the techniques, whereas the last one will provide additional conclusions about the procedure.

Chapter 4: Monte Carlo method is analyzed. Interesting results, as well as the basis of this procedure are displayed.

Chapter 5: In this chapter, Differential Algebra is explained and developed. Uncertainty in initial velocity is analyzed as well.

Chapter 6: The linearized covariance method is presented. Results are compared with several articles and hence the accuracy of results is evaluated.

Chapter 7: The probability transformation method (PTM) is presented next. This method focuses on the evolution of PDFs that model certain parameters. It then follows that a different point of view of the project is considered, though similar conclusions are obtained.

Chapter 8: Finally, the Polynomial chaos expansion (PCE) is developed. The strong mathematical developments of this technique, as well as interesting conclusions, are presented in the chapter.

Chapter 9: In this chapter, the five methods are compared. Their strenghts and weaknesses are remarked, as well as the time of compilation and accuracy.

Chapter 10: To sum up, several conclusions based on the previous results are listed. In addition, some future work is proposed.

2 Basics of orbital mechanics

In this chapter, the motion equation, as well as perturbations' models are introduced. The goal of this part is to provide all the mathematical expressions that enable us to determine the satellite's position and velocity. Moreover, the reference frames that are used along the project are presented as well. Equations have been extracted from [27] and [25].

2.1 Motion equation

In order to study the movement of two massive bodies attracted by gravity forces, two simplifying hypotheses are considered:

- First at all, it is supposed that the Earth and the satellite are isolated in the universe, so that we do not consider the effect of other planets or even the Sun.
- The considered bodies are modelled as a punctual mass, which are located in the mass centre of the body.

Although these assumptions are not verified in the real world, we work initially with them and later, perturbations are included to be more realistic.

The attraction force created by every point is defined as follows:

$$\vec{F_1} = \frac{Gm_1m_2}{r^2}\frac{\vec{r}}{r} \tag{2.1}$$

$$\vec{F_2} = -\frac{Gm_1m_2}{r^2}\frac{\vec{r}}{r} \tag{2.2}$$

Developing Equations (2.1) and (2.2):

$$m_1\ddot{\vec{R}}_1 = \vec{F_1} \rightarrow \ddot{\vec{R}}_1 = \frac{Gm_2}{r^2}\frac{\vec{r}}{r} \tag{2.3}$$

$$m_2\ddot{\vec{R}}_2 = \vec{F_2} \rightarrow \ddot{\vec{R}}_2 = -\frac{Gm_1}{r^2}\frac{\vec{r}}{r} \tag{2.4}$$

Using the definition of $\vec{r}$ the motion's equation is obtained :

$$\ddot{\vec{r}} = \ddot{\vec{R}}_1 - \ddot{\vec{R}}_1 = -G(m_1+m_2)\frac{\vec{r}}{r^3} = -\mu\frac{\vec{r}}{r^3} \tag{2.5}$$

Where $\vec{r} = (r_x, r_y, r_z)$ is the position vector and $\vec{v} = (v_x, v_y, v_z)$ is the velocity vector.

Most of the time, it is supposed in Orbital Mechanics that one body is much more massive than the other ($m_1 >> m_2$) and then the gravitational parameter is defined as follows:

$$\mu = G(m_1 + m_2) \sim G \cdot m_1 \tag{2.6}$$

This assumption enables us to consider the single body's problem, which states that the movement is carried out by one body (m_2) around the massive one (m_1).

As explained before, in order to obtain Equation (2.5) several hypotheses were assumed; to obtain more realistic results, perturbations should be included in (2.5).

2.2 Orbital elements

Once the motion equation has been determined, the calculation of the orbital elements, position and velocity is presented. Keplerian elements (as known as orbital elements) are six parameters that define the orbital plane's position in the space, the orbit's size and shape, the position of periapsis and the location in the orbit.

First at all, several variables that are used to calculate them are showed.

$$\vec{h} = \vec{r} \times \vec{v} = rv\cos\gamma \tag{2.7}$$

$$\vec{n} = \frac{\vec{k} \times \vec{h}}{||\vec{k} \times \vec{h}||} \tag{2.8}$$

$$\vec{e} = \frac{\vec{v} \times \vec{h}}{\nu} - \frac{\vec{r}}{r} \tag{2.9}$$

Where $\vec{h}$ is the specific angular momentum, $\vec{e}$ the eccentricity vector and $\vec{n}$ the nodal vector. All these are constant under the two-body problem hypothesis. Once these parameters have been obtained, we are able to calculate the orbital elements :

- **Semi major axis (a)**: It is the parameter of the orbit which enables us to define the orbit's size. It is only consistent when the orbit is not parabolic. In the project only elliptical orbits are considered. Numerically we calculate it using the specific mechanical energy as follows:

$$\varepsilon = \frac{v^2}{2} - \frac{\mu}{r} = -\frac{\mu}{2a} \rightarrow a = -\frac{\mu}{v^2 - \frac{2\mu}{r}} \tag{2.10}$$

- **Eccentricity (e)**: This parameter indicates the kind of conic that our orbit is, as well as its shape. There are three possibilities: an ellipse, a parabola or a hyperbola:

  1. e=0 $\rightarrow$ Parabola
  2. $e \in (0,1) \rightarrow$ Ellipse
  3. e>1 $\rightarrow$ Hyperbola

  Analytically, the eccentricity is calculated as follows:

$$p = \frac{h^2}{\mu} \rightarrow a(1-e^2) = \frac{h^2}{\mu} \rightarrow e = \sqrt{1 - \frac{h^2}{\mu a}} \tag{2.11}$$

- **Inclination (i)**: This is the angle between the equator and the orbital plane. It gets analytically defined as:

$$i = \arccos(\frac{h_z}{h}) \tag{2.12}$$

The inclination is defined as an angle between 0º and 180º.

- **Argument of the perigee (ω)**: It is the angle between the ascending node and the eccentricity vector.

$$\omega = \arccos(\frac{\vec{n} \cdot \vec{e}}{e}) \tag{2.13}$$

ω is calculated using Equation (2.13). However, this expression is only properly used when $e_z > 0$. If $e_z < 0$, then the argument of periapsis would be calculated as $360 - \omega$, where such ω was calculated following (2.13).

- **RAAN (Ω)**: This parameter is defined as the angle between the vernal equinox and the ascending node. In order to calculate Ω, one uses the following formula.

$$\Omega = \arccos(n_x) \tag{2.14}$$

The expression is only valid for $n_y > 0$. If $n_y < 0$, then the RAAN would be calculated as $360 - |\Omega|$, where such Ω was calculated following 2.14.

- **Mean anomaly (M)**: This value indicates the body's position in the orbit. Although the true anomaly (θ) could be used as well, mean anomaly is easily obtained and has got mathematical advantages that are introduced later. Mean anomaly is obtained as:

$$M = \sqrt{\frac{\mu}{a^3}}t \tag{2.15}$$

Figure 2.1 displays the orbital elements. In this figure, the parameters are described in an inertial geocentric equatorial reference frame.

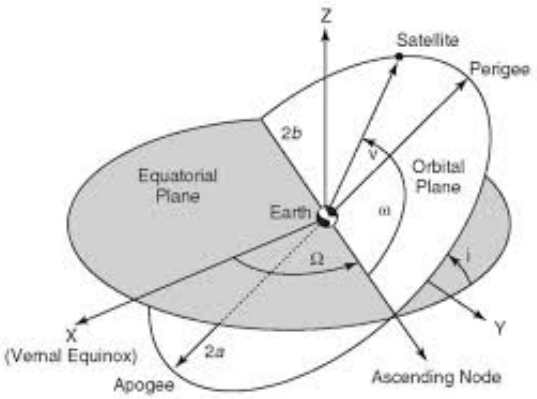

Figure 2.1 Keplerian elements.

This reference frame is the one that is used to integrate the equations. This fact is crucial, as several functions and parameters are sometimes defined in other reference frame, and thus a rotation matrix to carry out the correct change should be calculated.

To conclude this section, two different methods that enable us to deal with perturbations are presented:

1. **General perturbation method.** It calculates the orbital element's variations as a function of time using the planetary equations in Lagrange's or Gauss' form. This procedure is used in [25].

2. **Special perturbation method.** This method calculates the orbital elements using the motion equation. There are two possibilities:

   - **Encke's method.** The mathematical model of the perturbations is directly included in the motion equation and then it is integrated. Nowadays it is the most common method as a result of the computational power and efficiency available at the moment.

   - **Cowell's method.** Equation (2.5) is integrated and then a few corrections are computed in order to obtain a reference solution. If the error between the reality and the calculations becomes bigger, the reference solution should be recalculated.

In this project, Encke's method is implemented.

2.3 Reference frames

The purpose of this section is to present the two main reference frames that are used in the project.

1. The reference frame used in Section 2.2 is the inertial geocentric equatorial reference frame. In this frame, motion equation plus perturbations' models are integrated.

2. On the other hand, there is another frame that is considered in the test cases because of its physical meaning, the local axes. These axes are more intuitive and offer deeper conclusions about position and velocity's oscillations as well.

   Figure 2.2 shows the local frame in a satellite orbiting the Earth.

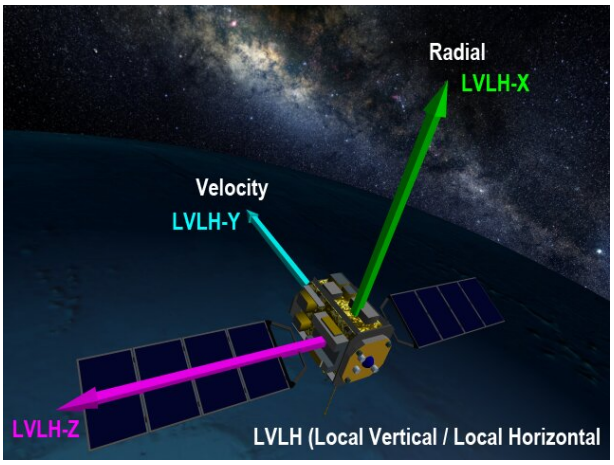

Figure 2.2 Local reference frame. Image from STK.

The local frame is analytically defined as follows, where $\vec{R}$ and $\vec{V}$ are the position and velocity vectors in the inertial frame.

$$\vec{i}_{local} = \frac{\vec{R}}{R} \tag{2.16}$$

$$\vec{k}_{local} = \frac{\vec{R} \times \vec{V}}{|\vec{R} \times \vec{V}|} \tag{2.17}$$

$$\vec{j}_{local} = \vec{k}_{local} \times \vec{i}_{local} \tag{2.18}$$

Local axes have got a powerful physical meaning that gets described as follows:

a) **OX**. The X axis is along the position vector. It points opposite to Earth. Its oscillations are related to satellite's position variations.

b) **OY**. The Y axis is toward velocity. It goes along the satellite's velocity when eccentricity tends to zero. As LEO usually have small eccentricity, this assumption is valid in most cases.

c) **OZ**. The Z axis is along the orbit normal. Its oscillations are related to the variations in the specific angular momentum.

3 Perturbation Analysis

Once the equations, the orbital elements and the main ideas of the project have been presented, a perturbation analysis is developed.

Obtaining the motion equation implied simplifying hypotheses that introduce small errors in the results. Although these errors could be neglected in the short-term, the solution would lack precision. Thus, perturbations should be included in order to be more realistic. Then, the motion equation is written as:

$$\ddot{\vec{r}} = -\mu \frac{\vec{r}}{r^3} + \vec{a}_{nonspherical} + \vec{a}_{drag} + \vec{a}_{Third-Body} + \vec{a}_{SRP} \tag{3.1}$$

Equation (3.1) is known as the acceleration model. In this method Equation (2.5) is combined with the perturbation's accelerations, and hence their effect is considered.

The aim of this chapter is to obtain and develop such perturbations' models, studying then the behaviour of the orbital elements when Equation (3.1) is integrated, and describing some observed phenomena.

Results are compared with [25] and [27]. This allows us to validate our outcomes.

3.1 Third body perturbations

One of the simplifying hypotheses that has been supposed is the fact that the Earth and the satellite are isolated in the universe. Obviously this assumption is not verified in the real world. As Figure 3.1 shows, the Solar System is full of massive bodies whose effect cannot be neglected in a long-term propagation.

To quantify the effect of third body perturbations, we should work with Equations (3.2) and (3.3). They consider the presence of the Sun ($\odot$) and the Moon ($\leftmoon$) respectively as follows:

$$\ddot{\vec{r}} = -\mu_{\oplus} \frac{\vec{r}}{r^3} + \mu_{\odot} \frac{\vec{r}_{\odot} - \vec{r}}{|\vec{r}_{\odot} - \vec{r}|^3} - \mu_{\odot} \frac{\vec{r}_{\odot}}{r_{\odot}^3} \tag{3.2}$$

$$\ddot{\vec{r}} = -\mu_{\oplus} \frac{\vec{r}}{r^3} + \mu_{\leftmoon} \frac{\vec{r}_{\leftmoon} - \vec{r}}{|\vec{r}_{\leftmoon} - \vec{r}|^3} - \mu_{\leftmoon} \frac{\vec{r}_{\leftmoon}}{r_{\leftmoon}^3} \tag{3.3}$$

Instead of using the position vector ($\vec{r}$) and the gravitational parameter (μ) of the Sun or the Moon, we may consider these of another planet.

Although all planets' effect could be considered, it would make our equations computationally demanding. Due to this reason the order of magnitude of their effect has been calculated to decide which ones should be implemented.

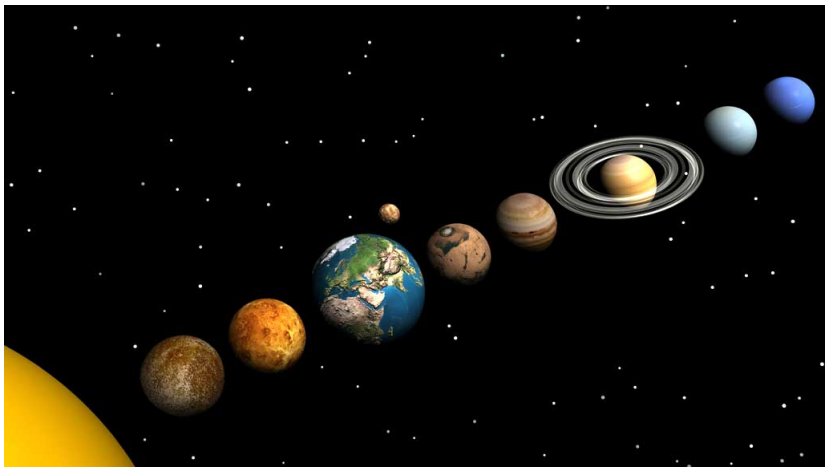

Figure 3.1 Solar System.

For LEO one obtains that $(\mu_{☾}/\mu_{\oplus})(r/r_{☾})^3 \sim 10^{-7}$ and $(\mu_{\odot}/\mu_{\oplus})(r/r_{\odot})^3 \sim 5 \cdot 10^{-8}$. These values compare the influence of the third body's perturbation in the satellite's acceleration. As it can be observed, the Moon and the Sun weakly perturb (3.1). However, the other planets' influence is around 10^{-10}, and thus only the gravitational attraction of the star and the Moon are considered along the project.

This result is expected, as the Moon is closer to the Earth than any other planet and the Sun is much more massive than any other body in the Solar System.

In spite of the fact that this effect could seem to be small and, in fact, it is, third bodies such as the Sun or Moon have an important effect on satellites at higher altitudes.

Finally, the motion equation with the new terms is:

$$\ddot{\vec{r}} = -\mu_{\oplus}\frac{\vec{r}}{r^3} + \mu_{\odot}\frac{\vec{r}_{\odot}-\vec{r}}{|\vec{r}_{\odot}-\vec{r}|^3} - \mu_{\odot}\frac{\vec{r}_{\odot}}{r_{\odot}^3} + \mu_{☾}\frac{\vec{r}_{☾}-\vec{r}}{|\vec{r}_{☾}-\vec{r}|^3} - \mu_{☾}\frac{\vec{r}_{☾}}{r_{☾}^3} \tag{3.4}$$

Integrating Equation (3.4) over a year for a low Earth orbit whose initial orbital elements are presented in Table 3.1, the Keplerian elements that are displayed in Figure 3.2 are obtained.

Table 3.1 Initial Keplerian elements.

a	e	i	ω	Ω	M
6878.14 km	0.01	20º	90º	45º	0º

Several conclusions about the orbital elements' behaviour are presented:

- The semi-major axis suffers periodical changes. Its value range between 6878.129 and 6878.141 km. In the figure it is observed that oscillations take place around a_0, which is the initial value.
- The eccentricity's behaviour shows both long-term and short-term periodical changes. Furthermore, the value does not noticeably change , as the oscillation's order of magnitude is around 10^{-4}.
- The inclination suffers great changes. There are secular variations and periodical oscillations. The most important effects are secular. Although its impact in LEOs is clearly seen in the figure, for a GEO the effect is highly detrimental, as it modifies inclination about 1 per year and station keeping manoeuvres are required.
- The argument of the perigee, analogously to the inclination, has both secular and periodical changes.
- The RAAN changes like ω. There are not only periodical changes, but also secular variations. The mean value decreases, although it is so slow that in one year's time, Ω decreases only 0.5º, making this shift almost imperceptible.

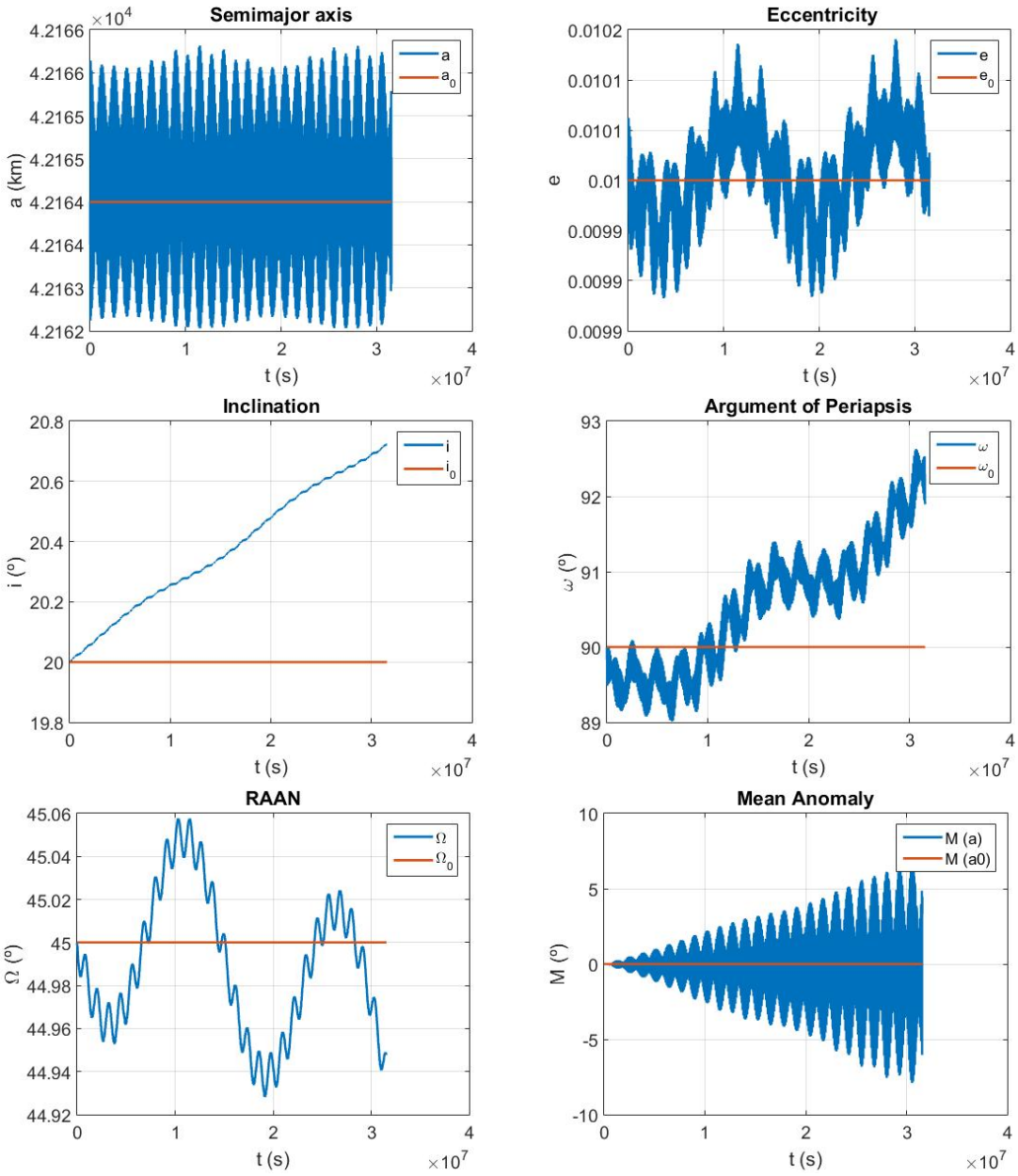

Figure 3.2 Evolution of orbital elements for third body perturbations.

- To properly analyse the perturbations that mean anomaly suffers, it is necessary to subtract $n \cdot t$ from the value that has been obtained from the integration of Equation (3.4). It enables us to observe the periodical changes of this orbital element, as the term $n \cdot t$ dominates the parameter.

3.2 Earth's gravitational potential

One of the hypotheses that was supposed in the previous chapter to develop the motion equation stated that bodies could be considered as a point which is as massive as the planet or satellite. However, this simplification can only be assumed if bodies were solid and homogeneous spheres, which is not the case.

Planets, stars, satellites, vehicles and other kind of elements are no spheres. They have irregular faces or, at least, they are not perfect spheres.

First at all, to consider the perturbation created by a non-spherical central body we must analytically calculate the gradient of the potential function. It then follows that the acceleration due to nonspherical central body is obtained, so that we are able to calculate and analyse the effect of this perturbation.

However, to develop these concepts an accurate model of the gravitational potential of the Earth is necessary:

$$U = \frac{\mu}{r}\left[1 - \sum_{n=2}^{\infty}\sum_{m=0}^{n} J_{nm}\left(\frac{R_{\oplus}}{r}\right)^{n} p_{nm}\sin(\phi)\cos(m(\lambda-\lambda_{nm}))\right] \tag{3.5}$$

In Equation (3.5) two terms are distinguished. The first one represents the potential function of a sphere ($U = \frac{\mu}{r}$). The other is the sum of the spherical harmonics, which are deviations and corrections to get the nonspherical function.

On the other hand, J_{nm} and λ_{nm} are coefficients related to the harmonic nm and p_{nm} is the Legendre's polynomial whose grade is n and order m. The mathematical expression of Legendre's polynomial are written as follows:

$$p_m(x) = (1-x^2)^{n/2}\frac{d^m p_n(x)}{dx^m} \tag{3.6}$$

Combining different values for n and m, three different harmonics are obtained: zonal (m=0), sectorial (n=m) and tesseral (n≠m). We develop two different potential functions based on the first two harmonics. These two models are named as J_2 and C_{22}, which are exhaustively developed in the next subsections.

3.2.1 Earth oblateness

First at all, the J_2 perturbation term is studied.

In this perturbation, all terms except the first are eliminated, since these coefficients' order of magnitude is usually overly small, around 10^{-6}, except for the first coefficient ($J_2 \sim 10^{-3}$).

In this case, the potential function of the nonspherical central body is presented next. It has been obtained from [27] and [3].

$$U = \frac{\mu}{r}\left[1 + \frac{J_2}{2}\left(\frac{R_{\oplus}}{r}\right)^{2}(1 - 3\sin^2(\phi))\right] \tag{3.7}$$

In Equation (3.7), ϕ is the satellite's latitude. In order to obtain an equation for the acceleration, it is necessary to calculate the partial derivatives. Furthermore, it is required to properly choose the reference frame which equations are integrated in. As explained before, this reference frame is the inertial geocentric equatorial. In Equations (3.11), (3.12) and (3.12) partial derivatives are calculated in such axes (x,y,z).

In order to obtain the partial derivatives, variable ϕ has to be expressed in terms of r_x, r_y and r_z. Figure 3.3 shows the axes, latitude and longitude in the reference frame that is being used. The X label coincides with the vernal equinox. Using geometric correlations ϕ is defined as a function of r_x, r_y and r_z.

$$\sin(\phi) = \frac{r_z}{r} \tag{3.8}$$

$$\cos(\phi) = \frac{\sqrt{r_x^2 + r_y^2}}{r} \tag{3.9}$$

The mathematical functions that link latitude and position are presented in Equations (3.8) and (3.9).

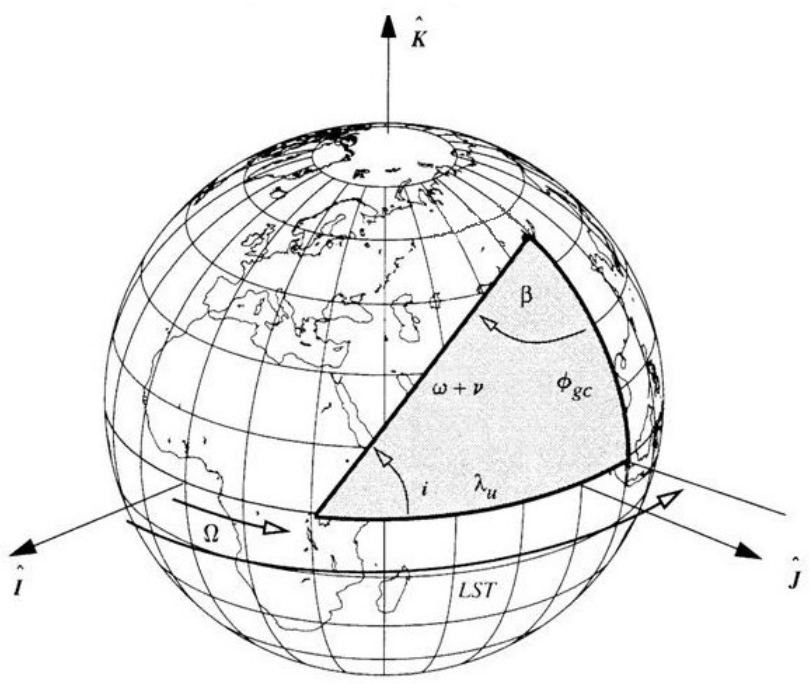

Figure 3.3 Axes and latitude in the reference frame.

In (3.7), ϕ is replaced by Equations (3.8) and (3.9). Once the nonspherical gravitational potential function has been obtained and particularized, we are able to properly derive the potential in order to obtain the accelerations.

First, there is a value that should be defined: $r = \sqrt{r_x^2 + r_y^2 + r_z^2}$. This parameter is often used in this chapter.

The components of the acceleration vector that are included in the motion equation ($\vec{a} = (a_x, a_y, a_z)$) are computed as follows:

$$a_x = \frac{\delta U}{\delta r_x} = -\frac{3J_2\mu R_\oplus^2 r_x}{2r^5}\left(1 - \frac{5r_z^2}{r^2}\right) \tag{3.10}$$

$$a_y = \frac{\delta U}{\delta r_y} = -\frac{3J_2\mu R_\oplus^2 r_y}{2r^5}\left(1 - \frac{5r_z^2}{r^2}\right) \tag{3.11}$$

$$a_z = \frac{\delta U}{\delta r_z} = -\frac{3J_2\mu R_\oplus^2 r_z}{2r^5}\left(3 - \frac{5r_z^2}{r^2}\right) \tag{3.12}$$

Once accelerations due to J_2 have been obtained, the equation that is used to propagate over the time and determine the Keplerian elements' behaviour is presented. The initial elements are displayed in Table 3.1. The results are presented in Figure 3.4. In these plots we can evaluate the oscillations that the six orbital elements suffer along one and a half day.

$$\ddot{\vec{r}} = -\mu\frac{\vec{r}}{r^3} + \vec{a}_{J_2} \tag{3.13}$$

Relevant conclusions are presented to clearly understand the results that are shown:

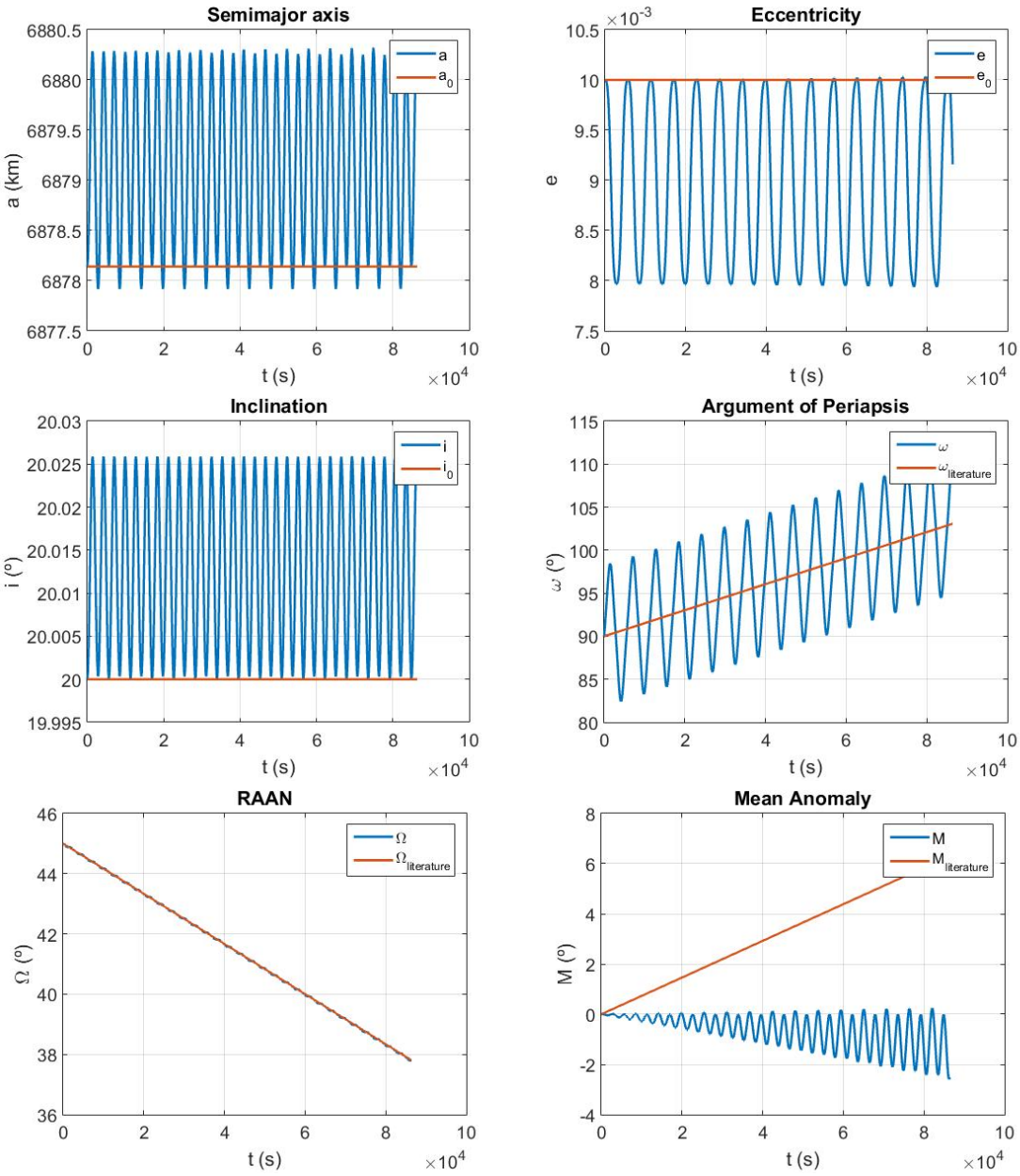

Figure 3.4 Evolution of orbital elements for J2 perturbation.

- The semi-major axis suffers periodical changes. Its value range between 6878 and 6880.5 km. It is relevant to remark that this variable has no secular variations. The mean value of the semi-major axis does not exactly coincide with a_0. This is due the presence of perturbations in Equation 2.5. On the other hand, as there are not secular changes, it is concluded that the energy stays constant.
- The eccentricity's behaviour is similar to the changes that the semi-major axis shows. There are no secular changes, only periodical ones. Analogously to the semi major axis, the mean value of the eccentricity is not the same as e_0. Although the order of magnitude of the periodical oscillations is quite small (around 10^{-3}), its effect in the orbit is extremely relevant, as the shape of the orbit substantially changes.
- The inclination behaves analogously to eccentricity and semi-major axis. There are short-term and long-term oscillations and the mean value does not coincide with i_0.
- The argument of the perigee shows not only short-term and long-term oscillations, but also a secular variation. In this case, the mean value of ω is the same as w_0.

There is an interesting term connected with this orbital element: "The advance of the perigee". As $\dot{\omega} \neq 0$, the perigee's and apogee's position varies, which could cause failures in missions. Due to this reason there are orbits, like "Molniya", which use the critic inclination(63.4º) cancelling this phenomenon. Figure 3.5 shows its effect.

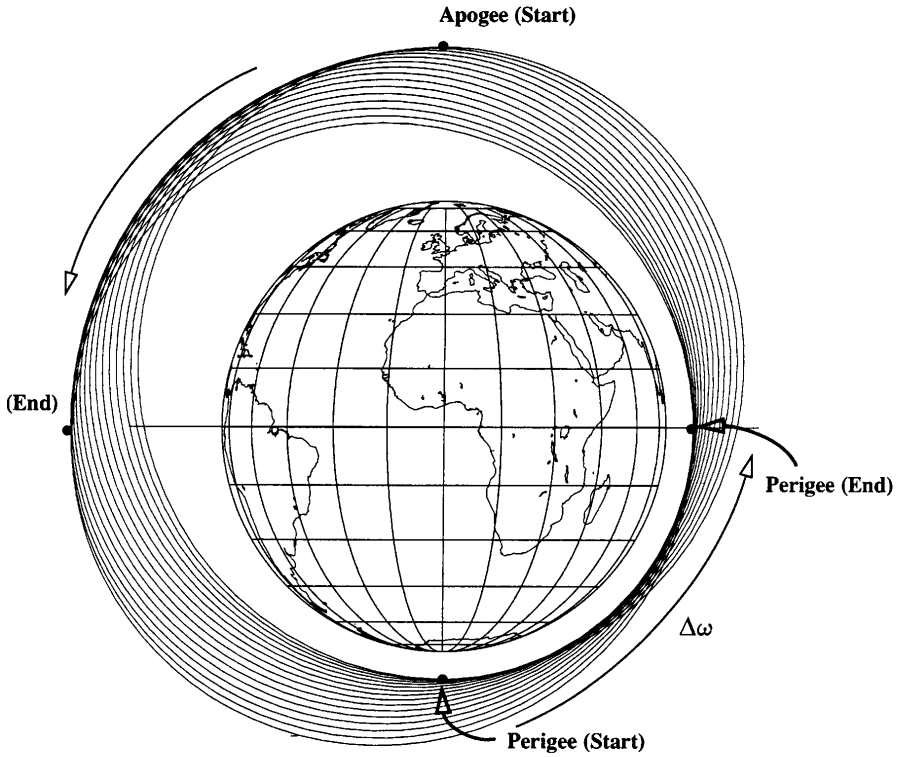

Figure 3.5 Advance of the perigee.

- The RAAN changes like ω. We difference between periodical and secular variations. One more time, as it happened for the argument of the perigee, the mean value of Ω coincides with the one obtained analytically.

  Analogously to ω, as $\dot{\Omega} \neq 0$, other phenomenon is called as "Precession of the nodes". It changes the orbital plane and only becomes zero when the inclination's value is 90º, called as polar orbit. Obviously, station-keeping manoeuvres are sometimes necessary to keep the satellite in the correct plane. Figure 3.6 shows this effect.
- Finally, to display the mean anomaly, the term $n \cdot t$ has been subtracted from results, avoiding the effect of the main term and considering only the deviation to the Keplerian solution. Both periodical and secular changes are observed.

To sum up, it should be remarked that J_2 perturbation, in combination with atmospheric drag, are the biggest phenomena that disturb a low Earth orbit and thus both of them are considered along the project.

3.2.2 Triaxiality

Equation (3.5) shows the gravitational potential function for a general body.

$$U = \frac{\mu}{r}\left[1 - \frac{J_2}{2}\left(\frac{R_\oplus}{r}\right)^2 (1 - 3\sin^2(\phi)) - 3J_{22}\cos^2(\phi)\cos(2(\lambda - \lambda_{22}))\right] \tag{3.14}$$

The potential function that considers this triaxiality's perturbations is described in (3.14). Both sectorial and tesseral harmonics are considered. Triaxiality is based on the consideration of the Earth as a general

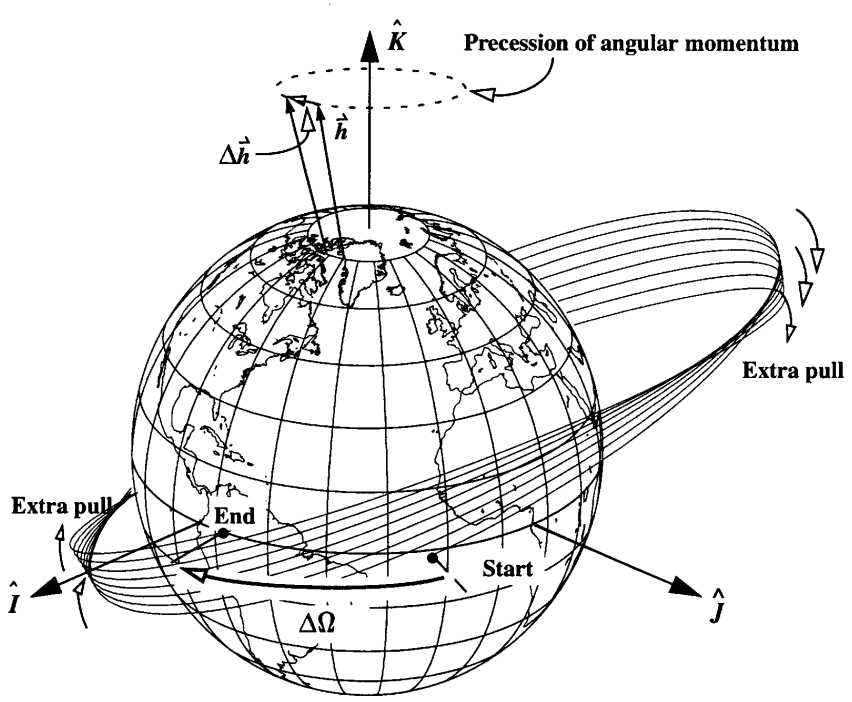

Figure 3.6 Regression of nodes.

ellipsoid. Equation (3.14) combines J_2 and J_{22}.

$$\alpha = \lambda - \omega_{\oplus} - GST_0 \tag{3.15}$$

The gravitational potential has to be defined as a function of r_x, r_y and r_z. One more time Figure 3.3 is used to determine the satellite's longitude, λ, in the reference frame that is used to integrate the motion equation. Furthermore, λ has to be defined according to this reference frame and thus a change is required. As the Greenwich meridian changes its position every day, a new variable, called Greenwich Sidered Time (α), is defined of variables in Equation (3.15). This parameter is the angle between Greenwich and the vernal equinox.

On the other hand, $\lambda(x,y,z)$ is developed next:

$$cos(\lambda - \omega_{\oplus} - GST_0) = \frac{r_x}{\sqrt{r_x^2 + r_y^2}} \tag{3.16}$$

$$sin(\lambda - \omega_{\oplus} - GST_0) = \frac{r_y}{\sqrt{r_x^2 + r_y^2}} \tag{3.17}$$

$$\beta = \lambda_{22} + \omega_{\oplus} t + GST_0 \tag{3.18}$$

Then, the acceleration can be written as:

$$a_x = -\frac{3J_{22}R_{\oplus}^2\mu}{r^7}\left(2\cos^2(\beta)(2r^2r_x - 5r_x^3) - 10\sin^2(\beta)r_y^2r_x + 2\sin(2\beta)(r_yr^2 - 5r_x^2r_y) - 2r_xr^2 + 5r_x^3 + 5r_xr_y^2\right) \tag{3.19}$$

$$a_y = -\frac{3J_{22}R_{\oplus}^2\mu}{r^7}\left(2\sin^2(\beta)(2r^2r_y - 5r_y^3) - 10\cos^2(\beta)r_x^2r_y + 2\sin(2\beta)(r_xr^2 - 5r_y^2r_x) - 2r_yr^2 + 5r_y^3 + 5r_yr_x^2\right) \tag{3.20}$$

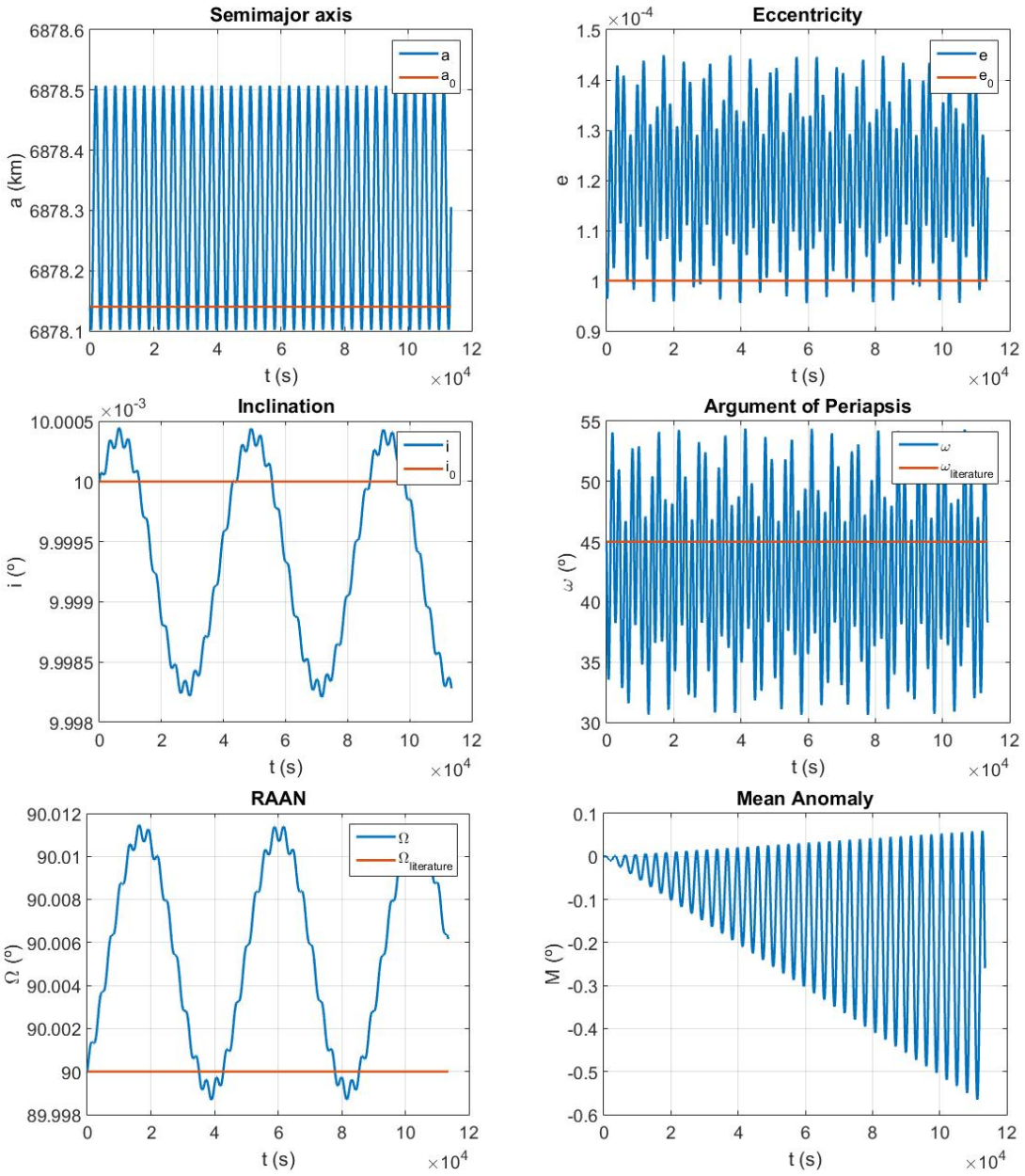

Figure 3.7 Evolution of orbital elements for C22 perturbation.

$$a_z = -\frac{3J_{22}R_{\oplus}^2\mu}{r^7}\left(-10\cos^2(\beta)r_x^2r_z - 10\sin^2(\beta)r_y^2r_z - 10\sin(2\beta)r_xr_yr_z + 5r_z(r_x^2+r_y^2)\right) \tag{3.21}$$

Partial derivatives are calculated in order to obtain the accelerations caused by the consideration of the triaxiality. These partial derivatives are: $a_x = \frac{\delta U}{\delta r_x}$, $a_y = \frac{\delta U}{\delta r_y}$ and $a_z = \frac{\delta U}{\delta r_z}$. Equations (3.18), (3.19), (3.20) and (3.21) show the final expressions.

All these mathematical equations are used in the acceleration model to obtain the orbital element's changes along one and a half day. The initial Keplerian elements are presented in Table 3.1 and results in Figure 3.7. Several suitable conclusions are included to properly analyse and understand this perturbation.

- The semi-major axis has periodical changes. Its value range between 6878.1 and 6878.5 km. The initial value, a_0 is also showed. The mean value of the semi-major axis does not coincide with a_0. This

fact has previously been presented for the J_2 perturbation. This orbital element presents short-term and long-term periodical oscillations.

- The eccentricity's behaviour is similar to the changes in semi-major axis. Instead of secular changes there are only periodical oscillations, but negligible.
- The inclination clearly shows short and long-term oscillations. Similarly to the semi-major axis, this parameter's variations are close to i_0.
- The argument of the perigee is analogous to the previous elements. There are only periodical changes and the mean value is close to the initial one, ω_0.
- The RAAN behaves similarly to the inclination. It clearly shows the two kind of periodical oscillations. However, its mean value does not coincide with the initial one Ω_0.
- Finally, to study the mean anomaly the term $n \cdot t$ has been subtracted from results, avoiding the effect of the main term and considering only the deviation to the Keplerian solution. This is the only case where we could observe some secular changes. However, the most important variations are the periodical ones.

3.3 Atmospheric Drag

The most relevant perturbation for low Earth orbits in a long-term propagation is the atmospheric drag because of the effect this phenomenon has in the satellite's altitude. It is defined as the effect of the highest layers of the atmosphere on an object as in the troposphere and the ionosphere there is some residual atmosphere. This non-zero density means that, while the object is moving, the body is impacting with a fluid. It creates a drag force, opposite to the motion, that disturbs the satellite's behaviour. Then, as the energy of the object increases, its velocity also increases, as the body is getting closer to the Earth. For a circular orbit, the speed is calculated as follows: $v = \sqrt{\frac{\mu}{r}}$. As the radius disminishes, the velocity gets bigger.

This perturbation is quite complicated to analyse because of a few reasons:

1. The Sun is crucial to determine the atmospheric density. Several phenomena like solar flux, solar winds, solar eruptions or magnetic storms change the atmospheric particles, volume and mass. Moreover, electromagnetic fields perturb those particles as well.
2. The presence of complex chemistry and thermodynamic reactions provokes unexpected behaviours, which are complicated to predict and model.
3. Due to friction, total energy is not conserved. This non-conservative movement changes not only the semi-major axis, but also the eccentricity, as it is shown in Figure 3.8. This makes even more difficult to predict the satellite's position and the atmospheric characteristics past a certain point.

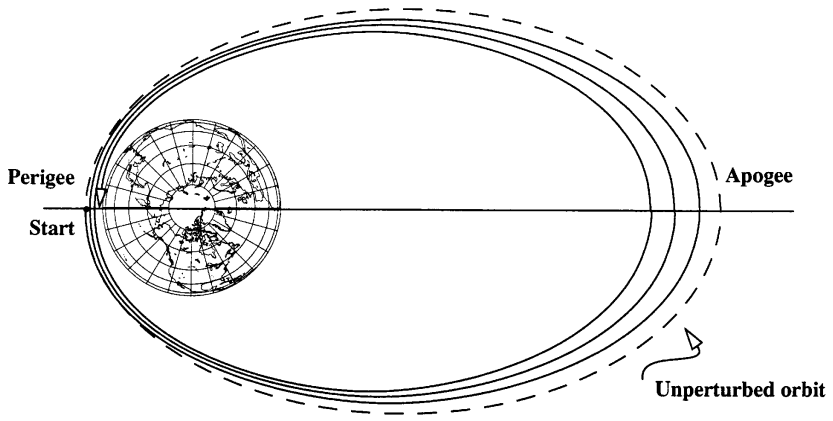

Figure 3.8 Atmospheric drag.

4. In addition, 27-day solar-rotation cycles, the relative position between the Sun and the Earth, ocean tides, pollution or diurnal variations are other phenomena that change the density's value.

5. Finally, gravitational attraction and temperature changes also perturb the density.

According to all of these facts, it is almost impossible to accurately determine the atmospheric's characteristics. Most methods try to give a close approximation to the real values and hence there are two families of density models. On the one hand, few models consider time as a parameter. This method needs an epoch and is very computationally demanding. On the other hand, analytical and numerical methods without considering time, are proposed. They are less accurate but easier to work with. Most of them are based on experimental results and observations. One of these methods is the exponential model, which states that the atmosphere's density decays exponentially with increasing density and taking into account experimental parameters. This last model is described in detail in [27].

The equation that defines this model is as follows:

$$\rho = \rho_0 \cdot e^{\left[-\frac{h_{ellipsoid}-h_0}{H}\right]} \tag{3.22}$$

Where ρ_0 is the reference density, $h_{ellipsoid}$ the altitude above the Earth, considering the planet as an ellipsoid. Finally, h_0 is the reference altitude and H a parameter that could be obtained from a reference table. Such table is showed in Figure 3.9.

Altitude h_{ellp} (km)	Base Altitude h_o (km)	Nominal Density ρ_o (kg/m^3)	Scale Height H (km)	Altitude h_{ellp} (km)	Base Altitude h_o (km)	Nominal Density ρ_o (kg/m^3)	Scale Height H (km)
0–25	0	1.225	7.249	150–180	150	2.070×10^{-9}	22.523
25–30	25	3.899×10^{-2}	6.349	180–200	180	5.464×10^{-10}	29.740
30–40	30	1.774×10^{-2}	6.682	200–250	200	2.789×10^{-10}	37.105
40–50	40	3.972×10^{-3}	7.554	250–300	250	7.248×10^{-11}	45.546
50–60	50	1.057×10^{-3}	8.382	300–350	300	2.418×10^{-11}	53.628
60–70	60	3.206×10^{-4}	7.714	350–400	350	9.158×10^{-12}	53.298
70–80	70	8.770×10^{-5}	6.549	400–450	400	3.725×10^{-12}	58.515
80–90	80	1.905×10^{-5}	5.799	450–500	450	1.585×10^{-12}	60.828
90–100	90	3.396×10^{-6}	5.382	500–600	500	6.967×10^{-13}	63.822
100–110	100	5.297×10^{-7}	5.877	600–700	600	1.454×10^{-13}	71.835
110–120	110	9.661×10^{-8}	7.263	700–800	700	3.614×10^{-14}	88.667
120–130	120	2.438×10^{-8}	9.473	800–900	800	1.170×10^{-14}	124.64
130–140	130	8.484×10^{-9}	12.636	900–1000	900	5.245×10^{-15}	181.05
140–150	140	3.845×10^{-9}	16.149	1000–	1000	3.019×10^{-15}	268.00

Figure 3.9 Exponential density model.

As a consequence of the difficulties that are found when one models density, the consideration of uncertainty in this parameter is required and thus it has been considered in the next chapters.

The atmospheric drag causes lowering of the apogee. It is shown in Figure 3.8. It could provoke an unintended re-entry and, and thus it is vital to accurately model this perturbation.

Once a density model has been chosen, the drag acceleration's is defined as:

$$\vec{a}_{drag} = -\frac{1}{2B}\rho v_{rel}^2 \frac{\vec{v}_{rel}}{|\vec{v}_{rel}|} \tag{3.23}$$

Where B is the ballistic coefficient and is equal to $\frac{m_v}{Sc_D}$, m_v is the object's mass, c_D is the drag coefficient and S the satellite's exposed area. In addition to these parameters, ρ is the density and has its own expression depending on the model that we use. Finally, $\vec{v}_{rel}$ is $\vec{v} - \vec{v}_{atm}$ the relative speed. As the Earth is rotating, the atmosphere has a velocity $\vec{v}_{atm}$:

$$\vec{v}_{atm} = (\omega_{\oplus} r_y, -\omega_{\oplus} r_x, 0) \tag{3.24}$$

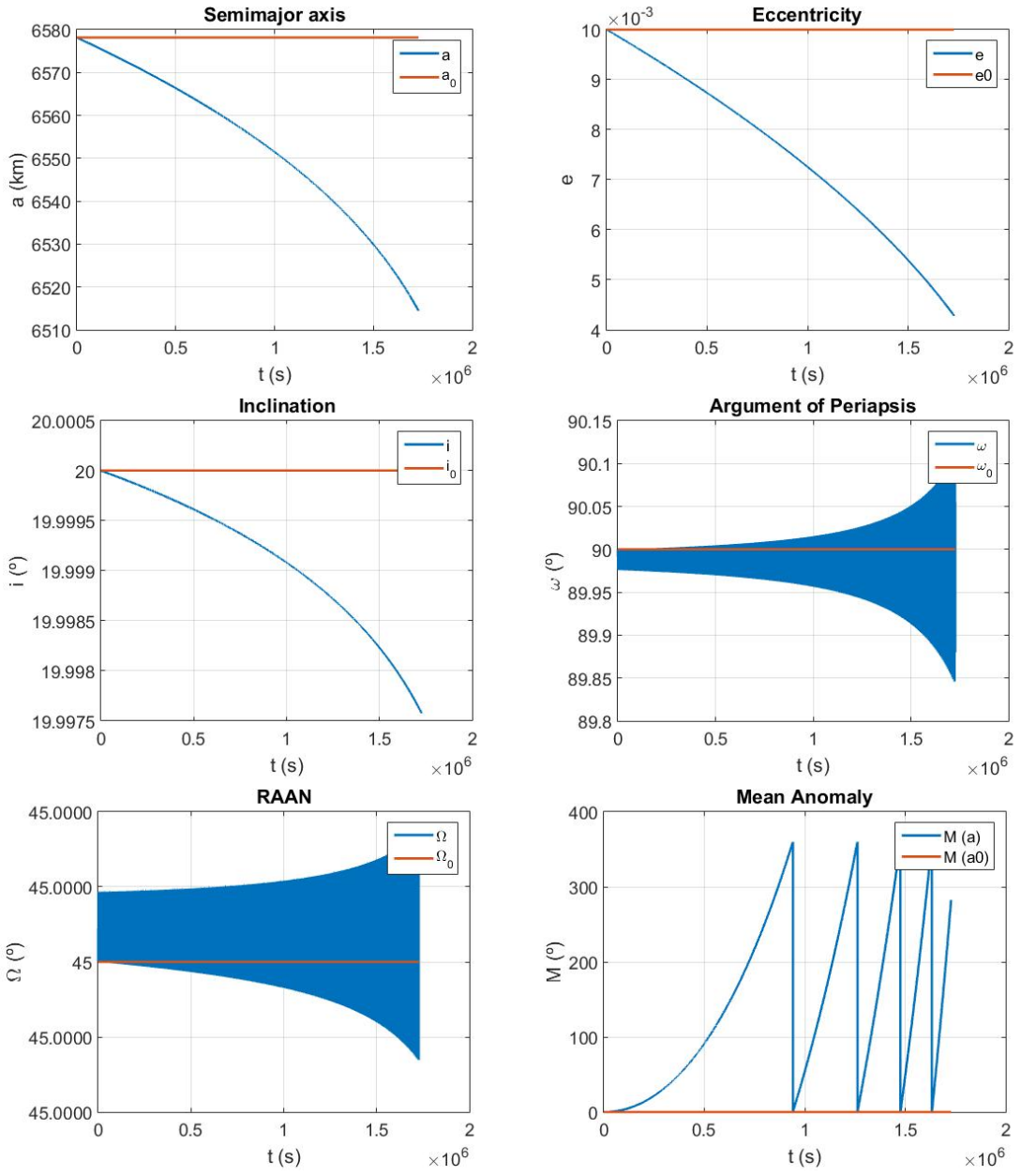

Figure 3.10 Evolution of orbital elements for atmospheric drag perturbation.

Instead of using the same initial conditions as in other sections, it was preferred to change the satellite's

altitude in order to clearly observe its variations. In Table 3.2 the initial orbital elements used to analyse this perturbation are presented. Furthermore, in Figure 3.10 their oscillations are displayed along 21 days.

Table 3.2 Initial Keplerian elements for atmospheric drag.

a	e	i	ω	Ω	M
6578.14 km	0.01	20º	90º	45º	0º

Several conclusions are presented in order to properly understand the periodical and secular variations. In addition, the relevance of this perturbation for low Earth orbits is proved.

- As it is showed in Figure 3.10, the semi-major axis' value decreases almost exponentially. The closer the satellite is to the Earth, the faster the semi-major axis decreases. This orbital element suffers not only secular changes but also periodical oscillations. Nowadays, high accuracy in this parameter is required to predict re-entrys.
- The eccentricity tends to reach the value $e = 0$, which means that the final orbit instead of being an ellipse, would be a circumference.
- The inclination shows a similar behaviour to the semi-major axis and the eccentricity as its value decreases over time. However, its variations are quite small in comparison with the other elements.
- The argument of the perigee does not suffer secular changes. There are only periodical changes around the initial value, ω_0.
- The RAAN only presents short-term and long-term periodical oscillations. Its changes could be neglected and it could be assumed that $\Omega = \Omega_0$.
- Finally, the mean anomaly displays an expected tendency. As the semi-major axis decreases, the value of the period gets smaller and the orbital angular velocity becomes higher. This causes that, in less time, the satellite goes over a greater angle range and hence the mean anomaly changes faster until the re-entry.

3.4 Solar Radiation Pressure

Finally, the solar radiation pressure perturbation is explained.

Solar radiation pressure is a non-conservative perturbation caused by the radiation from the Sun impinging on the satellite. This effect is based on the duality wave-corpuscle of the sunlight, which creates a mechanical effect on the object in the opposite direction to the satellite-to-Sun vector. Although the acceleration caused by this effect has a small order of magnitude (around $10^{-8} m/s^2$), its effect is extremely relevant in communication satellites or the international space station (ISS), which have large solar panels and long periods of time exposed to the sun.

This perturbation, as the atmospheric drag, is difficult to model because of a few reasons. First of all, during certain intervals of time, the Earth is between the Sun and the satellite. The shadow makes the effect disappear . Secondly, it is necessary to properly define and predict solar cycles and solar storms, which is often elaborate. Finally, the area exposed to the Sun cannot be easily calculated, as several parameters such as the satellite's attitude, the incidence angle or the relative position between the Earth and the Sun, are crucial to determine it.

However, to know how the orbit changes when affected by this perturbation, several simplifying hypotheses are made.

In this project, the non-shadow case is considered. Thus, solar rays impact the satellite all the time. This gives us an idea about how the orbital elements change, but is not realistic. Another simplifying hypothesis is considering a circular orbit of the Earth around the Sun. The inclination of the ecliptic ($\varepsilon = 23.5$) has been

considered in the calculations.

The net force created by the solar radiation pressure is:

$$F = pA(1+\varepsilon)\cos(\phi_{\odot}) \tag{3.25}$$

Where F is the force caused by the solar radiation pressure, p the solar radiation pressure, A the area, ε the reflectivity coefficient and $\phi\odot$ the incidence angle. This two last parameters are assumed to be zero in this mathematical developments.

Once the force has been determined, the acceleration that is included in the motion equation is calculated. This mathematical equation has to include the satellite's mass and $\vec{e}_{\odot}$, which is the unitary vector in the Sun-satellite direction. The acceleration's expression is:

$$\vec{a}_{SRP} = -\frac{F}{m_v}\vec{e}_{\odot} \tag{3.26}$$

Including $\vec{a}_{SRP}$ in the motion equation and integrating this expression, the orbital elements as a function of time are obtained. Because of the characteristics of this perturbation, it has been decided that Figure 3.11 shows the elements' variation for a year.

Table 3.3 Initial Keplerian elements for solar radiation pressure.

a	e	i	ω	Ω	M
6878.14 km	0.01	20º	90º	0º	0º

In this case, the initial orbital elements are specified in Table 3.3.

As this perturbation is not only quite challenging to implement, but also quite unrealistic because of the simplifying hypotheses that were necessary for its implementation, results have been compared with a handful of references. These articles and papers deeply deal with this perturbation. These references are [17], [2] and [20].

To sum up, several conclusions are presented:

- The semi-major axis suffers only long-term oscillations, which have a one-year period, and short-term changes. This element ranges between 6878.125 km and 6878.155 km, so that the effect of the solar radiation perturbation in this parameter is smaller that the variations that other perturbations created.
- The eccentricity's behaviour is similar to the semi-major axis as it displays one-year periodical oscillations, as well as short-term changes that are not easily seen. On the other hand, the eccentricity increases and decreases taking values far from e_0. Due to this reason it is so relevant this perturbation for GEO satellites, which need station keeping manoeuvres to face this element's oscillations. Eccentricity makes GEO satellites oscillate around their nominal longitude.
- The inclination shows also a periodical change. Curiously such behaviour would only be found when $\Omega_0 = 0$ and $\Omega_0 = 180$. It happens as in these situations, the ascending node of the satellite's orbit around the Earth and the Earth around the Sun lay in the same line. If we are not in this situation, there are asymmetries provoking secular variations in the inclination. On the other hand the element variations could be neglected and thus this parameter could be treated as a constant.
- The argument of the perigee does not suffer secular changes, but periodical oscillations are clearly observed in the figure.
- The RAAN experiments secular variations except for two situations: $\Omega_0 = 0$ and $\Omega_0 = 180$. The first one has been considered in the project. Little changes in this parameter cause important changes in the inclination, but they are out out of the scope of this project.

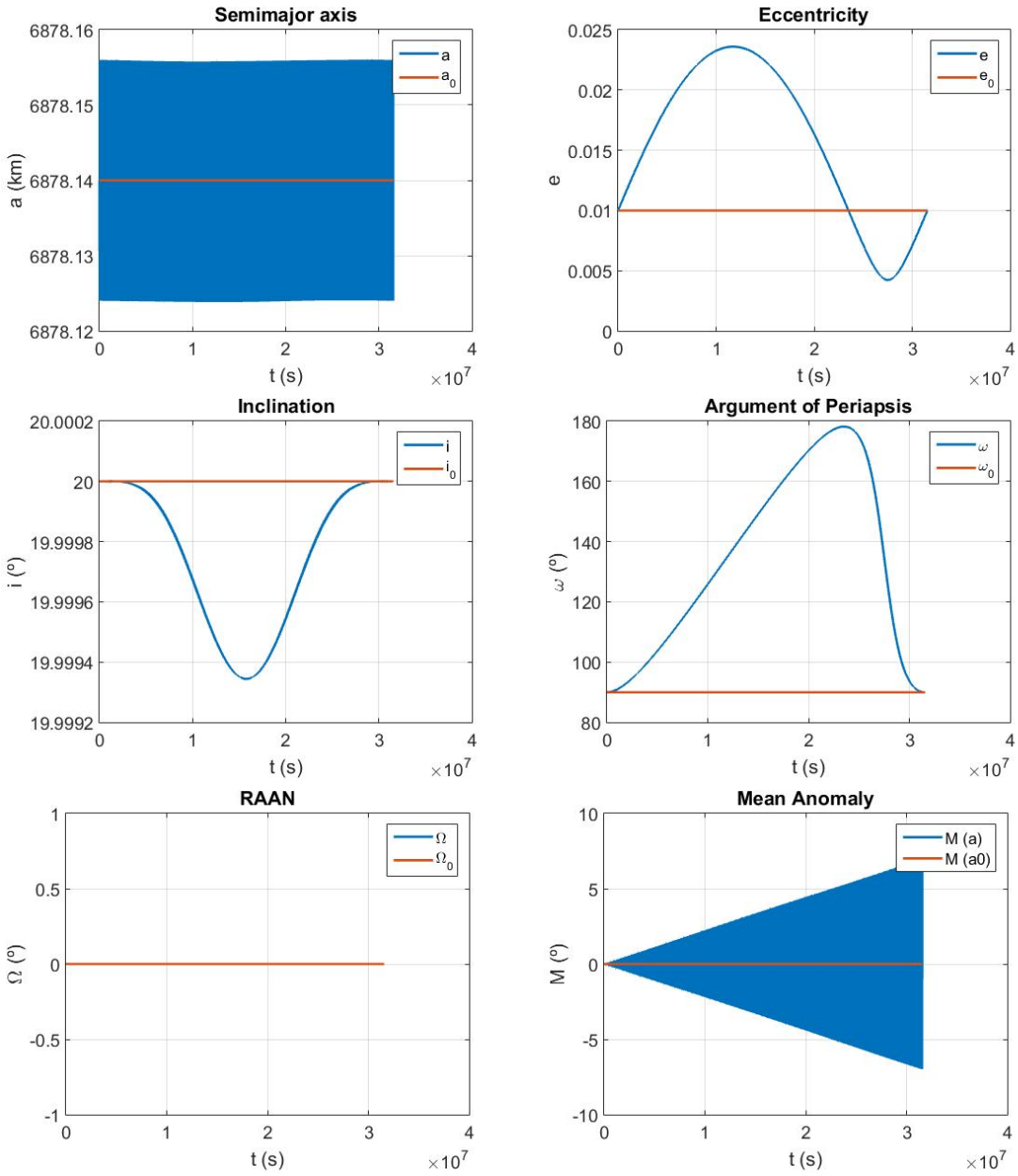

Figure 3.11 Evolution of orbital elements for solar radiation pressure perturbation.

- Finally, the mean anomaly shows symmetrical oscillations around the initial value M_0, which is zero.

3.5 Comparison with a real example

Perturbations have been described in detail. The initial values of the orbital elements are chosen in order to clearly analyse the variations.

However, it could be interesting to compare the results with the real satellite's position acquired from the database CelesTrack, where the current NORAD two line elements are included. Those results were obtained from [1]. It allows us to determine how realistic our model is.

As this project is focused on LEO, it is necessary to look for a low altitude satellite. Satellite "Landsat 7" has been chosen. This vehicle's characteristics are:

1. m_0 = 1973 kg
2. Height= 4.04 m
3. Diameter= 2.74 m

Moreover, the orbit should be defined in a certain epoch. The chosen one is: year 2001, the seventh of April, at 16h 18 min 13 sec. The simulation that is displayed finishes just one year later. In this case, the orbital elements of Landsat 7 have been displayed along five years, though the ones that were calculated by using the model have been displayed in the proper year of the ephemers.

Several additional remarks are:

1. In order to properly study perturbations, it has been necessary to work with simplifying hypotheses. However, there are also considerations related to the real missions that have not been considered in this project, despite the fact that they could play a decisive role in the elements' behaviour. For instance, station-keeping manoeuvres or an initial parking orbit may be relevant in the study.
2. The precision of the real values of the satellite position is around 1 km. Furthermore, it is necessary to refresh the satellite's position after every five hours approximately. This is coherent with the conclusions and results that are developed in the next chapters.
3. The fuel weight, ρ or the area faced to the Sun are important parameters that have been approximated by using a few hypotheses or considering them as a constant parameter, which could be quite unrealistic. Due to this reason, several differences between the real orbital elements and the one obtained by using literature models are expected.

In Figure 3.12 the comparison is displayed.

Several conclusions are presented:

1. The mathematical models give us accurate results for the semi-major axis, as the mean of the calculated orbital element almost concurs with the real value of it.
2. The eccentricity displays a dissimilarity between the TLE and the results from the mathematical models. However, these differences are not high (around $2 \cdot 10^{-3}$) and are supposed to be caused as a result of the simplifying hypotheses.
3. The inclination's behaviour is quite similar to the eccentricity, as both do not coincide with the real results. However, in both cases case the order of magnitude coincides between the TLE plot and the one obtained from the mathematical model. The inclination's maximum variation is only 0.02º. Due to this reason, the model shows realistic results. Moreover, in this plot there is a relevant fact that should be mentioned. As it could be seen, inclination suffers transient increments of its value, which are caused by station keeping manoeuvres. This kind of phenomena are not considered in this project, although they happen in the reality.
4. The argument of the perigee displays realistic results. Although the real values of ω seem to oscillate around 90º, there are transient variations, which are correctly captured by the model.
5. The analysis of Ω is the most significant, as Landsat 7 is a sun-synchronous satellite. The model provides accurate results (in the plot it is complicated to distinguish both curves), which shows the accuracy of the implemented model.
6. Mean anomaly does not offer relevant conclusions, as this value oscillates between 0 and 360º.

3.6 Conclusions

To sum up, several remarks related to perturbation are presented.

First at all, it is relevant to introduce Table 3.4, which shows the order of magnitude of the perturbations in LEO orbit, to understand the effect of all phenomena in the orbital elements. As it can be seen, the Keplerian

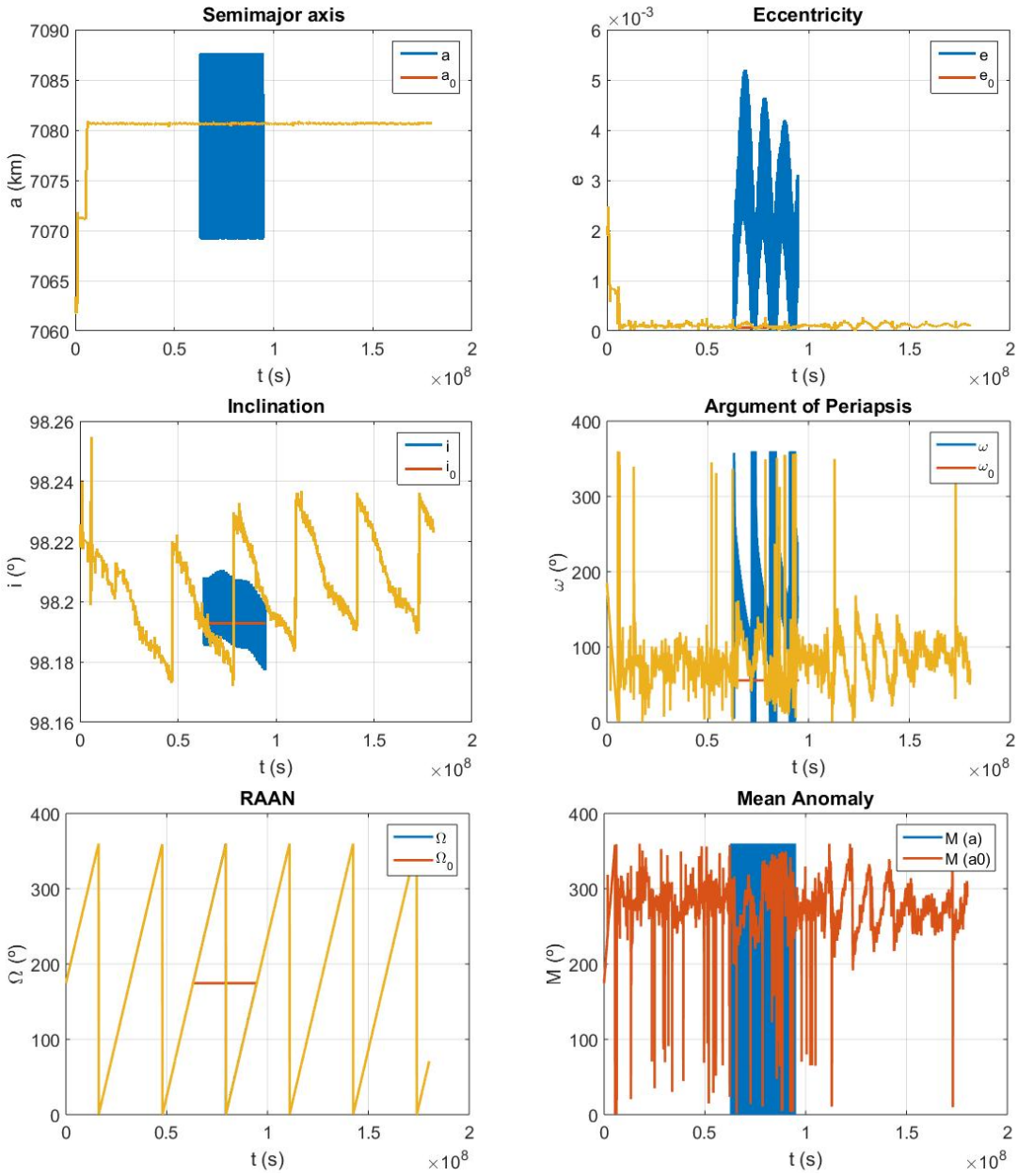

Figure 3.12 Landsat 7. Orbital elements.

acceleration is the most important one, three orders of magnitude above the J_2 effect, which is the most important perturbation. Moreover, one could observe that the smallest disturbances are related to third body's effect and solar radiation pressure, and thus, it could be accurate to neglect their effect.

Furthermore, Table 3.4 subtly shows the fact that perturbations should be logically considered when propagating for long-term periods. However, in the short-term it is quite accurate to neglect all of these phenomena.

Table 3.4 Perturbations' accelerations in LEO.

Perturbations	Kepler	J_2	C_{22}	SRP	TBP	Atmospheric drag
acceleration (m/s^2)	~ 10	~ 0.01	$\sim 10^{-5}$	$\sim 10^{-7}$	$\sim 10^{-6}$	$\sim 10^{-5}$

In addition to these conclusions, it is important to mention several applications of perturbations.

Although these effects change the orbit's behaviour, they could also bring some benefits. As it has been seen, they can change the satellite's attitude or increase or decrease its acceleration. Due to this reason perturbations can be used to save fuel, be more efficient or make a mission viable. For instance, the "Mars reconnaissance orbiter" used the atmospheric drag of Mars in order to save more than 600 kg fuel, and thus the mission became possible.

On the other hand, a few satellites nowadays use solar flaps. They are surfaces with a large area that allow us to control the body's attitude using only the solar radiation pressure's effect. Thanks to this it is possible to save fuel, and thus to extend the satellite's lifetime.

Furthermore, perturbations have benefits related to space waste. The atmospheric drag decreases altitude, which provokes a re-entry after some time. The disappearance of old, "dead" satellites enables us to replace them by new ones.

Finally, perturbations are nowadays a matter of study. Several ideas such as solar wings might be used in a few decades for space travel in the Solar System.

4 Monte Carlo Method

4.1 Method

Monte Carlo method is a probabilistic and computational algorithm based on randomness to solve problems. It is extremely powerful to simulate systems with many degrees of freedom. This method is not only often used in physics and maths but also in the calculation of risk in business, problems with several boundary conditions or even in gaming. Monte Carlo basically is based on working with a huge sample of initial conditions (about 1000 cases). The equations are solved for every case of the sample. The basis of this technique is deeply described in [14] and [19].

Monte-Carlo method was used in the second world war in order to analyse the neutron diffusion in the atomic bomb, as the behaviour of such particles is incredibly random. Nowadays, as a result the development of computers we are able to quickly solve problems using this algorithm.

Several advantages and disadvantages of it are mentioned. They are defined in detail in [21].

1. Easy implementation by using computer programming.
2. Computationally intensive as samples are composed by a huge amount of points.
3. However, the bigger the initial sample is, the higher accuracy we have.
4. Monte-Carlo method allows us to study the interaction between different variables and parameters, analysing how certain changes in the initial conditions disturb orbital elements oscillations, as well as the satellite's position and velocity.
5. A realistic model of the problem is required. However, a deep perturbations' analysis has been carried out in the previous chapter. Furthermore, results have been compared with [27] and [6], as well as with values from a real case. Precision and realism of the model have been proved.
6. Monte Carlo method is defined as conservative if the initial sample is created using a normal distribution, as there can be initial conditions in the sample that are far from the expected values of such initial conditions.

Once the Monte Carlo method has been introduced, the mathematical development and implementation is developed.

4.2 Mathematical development

First at all, to use Monte Carlo method it is necessary to have an accurate and reliable model to propagate the satellite's position and velocity along the orbit. It is the main purpose of chapters 2 and 3. As mentioned before, the model has been proved to be realistic.

On the other hand, in order to define a domain of possible inputs, a statistical function is used. In this chapter two functions are considered and thus they are described next:

- **NORMAL DISTRIBUTION.** The normal distribution is used when several random variables are considered (multivariate case), as well as when the uncertainty is caused by the accumulation of small errors (for instance, measurement errors or the unknown effect of perturbations).

  A random variable which follows this distribution, gets defined as $X \sim N(\mu,\sigma^2)$, where μ is the mean value of the parameter and σ is the standard deviation.

$$f(x) = \frac{1}{\sigma\sqrt{2\pi}} e^{-\frac{(x-\mu)^2}{2\sigma^2}} \tag{4.1}$$

$$F(x) = \int_{-\infty}^{x} f(x)dt \tag{4.2}$$

  Its PDF appears in Equation (4.1), and its distribution function in (4.2).

  The values of the random variable X are defined in a confidence interval. There are three different possibilities that can be considered:

  1. **1-σ interval**: The possibility to find the variable X in (m-σ,m+σ)=68,3%.
  2. **2-σ interval**: The possibility to find the variable X in (m-2σ,m+2σ)=95.45%.
  3. **2-σ interval**: The possibility to find the variable X in (m-3σ,m+3σ)=99.74%.

  Along the project the 3σ case is considered.

  However, instead of working with only one variable, we are working with three, as the position is decomposed in its three components: r_x, r_y and r_z. Due to this reason, the confidence interval is not a curve, it is an ellipsoid. This fact is shown in Figure 4.1. Inside the ellipsoid several points that belong to the normal distribution have been displayed.

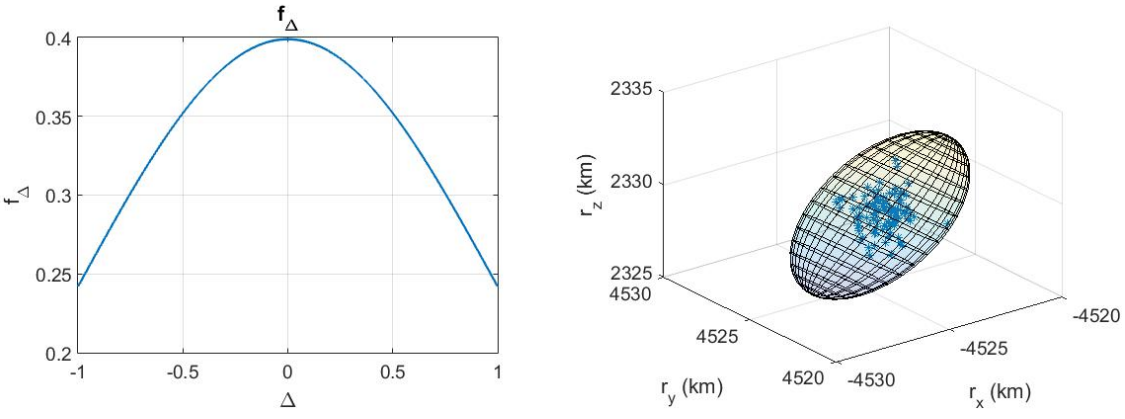

Figure 4.1 Normal distribution.

The calculation of the covariance matrix is presented. Its equation gets defined as follows: $(\underline{x}-\underline{\mu})^T \sum^{-1} (\underline{x}-\underline{\mu})$, where $\sum$ is the covariance matrix and is defined as follows:

$$\sum = \begin{bmatrix} \sigma_x^2 & E\left[(X-m_x)(Y-m_y)\right] & E\left[(X-m_x)(Z-m_z)\right] \\ E\left[(X-m_x)(Y-m_y)\right] & \sigma_y^2 & E\left[(Y-m_y)(Z-m_z)\right] \\ E\left[(X-m_x)(Z-m_z)\right] & E\left[(Y-m_y)(Z-m_z)\right] & \sigma_z^2 \end{bmatrix}$$

It is necessary to clarify that m_x, m_y and m_z are the position vector's means at a moment t_j in the propagation, while X,Y and Z are the position's components at that moment. Finally, σ is the standard deviation.

This covariance matrix is 3x3. In linearized covariance, $\sum$ is 6x6, as both position and velocity components are considered.

It should be clarified the fact that the covariance matrix has been propagated using the error transition state matrix. In this chapter the covariance matrix is calculated in each position and moment in the orbit.

- **UNIFORM DISTRIBUTION.** Uniform distribution offers additional conclusions to the project and hence it is considered.

$$f(x) = \frac{1}{b-a} \rightarrow a \leq x \leq b \tag{4.3}$$

$$f(x) = 0 \rightarrow else \tag{4.4}$$

The distribution function gets described by Equations (4.3) and (4.4).

Moreover, in Figure 4.2, the previous probability distribution function (PDF) gets displayed.

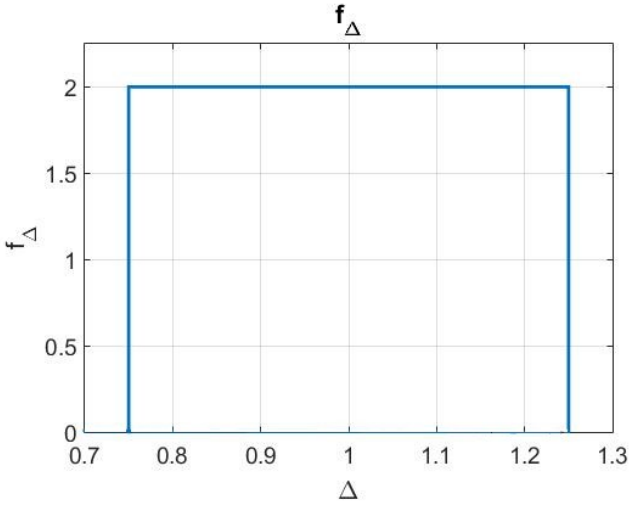

Figure 4.2 Uniform distribution.

The main advantage of this function is the definition of the two ends of the interval. Due to this reason, if a small value of σ is defined, the points of the sample are close to the mean and thus, this distribution is not as conservative as the normal one. In this distribution every point of the sample has the same importance, which does not happen with the normal one.

Once the initial points are defined, Monte Carlo method starts working. It just solves the problem as many times as initial points we have. Once all the simulations have finished, we are able to analyse how do

parameters change, comparing their behaviour in terms of the inputs and the tendency they have. As expected, the number of simulations depends on the area and the problem we are working with and the degrees of freedom. However, according to [21] and [19], an initial sample of one thousand points should be calculated, in order to obtain realistic results.

Once the mathematical basis of the method has been explained, results are shown.

4.3 Results

The results that are presented have been calculated using the orbital elements that appear in Table 4.1. These values allow us to calculate the initial conditions in position and velocity.

Table 4.1 Initial Keplerian elements.

a	e	i	ω	Ω	M
6878.14 km	0.01	20º	90º	45º	0º

4.3.1 Uncertainty in initial position

Because of the effect of perturbations, errors in the measurements or even station-keeping manoeuvres, it is quite complicated to know the exact position of a satellite in a certain moment. What's more, the huge velocity they have makes this knowledge even more uncertain.

Due to this reason, uncertainty in the initial condition in position is assumed in this subsection.

In order to generate the initial sample, the normal distribution has been used. The mean value of $r_x(t_0)$, $r_y(t_0)$ and $r_z(t_0)$ are the ones obtained using the orbital elements in Table 4.1, as well as the initial standard deviation is supposed to be 0.707 km in every axis, according to typical values extracted from [14] and [6].

The orbital elements that are obtained in this case are presented in Figure 4.3.

Several conclusions about Figure 4.3 are presented:

1. The orbital elements' behaviour is the same as the one showed in the previous chapter. It is caused because Monte Carlo method does not change the model, it just displays thousands of simulations, showing the tendency and deviations caused by uncertainty in the initial position.
2. As Figure 4.3 shows, semi-major axis (and due to this reason mean anomaly) has the biggest oscillations, whereas Ω almost does not get perturbed.
3. According to [3], oscillations in the semi-major axis are vital in LEO, as it can mean that the satellite's lifetime orbit increases or decreases around 10 days. In terms of money, if the satellite's life decreases ten days, the company loses around 1 million dollars, according information about the Landsat program.
4. Figure 4.3 shows a huge variety of colours, as each one is assigned to each simulation. As the initial sample is created by one thousand points, there is a simulation per initial point and thus a curve in the figure. The overly of such curves is shown in Figure 4.3.

Once the orbital elements have been calculated using Monte Carlo method, the covariance matrix propagation is presented. Covariance matrix is a good way to determine the place of the space where the satellite is expected to be. Furthermore, its propagation enables us know how does the satellite's position vary.

Results are displayed in Figure 4.4. As a figure of the orbit cannot show properly the ellipsoids that are related to the confidence interval, a zoom has been made in the highest latitude point. It allows us to notice clearly the ellipsoids' size variations. It is possible to differentiate not only different ellipsoid's orientations

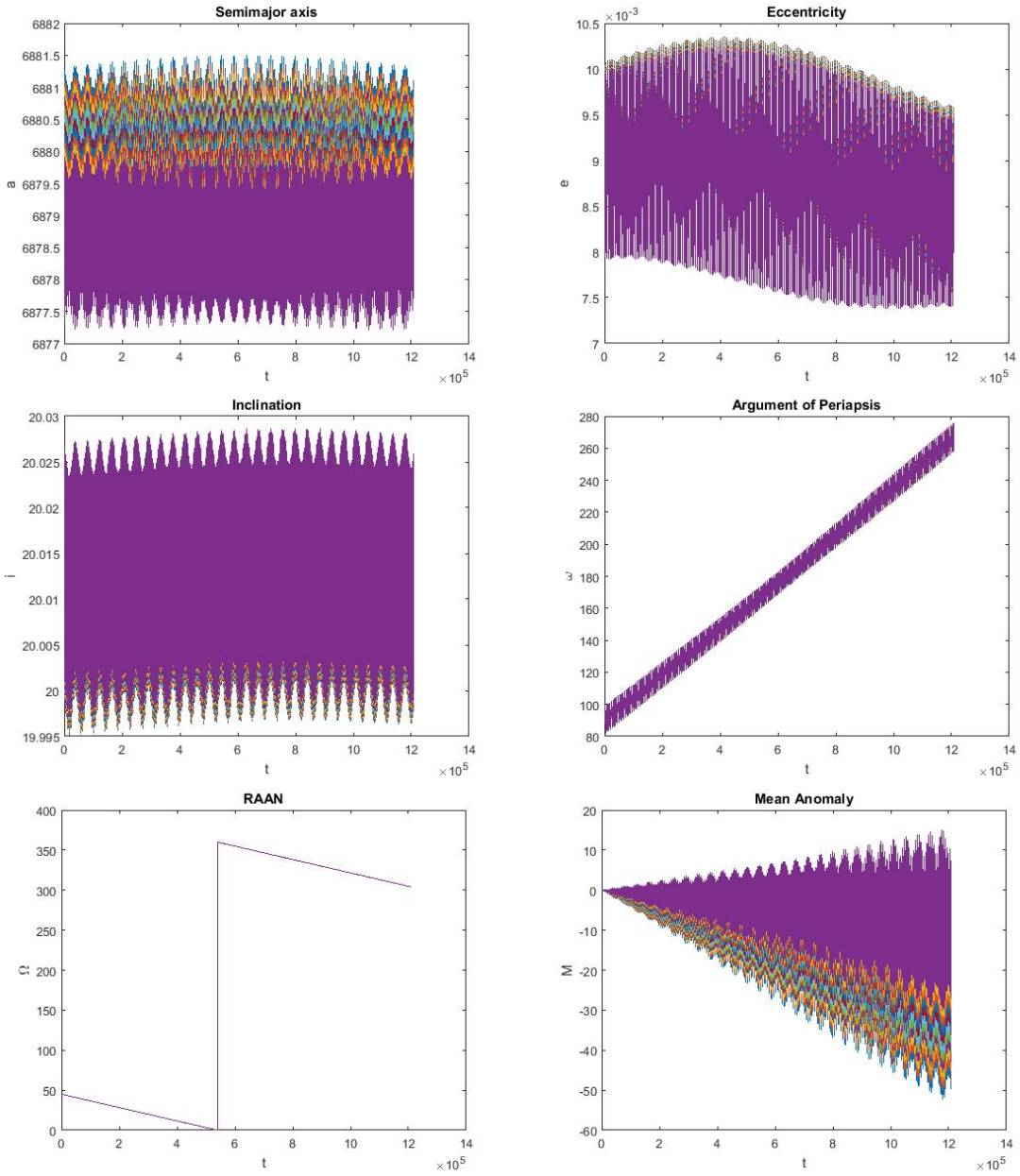

Figure 4.3 Orbital elements. Uncertainty in position. Monte Carlo method.

but also sizes.

On the one hand, the orientation of the ellipsoid depends on the eigenvectors of the covariance matrix. As displayed in Figure 4.4, this geometric form tends to line with the orbit. However, there are ellipsoid's size oscillations that should be mentioned as well. The size is a function of the eigenvalues of the covariance matrix, weight depending on the growth of the confidence region used. As said, in this project it is 3σ.

In order to enrich the conclusions, the previous results are displayed in a local reference frame. As these axes are more intuitive and have a physical meaning, they enable us to obtain more information about uncertainty propagation from this method.

Figure 4.5 displays the ellipsoids in local axis over time. In this test case, the ellipsoid has been propagated over 1 hour.

As it is presented in Figure 4.5, the covariance ellipsoid begins as a sphere and turns into an ellipsoid

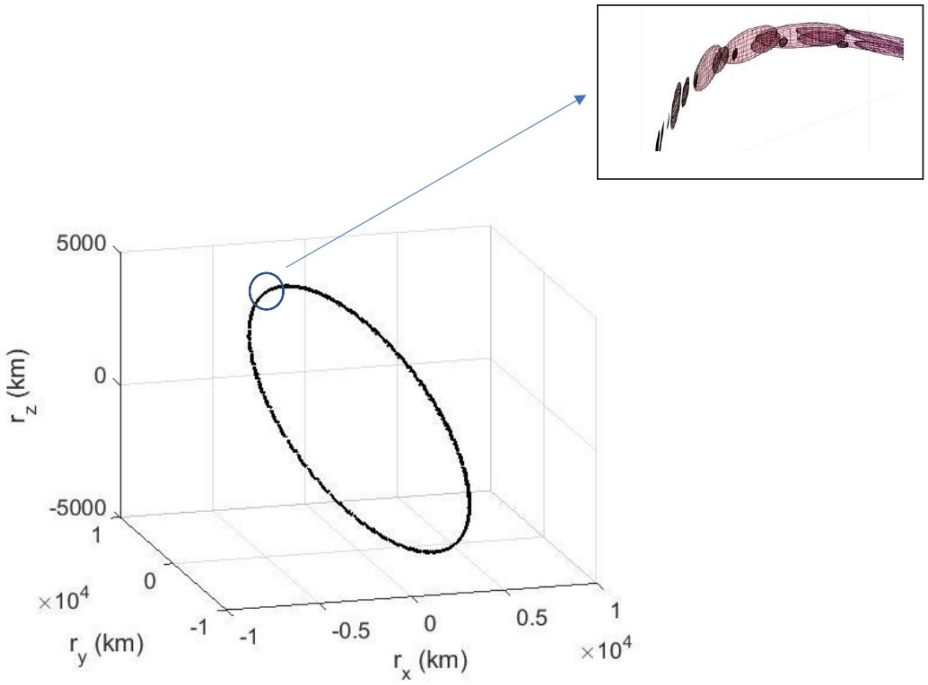

Figure 4.4 Results for Monte Carlo covariance matrix propagation.

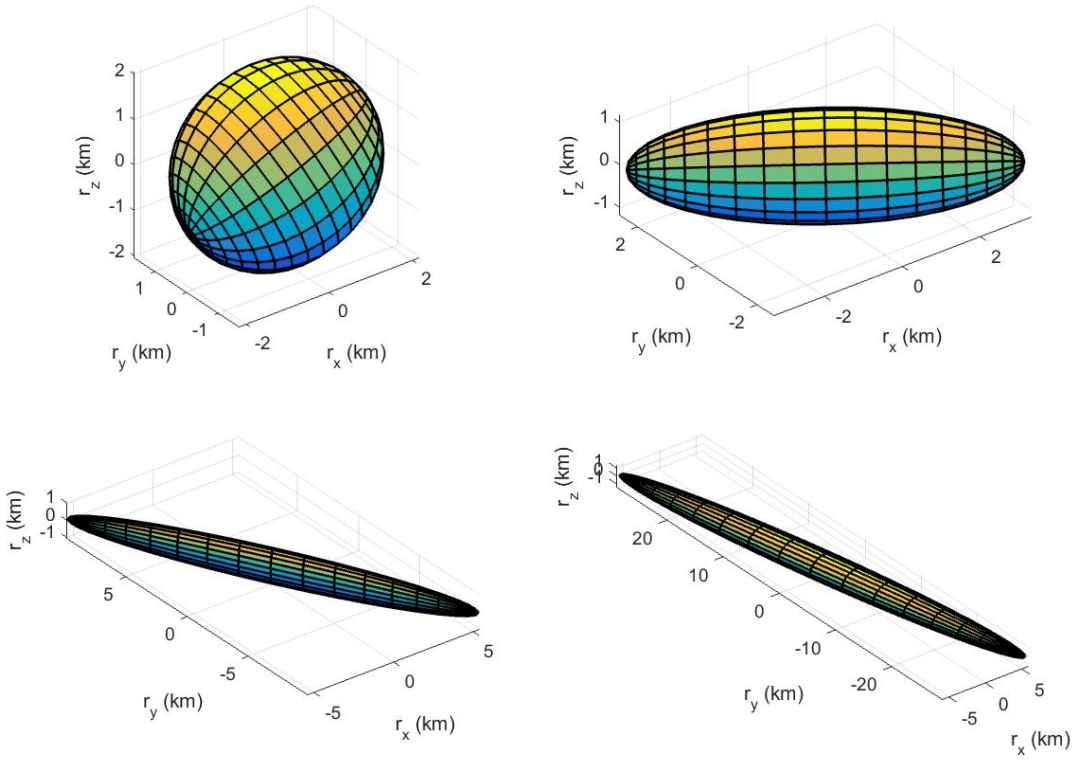

Figure 4.5 Position's ellipsoid after 3 minutes, 15 minutes, 30 minutes and 1 hour.

increasing its size in x-axis and y-axis, as well as its size decreases in z-axis. The growth in y-axis is much bigger than the one in x-axis, which shows the importance that uncertainty propagation has in velocity.

Other additional conclusion that are obtained from figure 4.5 is the fact that ellipsoid's size experiments oscillations. It is coherent with another idea that was noticed when analysing Figure 4.4. When the satellite reaches the maximum and minimum latitude point, the geometric figure becomes spherical, as well as when it reaches the ascending and descending nodes, it turns into a line. This fact can be noticed in the figure, as the ellipsoid gets wider when one hour has passed than when it was only 30 minutes.

4.3.2 Uncertainty in density

The consideration of uncertainty in ρ is completely logical, as phenomena such as solar storms or chemical reactions can cause huge oscillations in the density's value.

In this test case, instead of showing the orbital elements, the standard deviation is shown. Results fo uncertainty in initial position and density are displayed and compared. They are presented in local axis.

To enforce this test case, this analysis is repeated in two different altitudes, which are described in Table 4.2.

Table 4.2 Initial orbital elements.

h	a	e	i	ω	Ω	M
500 km	6878.14 km	0.01	20º	90º	45º	0º
200 km	6878.14 km	0.01	20º	90º	45º	0º

Density is modelled with a normal distribution. In the first test case (h=200 km), density's mean value is $5.464 \cdot 10^{-10} \frac{kg}{m^3}$ and its standard deviation equal to $1.82 \cdot 10^{-14} \frac{kg}{m^3}$, whereas in the second test case (h=500 km) density's mean value is $1.585 \cdot 10^{-12} \frac{kg}{m^3}$ and σ equal to $5.286 \cdot 10^{-16} \frac{kg}{m^3}$.

Results are displayed in Figures **??** and 4.7.

As observed in Figure 4.6, the impact of uncertainty in ρ is incredibly more important than the effect when the initial condition in position is not known exactly.

However, this assertion should be qualified, as the effect of atmospheric drag is only remarkable for tiny altitudes (less than 300 km) and hence, if h>300 km, uncertainty in ρ has almost no effect in satellite's position, as it is displayed in Figure 4.7. However, when h<300 km, specially in the case when h<200 km, little perturbations in the density's value turn into great oscillations in the satellite's position.

On the other hand, as showed in Figure 4.7, where the orbit's altitude is 500 km, an initial error in density has almost no effect in the satellite's position in comparison with the unknown initial position. As explained before, as the altitude is quite high and atmospheric drag has a small effect in the satellite's acceleration, this result is expected.

Moreover, there are several additional ideas that should be pointed. As results are displayed in local axis, OY is related to velocity (as the eccentricity tends to zero). It is curious the fact that the increase of time brings an increase in the standard deviation in OY. It means that uncertainty propagation specially perturbs the velocity. The effect of uncertainty propagation in OZ in both plots can be neglected if results are compared with the obtained ones for the other local axis OX and OY. OZ is related to the kinetic moment. This parameter is supposed to be constant according to the two bodies problem. Several small oscillations in its value can be expected because of the effect of the perturbations.

In [29], different heights and methods are developed to deeply study this topic, as well as [3] focuses more on the satellite's lifetime. In both projects, a deeper analysis can be found.

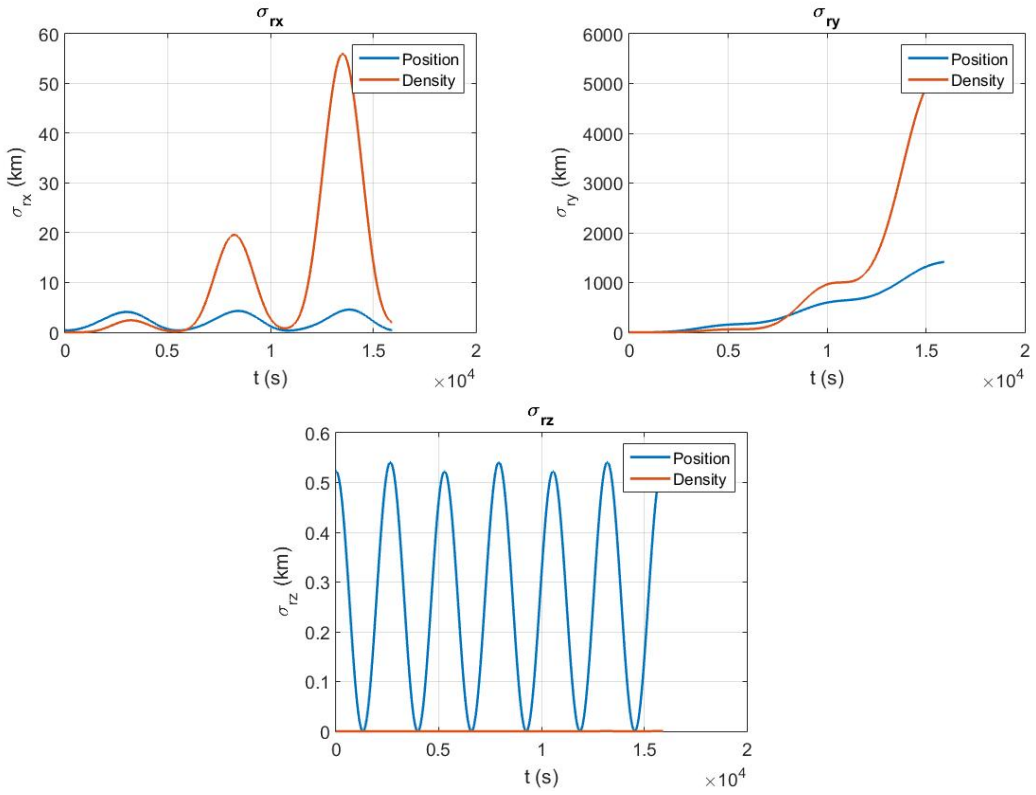

Figure 4.6 h=200 km. Typical deviation in local axis.

4.3.3 Uncertainty in each local axis in initial position. Uniform distribution case

To conclude the chapter, uncertainty in each local axis is considered. Each parameter is modelled using an uniform distribution and only the one parameter case is developed.

There are two reasons that support this analysis:

1. On the one hand, local axes offer more information about the variation of velocity and position than the inertial reference frame because of the physical meaning that local axes have.
2. On the other hand, this research enables us to work with a different PDF from the normal one.

Three test cases have been considered and in all of them, uncertainty in $r_x(t_0)$, $r_y(t_0)$ or $r_z(t_0)$ has been included. Each random variable follows an uniform distribution whose mean $\vec{r}_0$ is the value calculated using the orbital elements in Table 4.1 and the initial deviation is equal to 0.25 km.

In Figure 4.8 the interval where the satellite is expected to be is propagated for the test case of uncertainty in local OX.

Several conclusions about each test case are presented:

1. **Initial uncertainty in local OX**. The position in local axes OX and OY gets bigger, whereas there are no oscillations in OZ. As time increases, y-axis gets bigger faster than x-axis. It shows that an error in position turns into huge variations in the satellite's speed. This test case shows similar results to the ones obtained when the uncertainty is supposed in the three axis of the inertial reference frame.
2. **Initial uncertainty in local OY**. Position in local axes x and y changes at the same time and speed in both of them whereas z-axis does not oscillate. It displays that uncertainty in velocity changes the satellite's period, which changes the body's position as well.

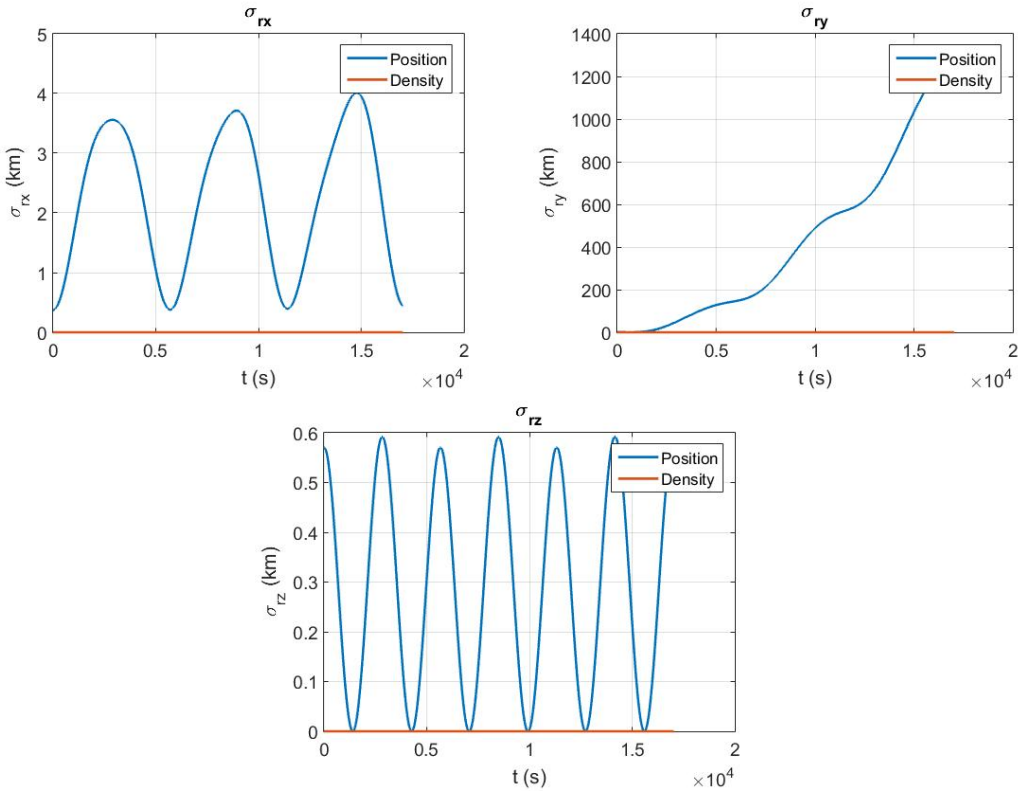

Figure 4.7 h=500 km. Typical deviation in local axis.

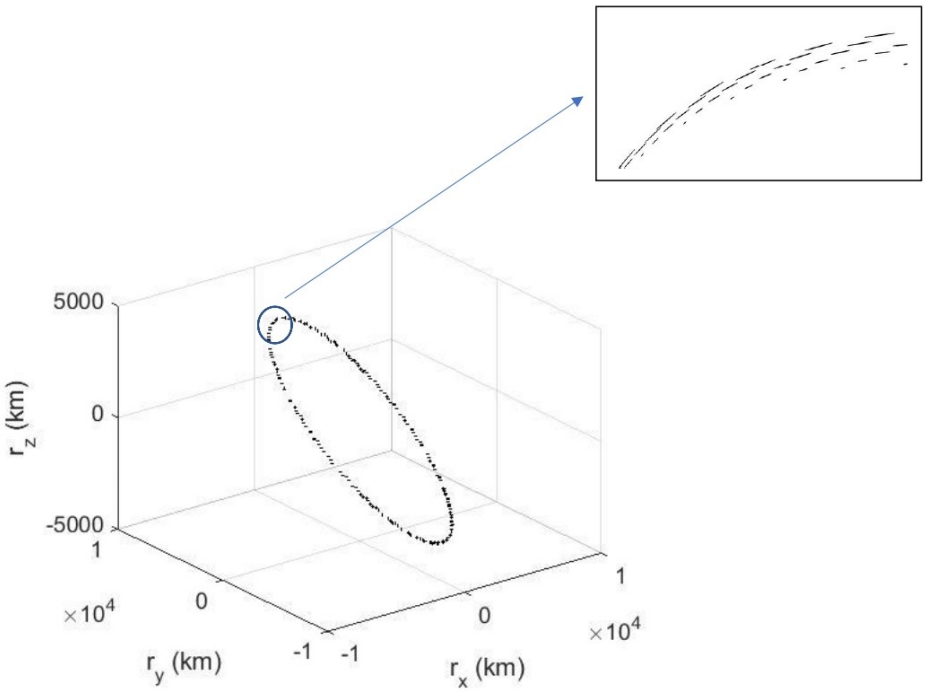

Figure 4.8 Results for Monte-Carlo. Uniform distribution. Uncertainty in local axes.

3. **Initial uncertainty in local OZ**. Position in z-axis has periodical oscillations but does not get increased. OX and OY become bigger if time increases. It displays properly the fact that kinetic moment stays almost constant along the orbit. Perturbations are the only reason why an initial perturbation in local

z-axis provokes changes in the satellite's position and velocity.

5 Differential Algebra

5.1 Method

In spite of the fact that Monte-Carlo methods offer high precision, they are computationally intensive and inefficient as well. On the other hand, several linearized models, as linearized covariance propagation, are not only more efficient, but also less accurate. Due to this reason we have to look for a method in order to obtain more realistic results than linearized models and reduce the computational cost of classical Monte-Carlo techniques.

As a result of these reasons, differential algebra (DA) is introduced. DA is a mathematical method based on approximating the solution by a Taylor expansion of order n. Moreover, instead of using standard automatic differentiation tools, differential algebra only works with polynomial algebra, which enables us to reduce the computational time.

As expected, if the order of the expansion gets increased, the precision of the solution turns bigger. However, it also implies more computational time and hence a compromise solution should be reached. In orbital mechanics, a maximum order of n=6 is often used. Along this project, an order n=4 has been considered. This assumption offers realistic results with high efficiency.

This method applies in most areas of the science, though it is mainly used in Orbital Mechanics. For instance, it is carried out in impact-probability computation or high-order filters as well.

5.2 Mathematical development

Once the main idea of the method has been explained, the implementation and mathematical developments that support this procedure are carried out.

First at all, Taylor's theorem is mentioned, as it is the basis of the differential algebra technique.

Theorem 5.2.1 (Taylor's theorem) *Let $k \geqslant 1$ be an integer and let the function $f : R \to R$ be k times differentiable at the point $a \in R$. Then there exists a function $h_k : R \to R$ such that:*

$$f(x) = f(a) + f^{'}(a)(x-a) + \frac{f^{''}(a)}{2!}(x-a)^2 + ... + \frac{f^k(a)}{k!}(x-a)^k + h_k(x)(x-a)^k \tag{5.1}$$

and $\lim_{x\to a} h_k(x) = 0$. *This is called the Peano form of the remainder.*

If we know the time derivatives of a variable, then we are able to approximate this variable in terms of its Taylor expansion.

As it was commented in the previous chapter, the motion equation is solved to calculate $r_x(t)$, $r_y(t)$, $r_z(t)$, $v_x(t)$, $v_y(t)$ and $v_z(t)$. Furthermore, the motion equation was written in terms of r_x, r_y and r_z and their time

derivatives and hence position and velocity's components have been defined in terms of $\vec{r}$, $\dot{\vec{r}}$, $\ddot{\vec{r}}$, ... yet. Due to this reason we are able to calculate their time derivatives from order k. It allows us to properly define the Taylor expansion of the parameters we want to calculate.

The value of time derivatives of $\vec{r}$ are known in t_0. Beginning with the initial conditions we can iterate and determine the derivative's value at t_1 of the simulation using Equation (5.1). Then, iterating this process along the interval of time of the simulation, all derivatives are defined. Then, the parameter's value can be calculated at every step of the time's interval.

In Figure 5.1 the flow diagram of this procedure is displayed.

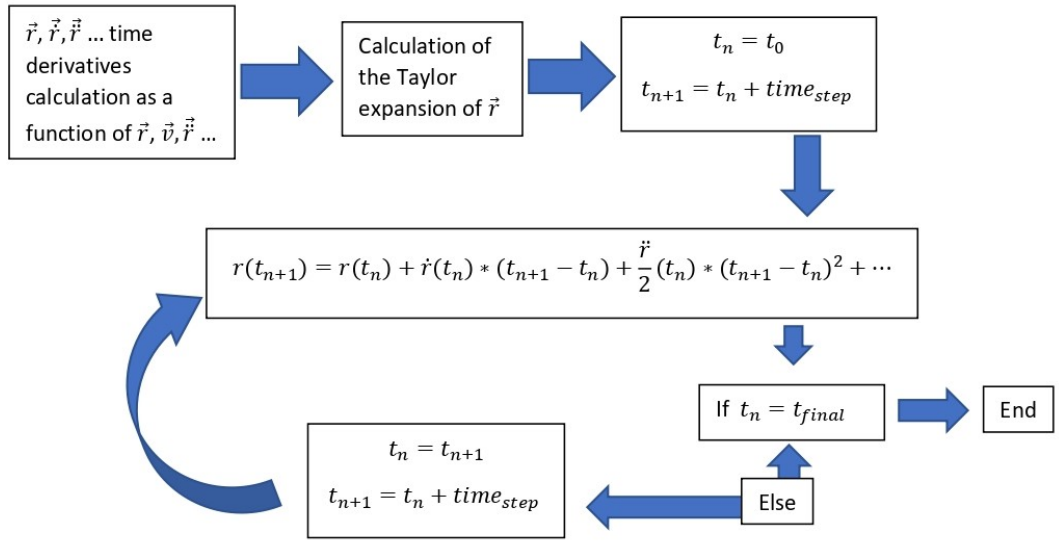

Figure 5.1 Flow diagram. Differential algebra.

In Figure 5.1, the calculation of a position's component was shown. However, to calculate other parameters, such as velocity, the same algorithm is followed.

According to [4] and [16] DA is analytically defined as follows:

1. First at all we initialize the initial conditions as a DA vector:

$$[x_0] = x_0 + \delta x_0 \tag{5.2}$$

2. Then, all operations of the integration scheme in DA should be performed:

$$x_1 = x_0 + f(x_0)h \tag{5.3}$$

Where x_0 will be replaced by $[x_0]$ in order to obtain the following expression:

$$[x_1] = [x_0] + f([x_0])h \tag{5.4}$$

And where $[x_1] = \tau_{x_0}(\delta x_0)$ is the Taylor expansion of the solution at t_1 from order k. Taylor's expansion's equation appears in (5.2.1). To calculate these expressions, several correlations are required:

- f(a)=$r_x(t_n)$
- f'(a)=$v_x(t_n)$
- f''(a)=$r_x(\ddot{t}_n)$, where the expression of $\ddot{r}_x$ has been written in Equation (2.5).

These correlations make the parameter r_x be defined as follows:

$$r_x(t_{n+1}) = r_x(t_n) + v_x(t_n)(t_{n+1} - t_n) + \frac{\ddot{r}_x(t_n)}{2!}(t_{n+1} - t_n)^2 + \ldots \tag{5.5}$$

As said before, the equations of the other parameters can be obtained following the same algorithm.

3. Finally, to determine $x(t)$, this process will be repeated for every step of the time's interval between t_0 and t_f. Figure 5.2 graphically shows the described algorithm.

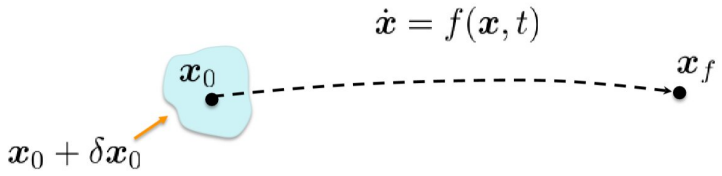

Figure 5.2 Dynamic evolution implemented in DA.

5.3 Results

In this section, results of three different test cases are presented. In all of them the initial orbital elements used for the calculation are presented in Table 5.1.

Table 5.1 Initial Keplerian elements.

a	e	i	ω	Ω	M
6878.14 km	0.01	20º	90º	45º	0º

Before showing the results, the Table 5.2 is presented, in order to compare the duration of different simulations using Monte Carlo and DA. As explained before, DA is more efficient than Monte Carlo technique. This table actually proves this idea.

Table 5.2 Integration time in terms of the interval and the integration step.

	1 week, step=10s	1 day, step=10s	1 day, step=1s
Motion equation using DA	1.455 s	0.8002 s	
J_2 using DA	4.405 s	1.728 s	4.94 s
Atmospheric drag using DA	4.42 s	2.065 s	5.364 s
Motion equation using ODE	8,2017 s	3,8005 s	
J_2 using ODE	7.219 s	3.58 s	5.7634 s
Atmospheric drag using ODE	6.745 s	3.455156 s	5.709 s

Finally, analogously to the previous chapter, uncertainty in initial position and in density are considered. However, for this method, uncertainty in initial velocity is studied as well.

5.3.1 Uncertainty in initial position

As explained in previous chapters, due to perturbation effect or measurement errors, it is common to deal with uncertainty in the initial position, and hence the consideration of this test case is logical.

Instead of displaying the orbital elements, whose behaviour is equal to the one that is displayed in Figure 4.3, the analysis introduced in paper [5] is followed. The main idea of this study is to define an initial interval

in the position's components, and thus a cube is defined. Propagating these position's intervals we notice how the initial cube changes. It shows us several conclusions that are explained later.

In this case, the initial intervals have been defined as follows:

$$r_x \in [r_x(t_0) - 0.25km, r_x(t_0) + 0.25km] \tag{5.6}$$
$$r_y \in [r_y(t_0) - 0.25km, r_y(t_0) + 0.25km] \tag{5.7}$$
$$r_z \in [r_z(t_0) - 0.25km, r_z(t_0) + 0.25km] \tag{5.8}$$
$$\tag{5.9}$$

Results are displayed in Figure 5.4. To obtain these results, Mathematica ©was required to calculate time derivatives, as well as MATLAB ©to implement them. However, the cubes have been obtained using a MATLAB code which has been subtracted from [7].

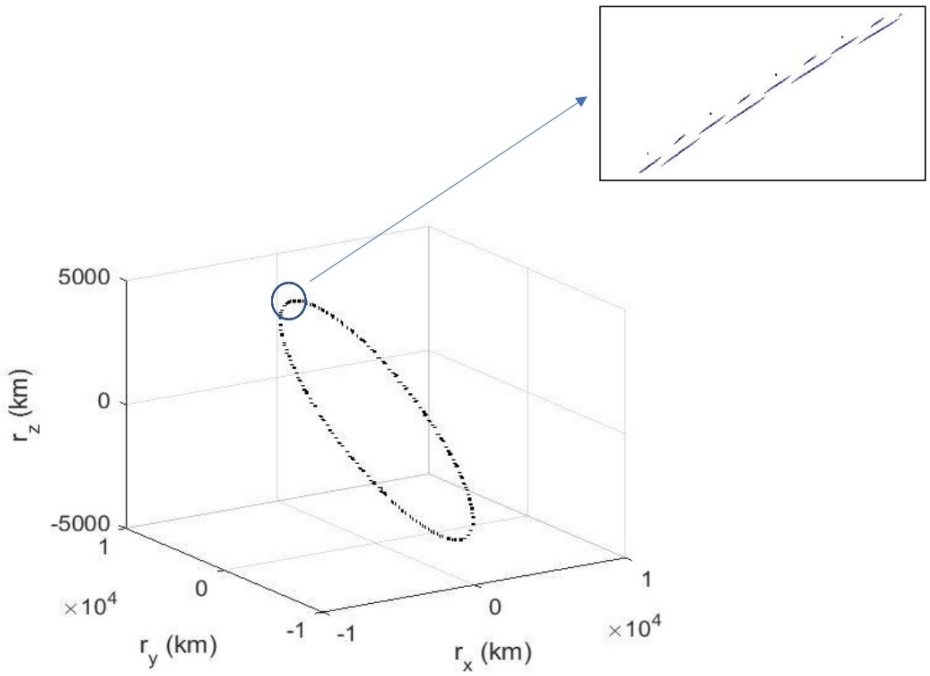

Figure 5.3 Results for DA position's propagation.

First at all, the position's cube propagation along the orbit has been shown in Figure 5.3. Cube's oscillations show the same tendency as the one that the covariance ellipsoid presented in the previous chapter.

The cube reaches its minimum size when it is in the maximum and minimum latitude point. On the other hand, it almost turns into a line when the satellite is in the ascending and descending nodes.

To enrich the conclusions and the analysis, Figure 5.4 is presented. A variety of ideas are developed:

1. Results are displayed in local axis. As showed in the previous chapter, z-axis stays almost constant, which means that kinetic moment stays almost constant as well. It is coherent with one assumption of Orbital Mechanics which states that in the two.bodies problem the kinetic moment is a constant parameter.

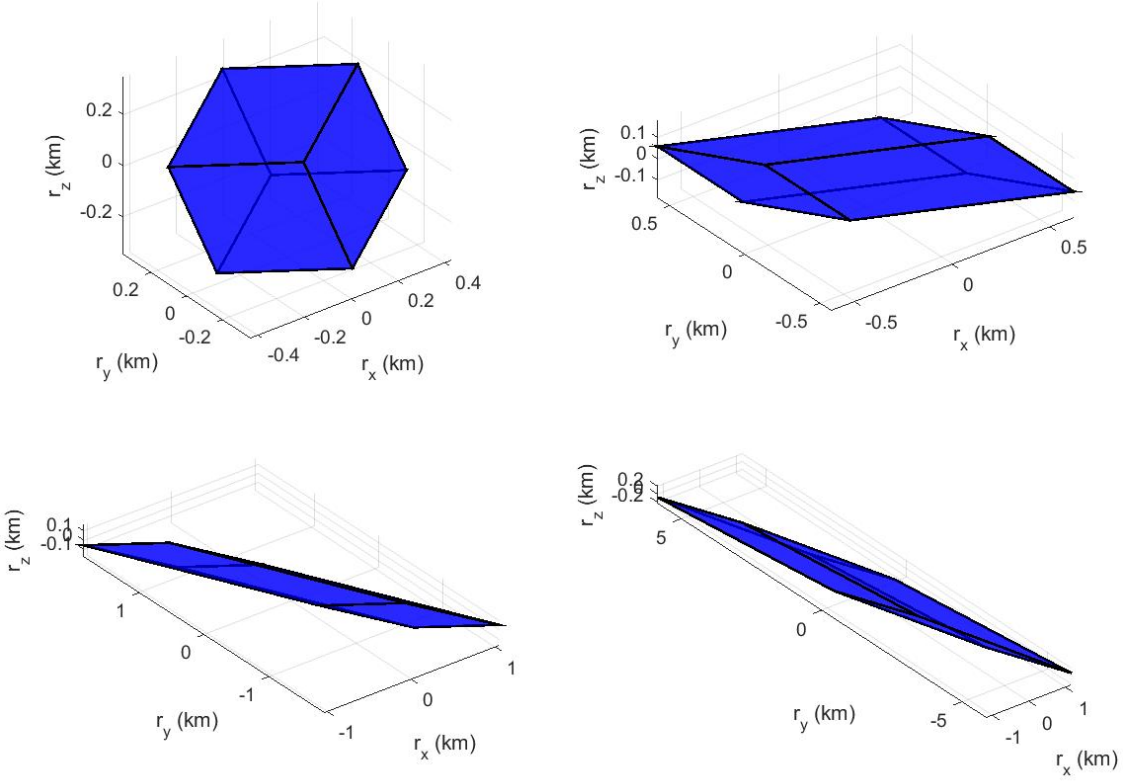

Figure 5.4 Position's cube after 3 minutes, 15 minutes, 30 minutes and 1 hour.

2. On the other hand, x-axis and y-axis increase their value, though OY does it faster than OX. It means that uncertainty propagation in position increases the uncertainty in position and velocity.
3. Simulations with both Monte-Carlo and DA were analysed. In this case, the cube took place inside the ellipsoid, although both displayed the same qualitative behaviour. As in Monte-Carlo the initial sample is generated by a normal distribution, results are more conservative. On the other hand, in DA it is necessary to define an interval and thus the sample is less conservative.

5.3.2 Uncertainty in density

As explained in chapter 3, there are several phenomena which are difficult to model. For instance, a realistic value of ρ at a certain moment is quite complicated to guess, as solar storms, natural phenomena or magnetic fields substantially perturb its value and hence, the analysis of the effect of uncertainty in ρ should be considered.

In this subsection, instead of displaying the covariance ellipsoid propagation, the standard deviation (σ) is calculated in local axis. It has been decided to show just two different test cases whose altitude's value are 200 km and 500 km.

As a result of that, Figure 5.5 shows σ in the three local axis when the initial altitude is h=200 km and whose density's model has been obtained from [27]. It was supposed that $\rho_0 = 5.464 \cdot 10^{-10} \frac{kg}{m^3}$ and $\sigma = 5.286 \cdot 10^{-13}$. The initial sample has been obtained using a normal distribution with a confidence region of 3σ. Altitude is h=200 km, as a higher one means that the atmospheric drag's effect decreases and the satellite's position is less perturbed.

As it is shown in Figure 5.5, the effect of unknown density in the position when we propagate in short-term period has strong consequences in OX and OY, as both present great oscillations whose order of magnitude is 1 and 100 respectively.

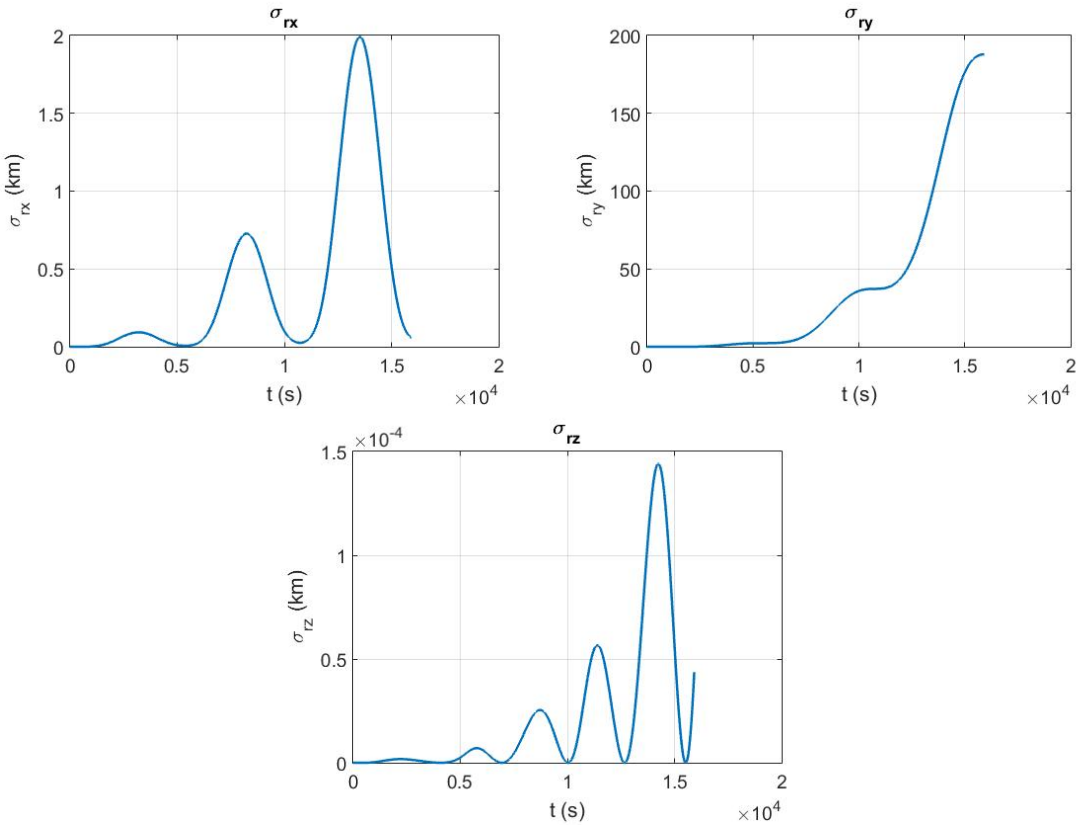

Figure 5.5 h=200 km. Typical deviation in local axes.

On the one hand, local OY is related to satellite's velocity (as eccentricity tends to zero). Figure 5.5 shows properly the incredible impact that ρ has in the satellite's velocity, as σ_{ry} varies from 0 km to 200 km.

On the other hand, local OZ axis has small changes that can be neglected if they are compared with the oscillations that can be found in OX and OY. As it was said, this result is coherent, as local OZ is referred to the kinetic moment and it is supposed to present small oscillations (almost zero). Such small variation are mainly caused by perturbations.

5.3.3 Uncertainty in initial velocity

Uncertainty in initial position and density has been studied.

Despite the fact that these analyses were focused on two relevant parameters according to the perturbations' chapter, there are thousands of parameters and distributions that can be considered as well. Although not all of them are taken into consideration, there are a few which can offer additional and relevant conclusions.

Due to this reason, the last test case is focused on studying uncertainty in initial velocity using DA method.

Results have been obtained supposing initial uncertainty in the velocity in the three inertial axis. To create this initial sample, a normal distribution has been carried out, considering an initial deviation of 0.01 km/s at every velocity's component. The confidence region's width was 3σ.

In Figure 5.6 the position's cube in four different moments of time in local axis is displayed.

Several remarks are presented:

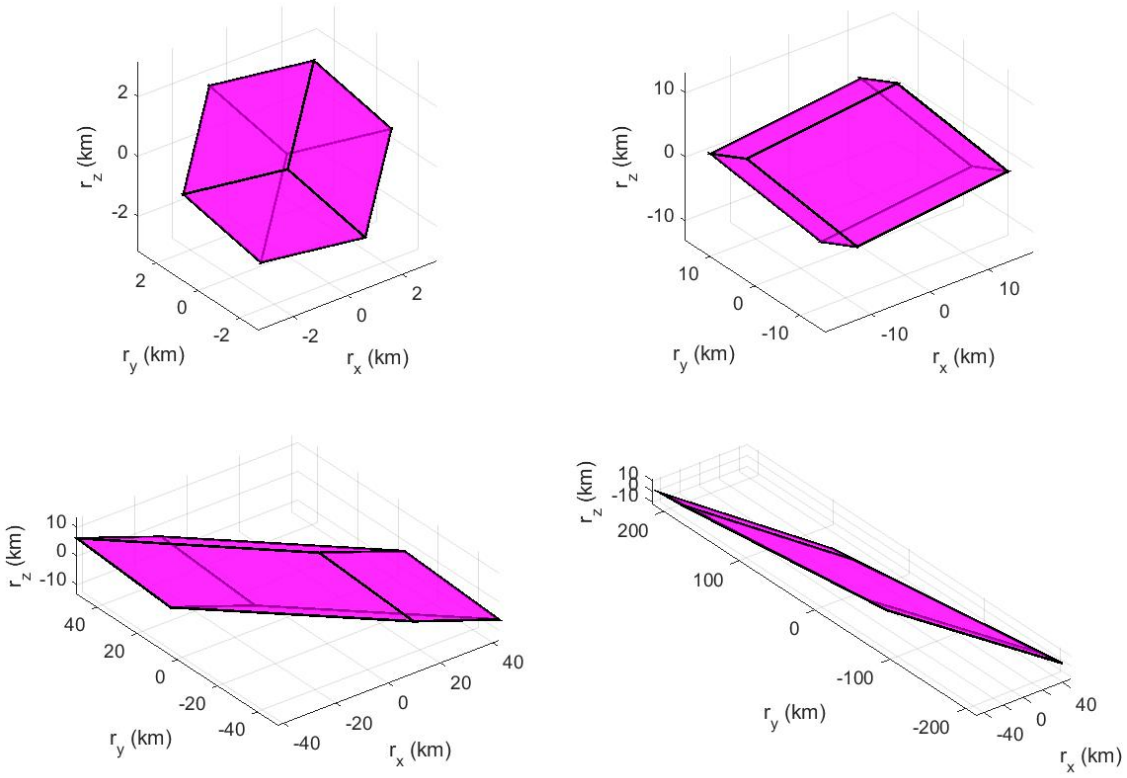

Figure 5.6 Position's ellipsoid after 3 minutes, 15 minutes, 30 minutes and 1 hour. Uncertainty in velocity.

Comparing the results from Figure 5.6 with Figure 5.4, there is a difference that can be easily noticed. In both Figure 5.4 and 5.6, the cube's size increased in OX and OY, while in the z-axis, variation were almost zero over time. However, considering initial uncertainty in velocity, the uncertainty in local axis OX and OY dramatically increase much more than in the case of uncertainty in initial position.

However, the qualitative behaviour of the uncertainty propagation is the same in both cases. It proves that, although the unknown parameter that is considered provokes quantitative oscillations in position, velocity and orbital elements, the qualitative tendency is a function of the equations and models that are considered. As equations are in both situations the same, qualitative behaviour does not change.

This test case has proved the importance of velocity in the knowledge of the object's position and thus this parameter should be realistically modelled and calculated with high precision.

6 Linearized covariance propagation

6.1 Method

According to [19], linearized covariance propagation is a method which approximates and propagated the covariance matrix. It is based on the local linearisation of $\vec{r}$ and $\vec{v}$ and its propagation along a reference trajectory. As equations have been linearized, this technique's efficiency is high, although it offers less realistic results as time increases.

Analogously to the other procedures, LinCov is used in a great variety of appliances, such as aeronautics, physics or orbital mechanics.

This method is sometimes used as a first approximation to study uncertainty propagation, because of its high efficiency, as the trajectory has to be calculated only once, whereas Monte-Carlo method has to repeat this process thousands of times. Once results have been obtained, the general idea about the parameter's behaviour is established. But then, to make a deeper study about uncertainty propagation, it is advisable to use other methods, as LinCov is not very realistic. Such fact has been presented in [4]. According to [13], to get enough accuracy, the integration step has to tend to zero ($\Lambda t \to 0$) . It makes the method more inefficient, which is not desired.

6.2 Mathematical development

Once the main idea of linearized covariance has been explained, the mathematical expressions that are the basis of this procedure are shown. They have been extracted from [26], where both discrete and continuous error propagation models were presented. In this project the continuous one has been developed.

$$\dot{P} = FP + PF^T + DQD^T \tag{6.1}$$

$$P(0) = P_0 \tag{6.2}$$

First at all, Equations (6.1) and (6.2) show the expressions used to propagate covariance. P is the covariance matrix, as well as F is the Jacobian matrix and the expression DQD^T is related to white noise, which is not considered.

The Jacobian matrix has the following expression, where $a_{\vec{perturb}}$ is the acceleration caused by perturbations and a_x, a_y, a_z are the components of the acceleration vector whose expression comes from Equation (3.1):

$$F = \begin{bmatrix} \frac{d\vec{v}}{d\vec{r}} & \frac{d\vec{v}}{d\vec{v}} \\ \frac{d\vec{a}}{d\vec{r}} & \frac{d\vec{a}}{d\vec{v}} \end{bmatrix} = \begin{bmatrix} 0_{3x3} & I \\ \frac{-\mu}{r^3} I_{3x3} + 3\frac{\mu}{r^5}\vec{r}\vec{r}^T + \frac{da_{\vec{perturb}}}{d\vec{r}} & \frac{da_{\vec{perturb}}}{d\vec{v}} \end{bmatrix} = \begin{bmatrix} 0 & 0 & 0 & 1 & 0 & 0 \\ 0 & 0 & 0 & 0 & 1 & 0 \\ 0 & 0 & 0 & 0 & 0 & 1 \\ \frac{\delta a_x}{\delta r_x} & \frac{\delta a_x}{\delta r_y} & \frac{\delta a_x}{\delta r_z} & \frac{\delta a_x}{\delta v_x} & \frac{\delta a_x}{\delta v_y} & \frac{\delta a_x}{\delta v_z} \\ \frac{\delta a_y}{\delta r_x} & \frac{\delta a_y}{\delta r_y} & \frac{\delta a_y}{\delta r_z} & \frac{\delta a_y}{\delta v_x} & \frac{\delta a_y}{\delta v_y} & \frac{\delta a_y}{\delta v_z} \\ \frac{\delta a_z}{\delta r_x} & \frac{\delta a_z}{\delta r_y} & \frac{\delta a_z}{\delta r_z} & \frac{\delta a_z}{\delta v_x} & \frac{\delta a_z}{\delta v_y} & \frac{\delta a_z}{\delta v_z} \end{bmatrix} \tag{6.3}$$

In order to determine and propagate the covariance matrix over time, it is necessary to calculate $\vec{r}$ and $\vec{v}$ at every step of the integration and hence it is required to add new equations to (6.1) and (6.2).

$$\begin{pmatrix} \frac{d\vec{r}}{dt} \\ \frac{d\vec{v}}{dt} \end{pmatrix} = \begin{pmatrix} \vec{v} \\ \frac{-\mu}{r^3}\vec{r} + a_{\vec{perturb}} \end{pmatrix} \tag{6.4}$$

$$\begin{pmatrix} \vec{r(0)} \\ \vec{v(0)} \end{pmatrix} = \begin{pmatrix} \vec{r}_0 \\ \vec{v}_0 \end{pmatrix} \tag{6.5}$$

Due to this reason, Equations (6.4) and (6.5) are presented. In these expressions, $a_{\vec{perturb}}$ is related to the accelerations induced by perturbations.

Joining of all these mathematical statements, a system with 42 differential equations in terms of partial derivatives is obtained.

As initial position is assumed to follow a normal distribution, instead of carrying out its parameter's value, it is required to deal with the mean value of this variable, and thus, the equations that are solved are presented next:

$$\frac{d\vec{m}_r}{dt} = \vec{m}_v \tag{6.6}$$

$$\frac{d\vec{m}_v}{dt} = \frac{-\mu}{m_r^3}\vec{m}_r + a_{\vec{perturb}} \tag{6.7}$$

$$\dot{P} = FP + PF^T \tag{6.8}$$

Whose initial conditions are: $(\vec{m_r(0)}, \vec{m_v(0)}, P(0)) = (\vec{m_{r_0}}, \vec{m_{v_0}}, P_0)$ and where "m" means "mean".

6.3 Results

Once the mathematical background has been defined, the results using this method are presented.

The initial orbital elements that have been considered are introduced in Table 6.1.

Table 6.1 Initial Keplerian elements.

a	e	i	ω	Ω	M
6878.14 km	0.01	20º	90º	45º	0º

Three test cases are explained: uncertainty in initial position, in density and in initial velocity.

6.3.1 Uncertainty in initial position

As explained before, due to perturbations effect or measurement error, it is logical to study uncertainty in initial position.

Results have been obtained creating an initial sample using uncertainty in the three inertial axis and supposing an initial σ_x, σ_y and σ_z equal to 0.5 km, while the mean is the calculated initial position with the orbital elements from Table 6.1.

First at all, Figure 6.1 is displayed. It shows how the covariance matrix gets propagated along the orbit.

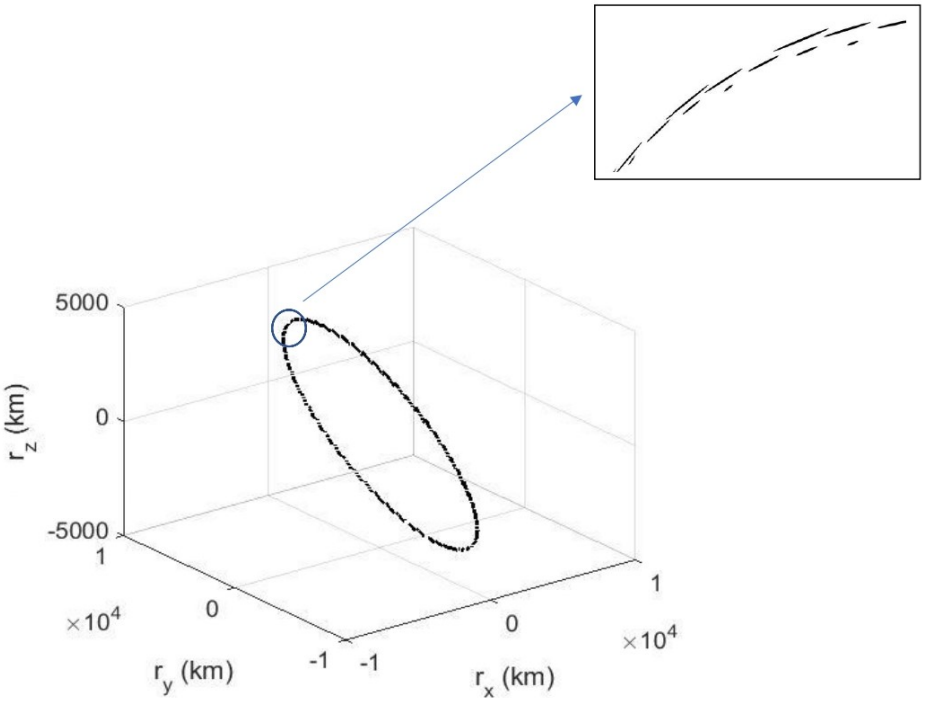

Figure 6.1 Results for Monte-Carlo covariance matrix propagation.

Although the mathematical and theoretical basis of this technique is different from the previous and next procedures, results are coherent in all of them. As it is shown in Figure 6.1, in the ascending and descending nodes, the ellipsoid turns into a line, while in the maximum and minimum latitude point it becomes almost a sphere. However, as time increases, the ellipsoid's size warps and stretches. These conclusions are similar to the ones obtained from Figures 4.4 and 5.3.

The propagation of the ellipsoid in local axis is shown in Figure 6.2.

As it is presented in Figure 6.2, the behaviour of the body is coherent with previous ideas: At the initial time, it begins as a sphere. However, as time increases, the geometric form turns into a line. In z-axis, the body decreases and then stays constant. It is expected, as the kinetic moment stays almost constant. On the other hand, the covariance ellipsoid increases in x-axis and y-axis, though it makes faster this size's change in OY than in OX. It claims the importance that uncertainty propagation in initial position has in the object's altitude and specially in the satellite's velocity.

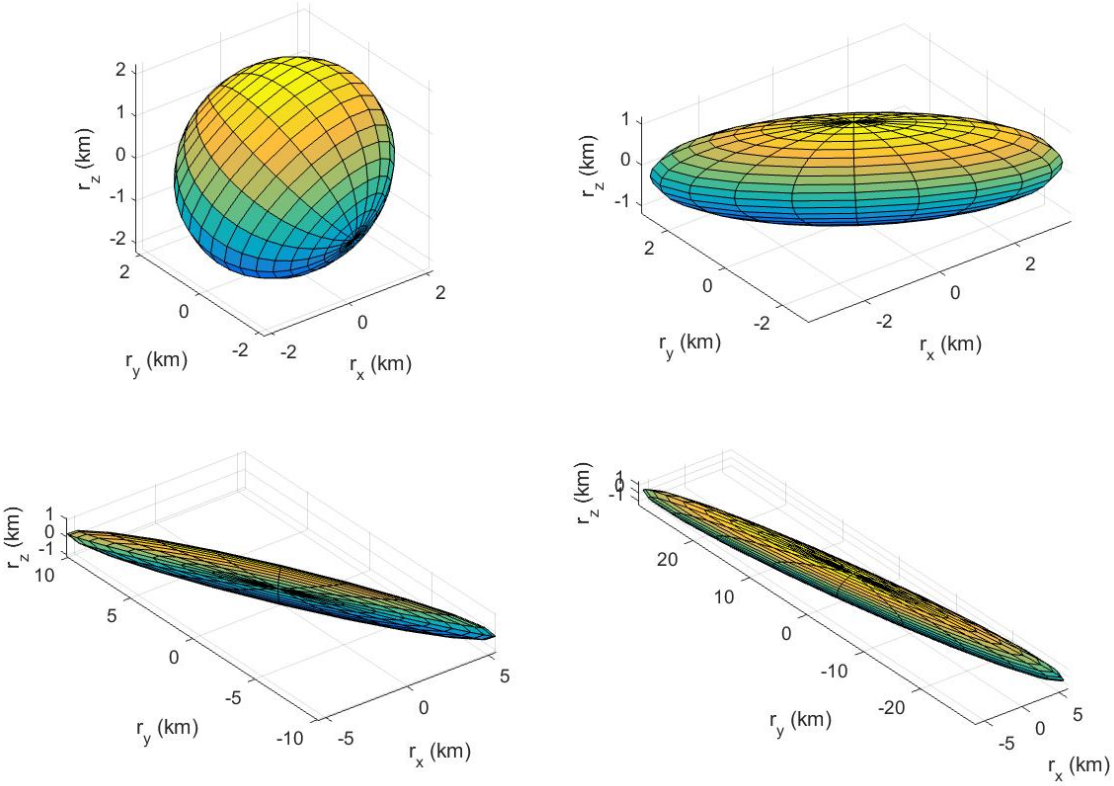

Figure 6.2 Position's ellipsoid after 3 minutes, 15 minutes, 30 minutes and 1 hour. LinCov. Unknown initial position.

6.3.2 Uncertainty in density

In previous chapters the importance and effect of uncertainty in ρ was discussed. It was proved that its effect is more relevant the closer the satellite is to the Earth.

In this test case, the standard deviation of the position in local axis is calculated and displayed. The altitude is h=500 km. Although it has been demonstrated that at this height the atmospheric drag's relevance can be neglected, a long-term simulation has been carried out. It allows us to determine the importance of such parameter when the propagation lasts more than one week.

In Figure 6.3 results are displayed. The density model that was chosen was obtained from [27]. For h=500 km, $\rho = 1.585 \cdot 10^{-12} \frac{kg}{m^3}$ and the standard deviation that was elected was $5.286 \cdot 10^{-16}$. A normal distribution was used to generate the initial sample. The confidence interval is 3σ.

Two main conclusions are obtained:

Firstly, the behaviour of σ in the three local axis is coherent with results from Figure 4.7. In both cases, because of the satellite's altitude (500 km), atmospheric drag's effect is small and for long-term simulations, it can be neglected.

But **secondly**, this uncertainty propagation over time brings a new idea. As it can be seen in Figure 6.3, the simulation's duration is 1 week, while in Figures 4.7, the duration was just 4 hours. Taking this fact into consideration, one can notice that, the more the time increases, the bigger effect that this uncertainty in ρ on position, velocity and kinetic moment has. This increase follows and exponential tendency. Due to this reason, although an unknown ρ has not great effects in most LEOs (which take place in an altitude h>300

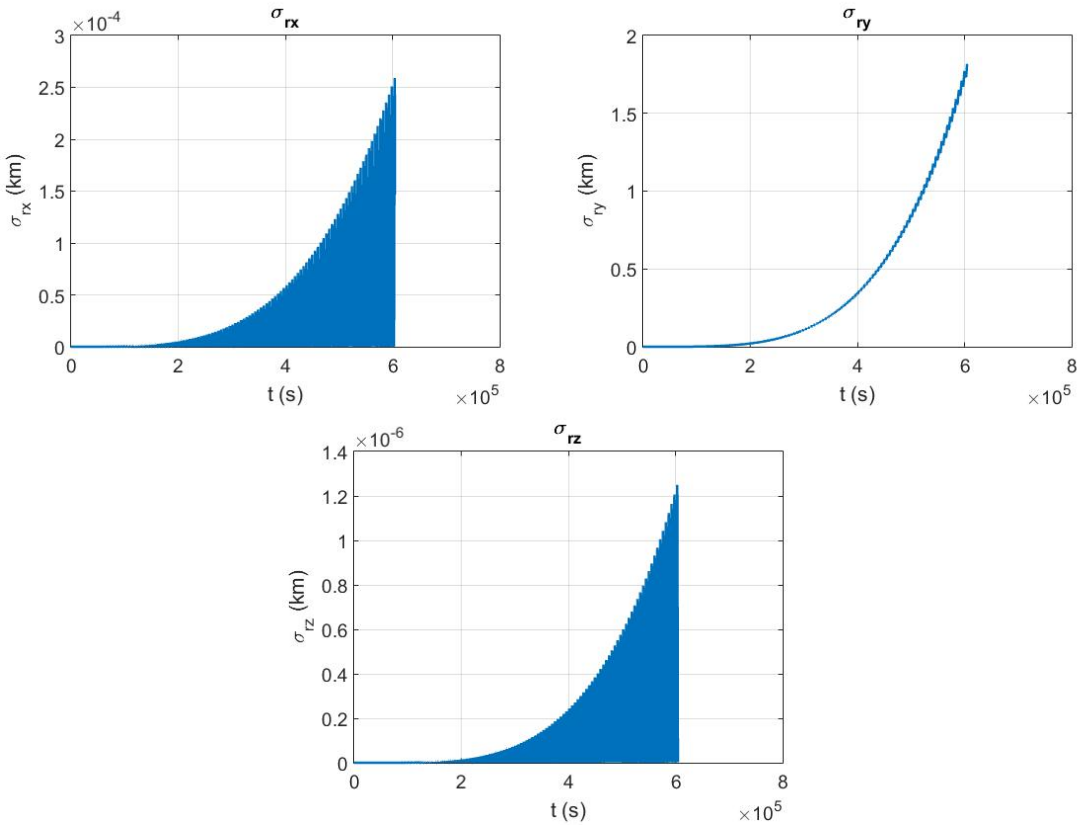

Figure 6.3 h=500 km. Typical deviation in local axes.

km) when we propagate in short-term periods, its relevance for long-term periods of time has been proved.

6.3.3 Uncertainty in initial velocity

In the previous chapter, the importance of uncertainty in the initial velocity was proved and thus the same test case is developed in this one.

The position's covariance matrix propagation is displayed in Figures 6.4. They coincide with the ones obtained in Figure 5.6. Instead of generating the initial sample using an interval, as it has been carried out in the previous chapter, the normal distribution has been considered in this one. The mean was the initial velocity calculated with the orbital elements from Table 6.1, whereas σ was supposed to be 0.01 km/s and the confidence region equal to 3σ. One hypothesis has been made. As the initial velocity follows a normal distribution, it has been supposed that position follows such distribution as well and thus, its covariance matrix is propagated and displayed.

The importance of an unknown initial velocity is noticed again, as the ellipsoid dramatically increases its size in the local axis OX and OY. Its strong influence requires that this parameter should be accurately calculated.

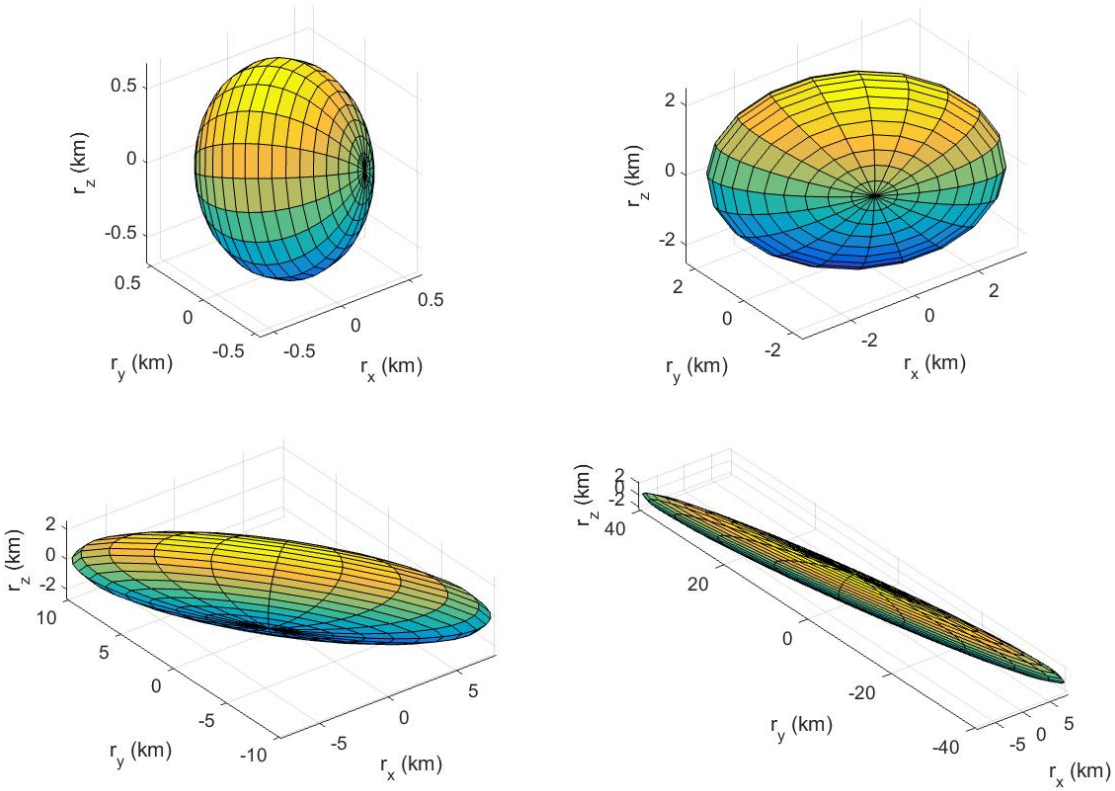

Figure 6.4 Position's ellipsoid after 3 minutes, 15 minutes, 30 minutes and 1 hour.

7 Probability Transformation Method: PTM

7.1 Method

The aim of this project is to explore and compare several uncertainty propagation methods. In previous chapter three techniques have been presented: Monte Carlo method, which is accurate, though very computationally intensive, DA and the linearized covariance, which are more efficient, though less realistic.

In search of more realistic result, whereas efficiency is higher than MC, the probability transformation method (PTM) is introduced. This probabilistic technique is based on the direct work on distribution functions and random parameters. Different mathematical and statistical transformations will be developed in order to obtain the final probability distribution function (PDF). Furthermore, once the final PDF has been calculated, this function allows us to determine the mean and the deviation.

Analogously to other methods, PTM applies in several areas of science, for instance: aeronautics, physics or even medicine.

Finally, several ideas about this method are summarized:

1. PTM offers realistic results and it is strongly computationally efficient. The two biggest benefits of this technique.
2. As it is presented later, PTM deals with equations that can be difficult to implement, as several singularities can appear, specially in the multivariate case.
3. The main goal of this technique is the calculation of the final PDF, which is a function that any of the previous procedures calculated.

7.2 Mathematical development

Once a general idea about the method has been explained, the mathematical development is presented. Two test cases are implemented: univariate and multivariate.

Equations that are used to develop this method have been subtracted from [3] and [11].

7.2.1 Univariate Analysis

For a random variable x, whose real value is unknown, though its distribution function actually is, the distribution function of other variable y can be calculated. This variable y should be a function of the previous

parameter x. The required transformation to carry out this development is described in the following Equation.

$$f_y(y) = \frac{f_x(F^{-1}(y))}{|F'(F^{-1}(y))|} \tag{7.1}$$

Different test cases are considered:

- First at all, uncertainty in initial position is taken into consideration. In this case, instead of supposing an initial uncertainty in the three inertial axis, such initial deviation is only supposed in the x-axis of the inertial reference frame.

  The initial condition in position $r_x(t_0)$ is defined using an uniform distribution. Because of that, $r_x(t_0) = r_I(t_0) \cdot U$, where U can be any value in the interval [0.99,1.01] and $r_I(t_0)$ is the initial position in the x-axis calculated using the initial orbital elements. On the other hand, $f_{r_x(t_0)}$ is the PDF of an uniform distribution.

  In this case, Equation (7.1) turns into:

$$f(r_\square(t_f)) = \frac{f_{r_x(t_0)}(g^{-1}(r_\square(t_f)))}{|g'(g^{-1}(r_\square(t_f)))|} \tag{7.2}$$

  Moreover, as $r^i_\square = g(r_x(t_0))$ and $g^{-1}(r^i_\square) = r_x(t_0)$, Equation (7.2) is written as:

$$f(r_\square(t_f)) = \frac{f_{r_x(t_0)}(r_x(t_0))}{|g'(r_x(t_0))|} \tag{7.3}$$

  It should be noticed that $r_\square$ can be r_x, r_y or r_z.

  In order to obtain the final PDF, it is necessary to raise a system of equations that properly define the considered case. Such equations are :

$$f_{r_x(t_0)} = \left\{ \begin{array}{c} \dot{\vec{r}} = \vec{v} \\ \dot{\vec{v}} = -\mu \frac{\vec{r}}{r^3} + \vec{f_{perturb}} \\ \dot{\vec{\xi}} = \frac{\delta f}{\delta \vec{x}}(\vec{r}, r_x(t_0)) \frac{\delta \vec{x}}{\delta r_x(t_0)} + \frac{\delta f}{\delta r_x(t_0)}(\vec{r}, r_x(t_0)) \end{array} \right\} \tag{7.4}$$

  Where $\frac{\delta f}{\delta \vec{x}}$ is the Jacobian matrix, whose expression has been developed in (6.3). And where $\vec{x}$ and $\vec{\xi}$ are presented next:

$$\vec{x} = \left\{ \begin{array}{c} r_x \\ r_y \\ r_z \\ v_x \\ v_y \\ v_z \end{array} \right\}; \xi = \left\{ \begin{array}{l} \xi_{rx} = \frac{\delta r_x}{\delta r_x(t_0)} \\ \xi_{ry} = \frac{\delta r_y}{\delta r_x(t_0)} \\ \xi_{rz} = \frac{\delta r_z}{\delta r_x(t_0)} \\ \xi_{vx} = \frac{\delta v_x}{\delta r_x(t_0)} \\ \xi_{vy} = \frac{\delta v_y}{\delta r_x(t_0)} \\ \xi_{vz} = \frac{\delta v_z}{\delta r_x(t_0)} \end{array} \right\} \tag{7.5}$$

  The equations presented in (7.4) are written in terms of time derivatives, and thus it is required to define the initial conditions. They are: $x(\vec{t_0}) = [r_x(t_0), r_y(t_0), r_z(t_0), v_x(t_0), v_y(t_0), v_z(t_0)]$ and $\xi(\vec{t_0}) =$

[1,0,0,0,0,0].

Once all the equations have been defined, as well as the initial conditions, they are solved using MATLAB©. Once $\vec{\xi}$ has been calculated, the final distribution function is obtained. As explained before, instead of using $\square$, one of the axis should be implemented (x,y or z). It allows us to determine the final distribution function in each of them, although the initial uncertainty was only considered in OX.

- Secondly, the case of uncertainty in density is considered as well. In this test case, the mathematical developments are similar to the ones that have been presented for uncertainty in initial r_x.

  ρ is defined as: $\rho = \Delta\rho \cdot \rho_0$ where ρ_0 has been obtained from [27]. In this case, $\Delta\rho$ follows an uniform distribution. This parameter takes values inside the interval [0.75, 1.25].

$$f(r_\square(t_f)) = \frac{f_{\Delta\rho}(g^{-1}(r_\square(t_f)))}{|g'(g^{-1}(r_\square(t_f)))|} \tag{7.6}$$

$$f(r_\square(t_f)) = \frac{f_{\Delta\rho}(\Delta\rho)}{|g'(\Delta\rho)|} \tag{7.7}$$

Equation (7.4) does not vary, although the expression of ξ changes. Due to this reason, the new equations that are integrated are introduced next:

$$f_{r_x(t_0)} = \left\{ \begin{array}{c} \dot{\vec{r}} = \vec{v} \\ \dot{\vec{v}} = -\mu \frac{\vec{r}}{r^3} + \vec{f_{perturb}} \\ \dot{\vec{\xi}} = \frac{\delta f}{\delta \vec{x}}(\vec{r},\Delta\rho)\frac{\delta \vec{x}}{\delta \Delta\rho} + \frac{\delta f}{\delta \Delta\rho}(\vec{r},\Delta\rho) \end{array} \right\} \tag{7.8}$$

Where $\xi = \frac{\delta \vec{x}}{\delta \Delta\rho}$. Solving Equations (7.8), the final PDF is calculated.

7.2.2 Multivariate Analysis

The multivariate case has been developed following the steps that are explained in [24].

In this case, there are two random variables that are initially known: u_1 and u_2, with a known joint density function $f_{u_1,u_2}(u_1,u_2)$. On the other hand, there are two random variables: v_1 and v_2, which are defined as:

$$v_1 = g_1(u_1,u_2) \tag{7.9}$$
$$v_2 = g_2(u_1,u_2) \tag{7.10}$$

The aim of the multivariate analysis is to calculate $f_{v_1,v_2}(v_1,v_2)$, which is the PDF of v_1 and v_2. Functions g_1 and g_2 are the transformation functions from the u_1u_2 plane into the v_1v_2 one.

$$f_{v_1,v_2}(v_1,v_2) = f_{u_1,u_2}(u_1,u_2) \cdot |J(v_1,v_2)| \tag{7.11}$$

In order to calculate $f_{v_1,v_2}(v_1,v_2)$, Equation (7.11) has been presented.

Where $|J(v_1,v_2)|$ is the determinant of the Jacobian matrix of the transformation and is calculated as follows:

$$J = \begin{bmatrix} \frac{\delta u_1}{\delta v_1} & \frac{\delta u_1}{\delta v_2} \\ \frac{\delta u_2}{\delta v_1} & \frac{\delta u_2}{\delta v_2} \end{bmatrix}$$

In order to simplify the calculations, it is advisable to calculate the marginal density function, using one random variable as an auxiliary one. For instance, if v_1 were the auxiliary variable, then $v_1 = v_2$. In this situation |J| is calculated as follows:

$$J = \begin{bmatrix} 1 & 0 \\ \frac{\delta u_2}{\delta v_1} & \frac{\delta u_2}{\delta v_2} \end{bmatrix}$$

And the PDF is:

$$f_{v_2}(v_2) = \int_{-\infty}^{\infty} f_{v_1,v_2}(v_1,v_2)dv_1 \tag{7.12}$$

Where $f_{v_1,v_2}(v_1,v_2)$ are obtained from Equation (7.11).

$$f_{v_2}(v_2) = \int_{u_1} f_{u_1,u_2}(u_1,u_2) \cdot |J| du_1 \tag{7.13}$$

The final expression of the marginal PDF is developed in (7.13).

The limits of the integral get defined by the transformation from the u_1u_2 plane into the v_1v_2 one.

In this project, for the sake of simplification it has been assumed that $u_1 = v_1 = r_x$ and $u_2 = v_2 = r_y$. This assumption makes the determinant of the Jacobian matrix equal to 1. Analogously to the previous development, the marginal PDF is calculated using (7.13). Their expressions appear next:

$$f_{r_y}(r_y) = \int_{r_x} f_{r_x,r_y}(r_x,r_y) \cdot dr_x \tag{7.14}$$

$$f_{r_x}(r_x) = \int_{r_y} f_{r_x,r_y}(r_x,r_y) \cdot dr_y \tag{7.15}$$

Finally, it should be mentioned that r_x and r_y have been chosen as random variables as it can enormously simplify the developments and implementations. However, other combinations are possible, for instance, $u_1 = r_x$, $u_2 = r_y$ and $v_1 = r_y$ and $v_2 = r_z$.

In spite of this idea, there are possible combinations in this method that converge into the same solution, which can perturb the final PDF introducing singularities. Due to this reason, the parameters combinations should be analysed previously in order not to find these singularities. In this case, the chosen random variables do not present this behaviour.

7.3 Results

In this chapter, instead of analysing different parameters, it was chosen to study uncertainty in position and density, though different statistical distributions were considered to generate the initial sample.

In Table 7.1, the initial orbital elements used for the simulations are displayed.

Table 7.1 Initial Keplerian elements.

a	e	i	ω	Ω	M
6878.14 km	0.01	40º	90º	45º	0º

As Gamma distribution has not been previously introduced, the main ideas about this PDF are presented next.

$$f(x) = \frac{a^p}{\Gamma(p)} e^{-ax} x^{p-1} \rightarrow x > 0 \tag{7.16}$$

Gamma distribution is defined by its distribution function, which is written in Equation (7.16) and two parameters: a (shape parameter) and p (scale parameter).

And where $\Gamma(p)$'s expression is:

$$\Gamma(p) = \int_0^\infty e^{-x} x^{p-1} \rightarrow x > 0 \tag{7.17}$$

When p=1, this distribution is also called as exponential distribution . For a=p=1, which is the considered case in the project, the distribution function is displayed in Figure 7.1.

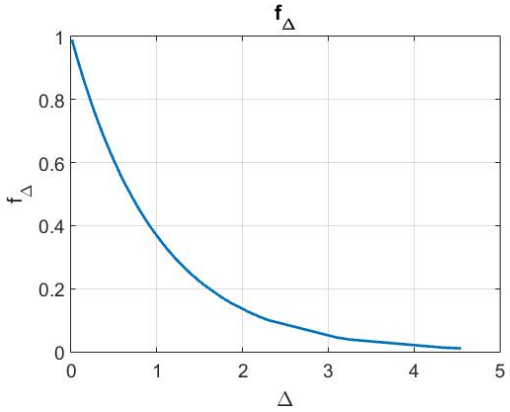

Figure 7.1 Gamma distribution function.

Finally, the reason why this distribution has been chosen is mentioned. First at all, Gamma distribution models quite well stochastic processes, as several references have shown. Furthermore, its function is similar to the one that is obtained when the uncertainty in initial position's case is analysed. To sum up, considering a statistical distribution different from the uniform and normal ones, can show additional conclusions about PTM's technique.

7.3.1 Uncertainty in initial position

As explained before, the consideration of uncertainty in initial position is completely logical because of the effect of perturbations. Moreover, measurement errors are also common and can disturb the expected location of the satellite.

Two test cases are studied. In the first one, $r_x(t_0)$ follows an uniform distribution, whereas in the second one a gamma distribution is considered.

Uniform distribution

The final PDF of the three components of the position's vector is shown in Figures 7.3. Results are displayed after $t = 2{,}5 \cdot N_{SAT} = 4$ hours.

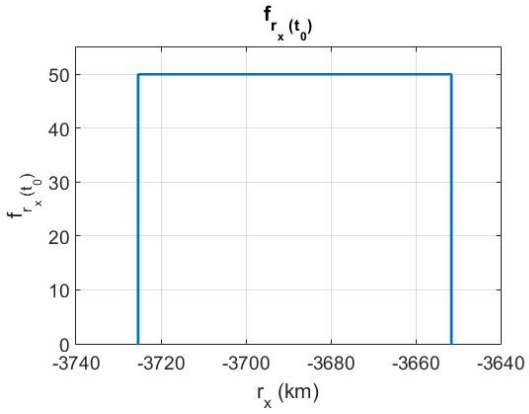

Figure 7.2 Initial PDF. Uncertainty in position. Uniform distribution.

The initial uniform distribution, which is displayed in Figure 7.2, was centred in the initial value of r_x, which was calculated using the orbital elements that appear in Table 7.1. In this test case it was initially supposed that mean=$r_x(t_0)$ and $\sigma = 1km$.

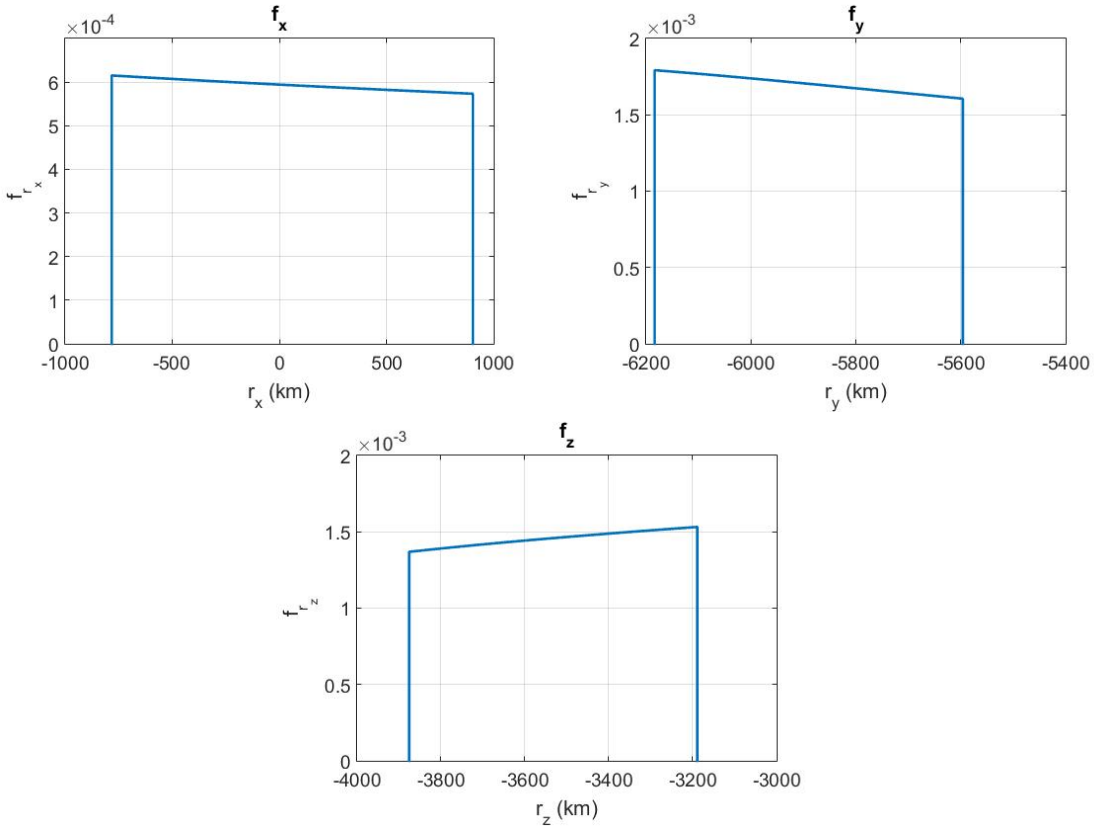

Figure 7.3 Final distribution functions in the position's components.

Once the final PDF has been calculated, it is possible to compute the expected value and its standard deviation in t_f. Such values are presented in Table 7.2.

Table 7.2 Expected values in position and typical deviation. Uniform distribution in position.

E_x	E_y	E_z	σ_x	σ_y	σ_z
3232.7 km	-4251.9 km	-4426.4 km	784.6546 km	197.4031 km	158.4076 km

The main conclusion that can be obtained from Figure 7.3 and Table 7.2 is the relevance that uncertainty in initial position has in the propagation of the position along the orbit. This conclusion is expected as it has been previously shown in the other chapters.

Gamma distribution

In the previous test case, the shape of the final PDF is similar to the density function of an exponential distribution, and thus $r_x(t_0)$ is assumed to follow such PDF in this test case. Initial parameters a=p=1 are considered, as well as a sample of 100 points. Simulation lasts 4 hours as well.

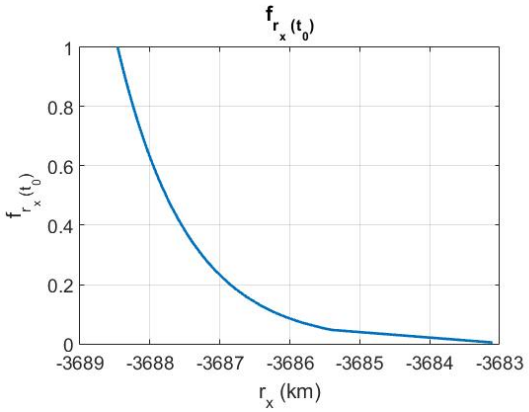

Figure 7.4 Initial PDF. Uncertainty in position. Gamma distribution.

The initial PDF is displayed in Figure 7.4. It allows us to compare graphically the distribution function's changes over time.

Results of final PDFs are displayed in Figure 7.5 and the expected value and σ are shown in Table 7.3.

Table 7.3 Expected values in position and typical deviation. Gamma distribution in position.

E_x	E_y	E_z	σ_x	σ_y	σ_z
3261.0 km	-4227.1 km	-4443.2 km	22.0716 km	21.5105 km	1.0100 km

As expected, gamma distribution (in this case, as a=p=1, it is an exponential distribution as well), models much better the uncertainty in initial r_x than it does the uniform one.

On the other hand, the expected values of r_x, r_y and r_z are quite similar when comparing Tables 7.2 and 7.3. Moreover, the coherence of results is proved because of the concurrence of such results. In chapter 9 it is shown that these values coincide with the ones obtained from other methods as well.

7.3.2 Uncertainty in density

Analogously to previous chapters, the propagation of uncertainty in ρ and its effect on the orbit are considered. As explained before, because of solar phenomena or atmospheric perturbations, density's value can change considerably.

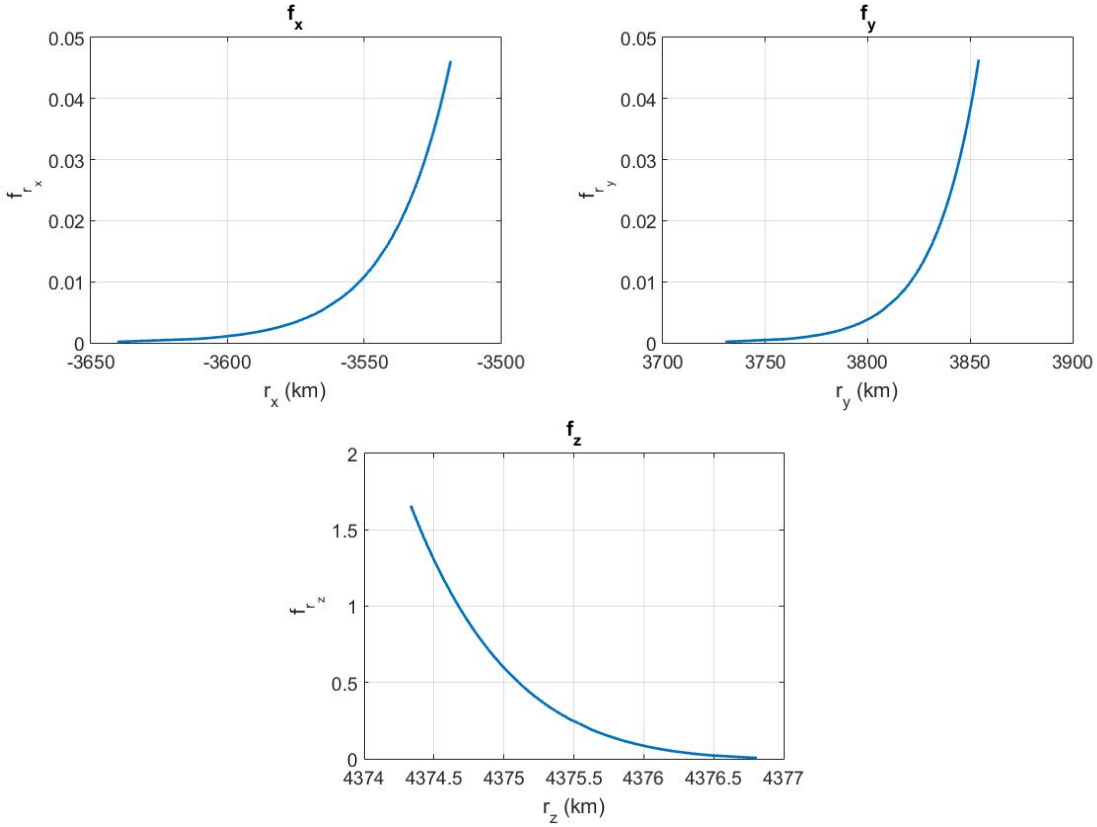

Figure 7.5 Final PDFs in the position's components.

Two cases are studied again: uniform and gamma distribution to model in $t = t_0$ this parameter.

Uniform distribution

In this case, ρ has been generated by using an uniform distribution whose mean is the value that is obtained from [27], and the initial σ is 0.25.

Simulation lasts 4 hours and the initial orbital elements are the ones that are shown in Table 7.1. As h_0=500 km, it is expected that ρ does not substantially perturb the orbit.

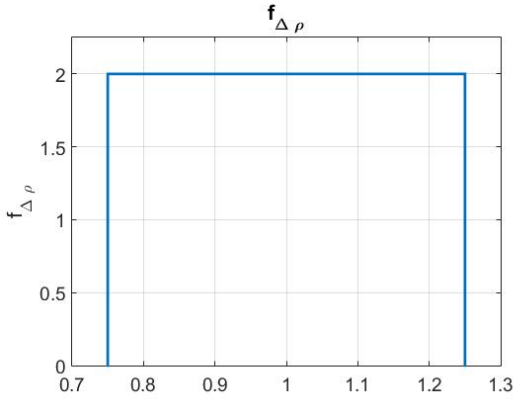

Figure 7.6 Initial PDF. Uncertainty in density. Uniform distribution.

The initial PDF is shown in Figure 7.6. Final PDF appears in Figures 7.7, whereas the expected value of the position's components are presented in Table 7.4.

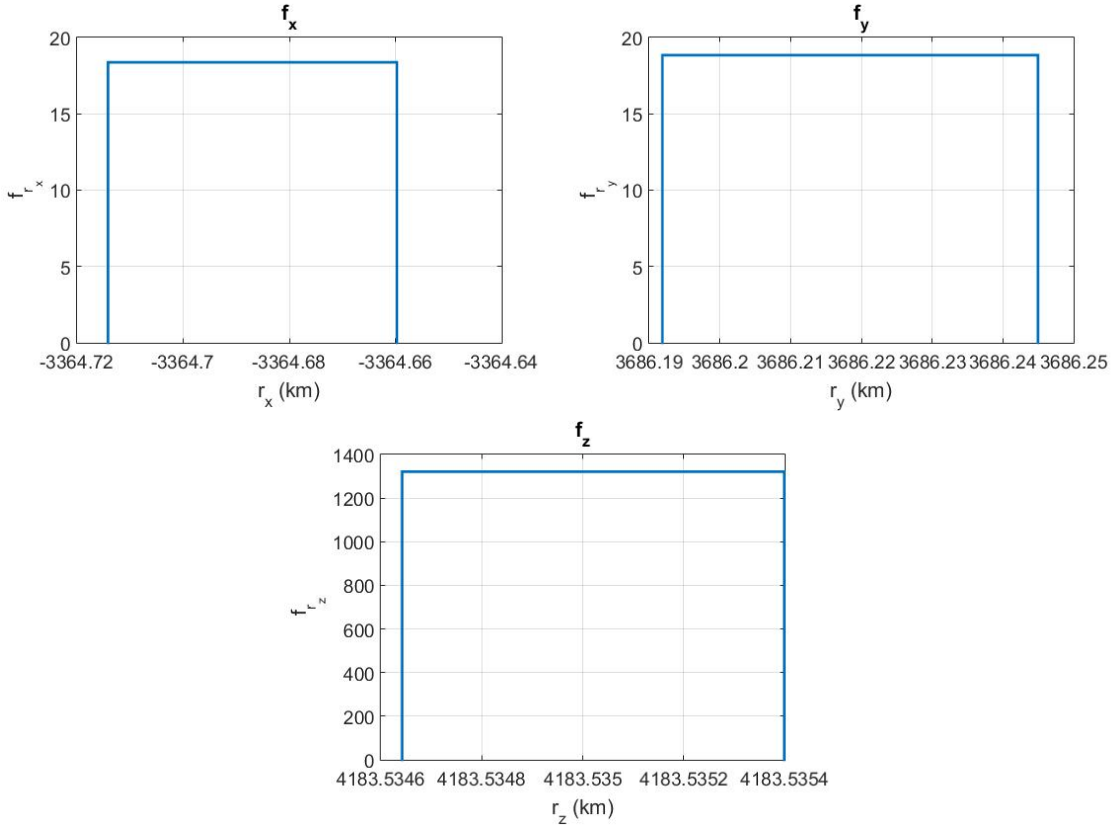

Figure 7.7 Final distribution functions in the position's components.

Comparing results from Table 7.4, with Tables 7.2 and 7.3, it is noticeable that density has only a small effect in position when propagating short-term periods of time. It is proved by the small values of σ and the expected values of r_x, r_y and r_z showed in Table 7.4, which are quite different from the ones displayed in Tables 7.2 and 7.3. The small values of the standard deviation agree with the conclusions that have been pointed in the previous chapters, which state that the atmospheric drag's effect for an initial altitude of 500 km can be neglected because of its order of magnitude.

Table 7.4 Expected values in position and typical deviation. Uniform distribution in density.

E_x	E_y	E_z	σ_x	σ_y	σ_z
3576.4 km	-3621.2 km	-4270.6 km	0.0098 km	0.0122 km	0.0014 km

Gamma distribution

Finally, gamma distribution is used to model the density. Parameters a and p will be again equal to 1, so that this distribution is actually the exponential one.

The initial PDF is displayed in Figure 7.8. Moreover, similar results to the previous test case are obtained. Figure 7.9 and Table 7.5 show these results for a 4 hours time simulation, whose initial orbital elements are the ones in Table 7.1.

The conclusions that can be obtained analysing the results are explained next.

In this situation σ is different from the one obtained before. Furthermore, the expected values of the position's components are quite different as well.

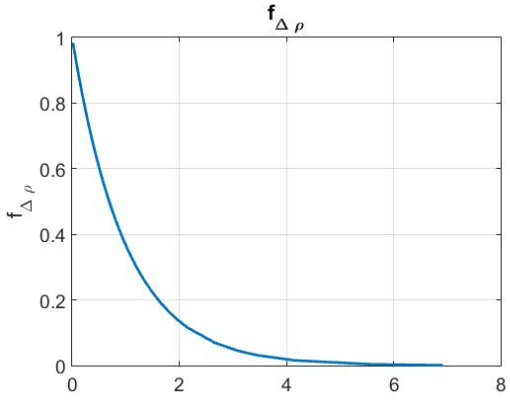

Figure 7.8 Initial PDF. Uncertainty in density. Gamma distribution.

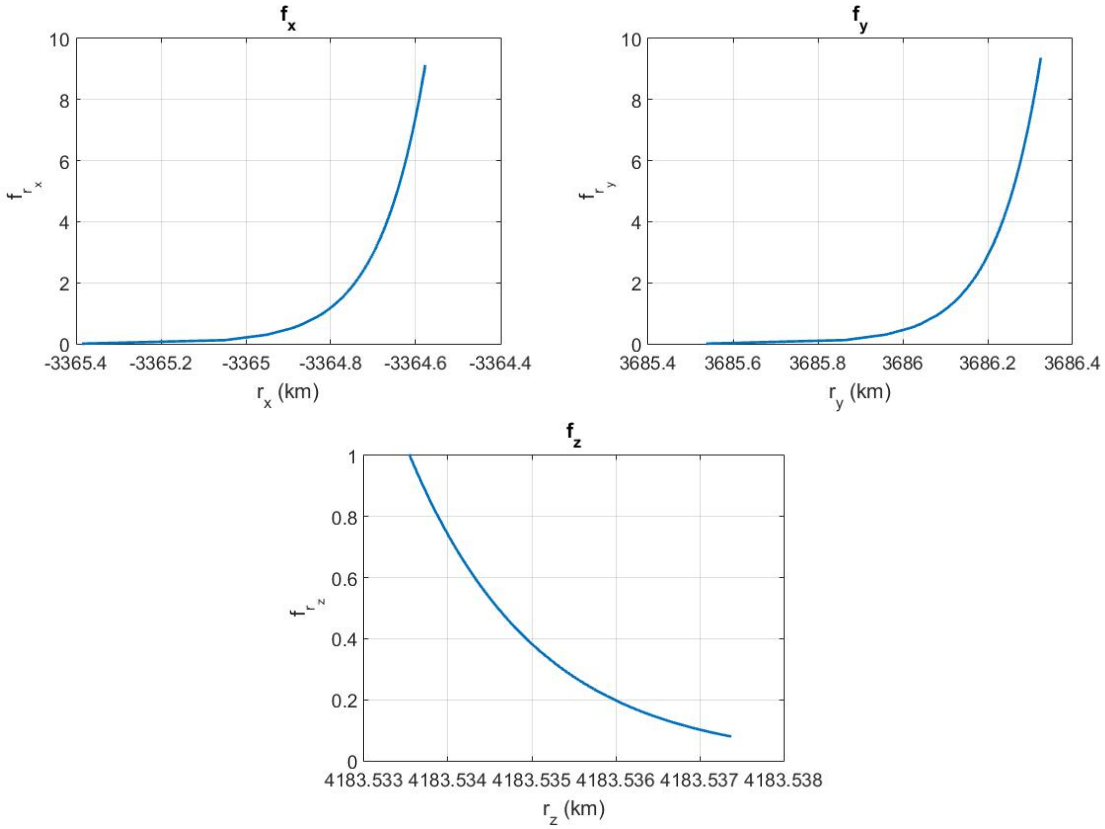

Figure 7.9 Final distribution functions in the position's components.

Table 7.5 Expected values in position and typical deviation. Uniform distribution in density.

E_x	E_y	E_z	σ_x	σ_y	σ_z
3182 km	-3988.8 km	-4254.7 km	0.1140 km	0.1253 km	0.0068 km

It is remarkable that, in spite of the fact that in both test cases the standard deviation values differ, in both situations the order of magnitude of this parameter is small. It shows one more time that the effect of the atmospheric drag in position when the initial altitude is 500 km can be neglected.

7.3.3 Multivariate case

As said before, in order to complete the analysis that is being developed in the project, the multivariate case should be considered as well.

However, the probability transformation method can converge into singularities for different combinations of parameters, Moreover, as it can be noticed from the mathematical development, a few combinations of parameters can complicate the implementation, as the marginal PDF turns complicated to calculate .

Due to these reasons, both initial and final variables are r_x and r_y. It simplifies the calculation of determinant of the jacobian matrix.

Initial and final PDFs, as well as the marginal PDF of each parameter are shown in Figure 8.3. Several conclusions about these plots are presented as well.

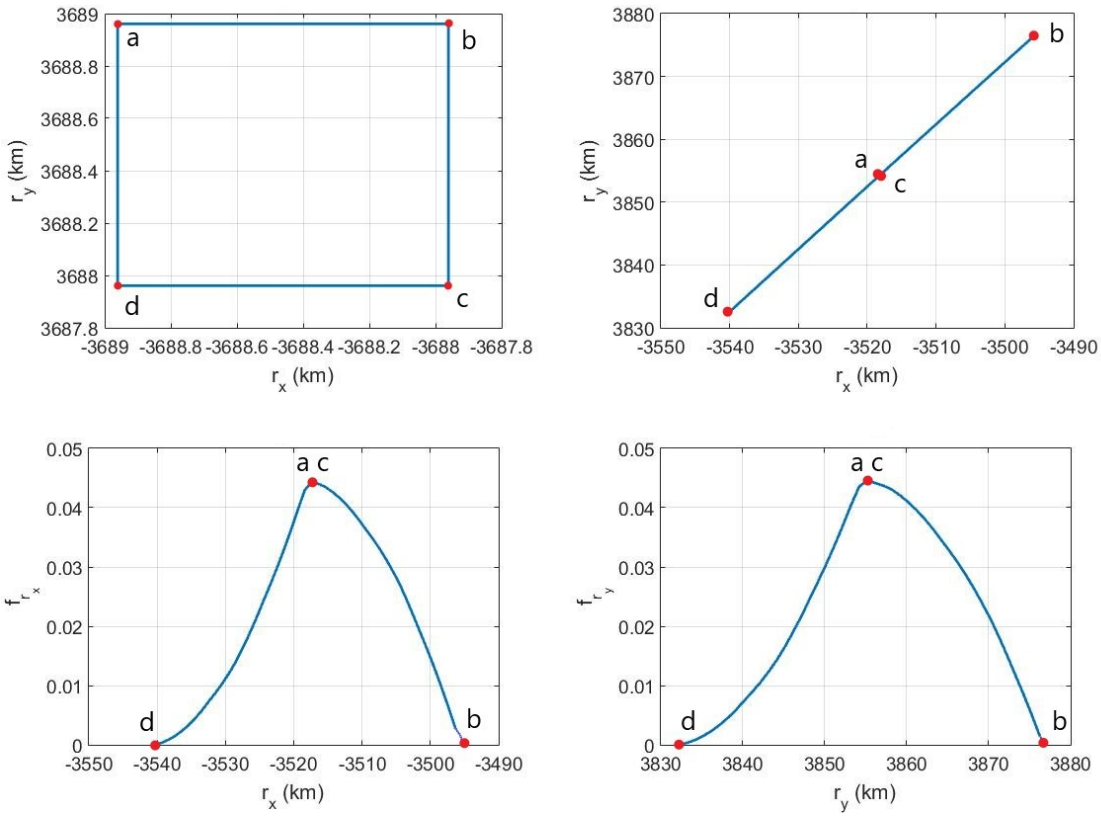

Figure 7.10 Final distribution functions in the position's components.

In Table 7.6 expected values and standard deviation values are shown.

Table 7.6 Expected values in position and typical deviation using PTM method. Multivariate case.

E_x	E_y	E_z	σ_x	σ_y	σ_z
-3514.8 km	3857.6 km	4374.3 km	8.5690	8.4960	0.3008

Three main conclusions about results are pointed:

1. As it can be seen, the initial PDF, which is square, turns into a line, as time increases. Such behaviour is expected, as it has previously been shown when Differential Algebra method was developed.

2. Expected values and σ are coherent with the ones obtained using other methods. This comparison is deeply analysed in chapter 9.

3. Finally, there is an interesting idea that must be mentioned. When the one-parameter case has been analysed, it has been noticed that the exponential distribution modelled with high accuracy an initial uncertainty in $r_x(t_0)$. However, when the uncertainty is considered in more than one parameter, it is realized that normal distribution approximates better the final PDF over time. Curiously, this result is expected, as normal distribution models with high accuracy stochastic processes when more than one initial uncertainty or several random parameters are considered, which is this final test case. This idea is coherent with [27], where this assumption is mentioned.

8 Polynomial Chaos Expansion

8.1 Method

The idea of stochastic process has been repeated along the project, as we are dealing with random variables that are defined in terms of time.

According to [18], polynomial chaos expansion (PCE), is one of the most used methods in science to study a stochastic process and thus this technique is considered in the project. PCE approximates the solution by an expansion of orthogonal polynomials which are chosen depending on the initial distribution that models the random variable.

Therefore, several uncertainty propagators use a polynomial chaos expansion combined with other methods in order to obtain a realistic propagation technique.

However, the more accurate the method is, the more polynomials the expansion needs, and hence the technique becomes more inefficient. A compromise solution should be reached in order to obtain realistic results without spending a huge amount of time.

Once the main idea of GPC has been explained, another concept is mentioned. In the expansion, only orthogonal polynomial are used because they satisfy a condition. This condition is:

$$\int_a^b p_m(x)p_n(x)dx = 0 \rightarrow m \neq n \tag{8.1}$$

This property is used in intrusive PCE to simplify the calculations.

On the other hand, Table 8.1 displays a correlation between the statistical distribution used to generate the initial sample and the sort of orthogonal polynomials used to develop such expansion.

Table 8.1 Correlation between random variable and kind of orthogonal polynomial.

Random variable	polynomial	Interval of definition
Normal	Hermite	(-∞,∞)
Gamma	Laguerre	(0,∞)
Beta	Jacobi	[a,b]
Uniform	Legendre	[a,b]

Finally, it is pointed that two different PCE techniques have been considered:

1. **Intrusive PCE.** The expression of the coefficients h_i is directly calculated from equations taking into consideration Equation (8.1) . In [8] this method is deeply developed.

2. **Non-intrusive PCE.** However, the coefficients' expressions cannot be easily obtained if equations were more complicated than a polynomial, as clearing h_i becomes impossible. Due to this reason, there are several references that develop different ways to approximate the coefficients of the expansion by several procedures as linear regression, Gaussian Mixture Models ... These non-intrusive techniques were extracted from [32], [9] and [10].

Once the main idea of PCE has been explained, the mathematical equations that define this method are developed.

8.2 Mathematical development

The equations and parameters that are implemented for this method are developed next:

$$\ddot{\vec{r}} = -\mu \frac{\vec{r}}{r^3} + \vec{a}_{perturb} \tag{8.2}$$

The motion equation is introduced in (8.2), where $\vec{a}_{perturb}$ is the acceleration caused by perturbations.

As explained before, there are two kinds of PCEs that can be implemented. Both of them are taken into consideration in this section.

8.2.1 Intrusive PCE

Two different cases are considered:

- Uncertainty in initial position. Analogously to the previous chapter, instead of supposing uncertainty in the three components of $\vec{r}_0$, it is only implemented in $r_x(t_0)$.

  This initial condition is as follows:

$$r_x = r_x(t_0)L_0(\Delta) + \delta L_1(\Delta) \tag{8.3}$$

$$r_x(t, r_x(t_0)) \simeq \sum_{i=0}^{P} h_i L_i(\Delta) \tag{8.4}$$

  On the other hand, r_x is calculated by the expansion introduced in Equation (8.4).

  Where P is the order of the expansion. Obviously, if $P \to \infty$, results are incredibly realistic, although the method is quite inefficien, and hence the chosen value of P is 3.

  On the other hand, it is known that $\dot{\vec{r}} = \vec{v}$. It allows us to determine the equations that are integrated, which are:

$$\left\{ \begin{array}{c} \sum_{i=0}^{P} \dot{h}_i L_i(\Delta) = v_x \\ \sum_{i=0}^{P} \ddot{h}_i L_i(\Delta) = -\mu \frac{r_x}{r^3} + \vec{a}_{x_{perturb}} \end{array} \right\} \tag{8.5}$$

  Where $r = \sqrt{r_x^2 + r_y^2 + r_z^2}$ and the expression of r_x is presented in (8.4).

  The next step is based on the main characteristic of orthogonal polynomials that has previously been presented . Due to this reason, in (8.5) all terms of all equations are multiplied per $L_l(\Delta)$, with l=0,1,2,3.

Then, calculating the hope with respect to Δ, the final equations are obtained. They are written as follows:

$$\left\{ \begin{array}{c} \dot{h_l} E[L_l^2(\Delta)] = E[v_x L_l(\Delta)] \\ \ddot{h_l} E[L_l^2(\Delta)] = E[(-\mu \frac{r_x}{r^3} + \vec{a}_{x_{perturb}}) L_l(\Delta)] \end{array} \right\} \tag{8.6}$$

$$\left\{ \begin{array}{c} \dot{r_y} = v_y \\ \dot{r_z} = v_z \\ \ddot{r_y} = -\mu \frac{r_y}{r^3} + \vec{a}_{y_{perturb}} \\ \ddot{r_z} = -\mu \frac{r_z}{r^3} + \vec{a}_{z_{perturb}} \end{array} \right\} \tag{8.7}$$

Combining Equation (8.6) with Equations (8.7), a system of 12 equations with 12 unknown parameters is established. But to solve it, it is necessary to include initial conditions. In this case, $h_0 = r_x(t_0)$, $h_1 = \delta$ and $h_l = 0$ for l=2,3,... whereas $\dot{h_l}$ for l=1,2,3,... is equal to zero and $\dot{h_0} = v_x(t_0)$.

Finally, as the purpose of this method is to calculate several statistical parameters, their equations in terms of the polynomial expansion are developed.

$$E(r_x(t, r_x(t_0))) = \sum_{i=0}^{P} \dot{h_i} E[L_i(\Delta)] = \sum_{i=0}^{P} \dot{h_i} E[L_i(\Delta) L_0(\Delta)] = h_0(t) E[L_0^2(\Delta)] = h_0(t) \tag{8.8}$$

The expression of the mean value appears in Equation (8.8), as well as the calculation of the variance, which is described next:

$$Var(r_x(t, r_x(t_0))) = \sum_{i=0}^{P} \sum_{j=0}^{P} h_i(t) h_j(t) E[L_i(\Delta) L_j(\Delta)] - h_0^2 \tag{8.9}$$

- On the other hand, the case of uncertainty in ρ is considered as well. The implementation is similar to the previous one. In this case, density is defined as:

$$\rho = \rho L_0 + \delta L_1 \tag{8.10}$$

Although equations do not change, there are two changes that must be considered. First at all, instead of writing ρ in the equations, (8.10) should be noted. Secondly, initial conditions are modified. In this case, $h_0 = r_x(t_0)$, and $h_l = 0$ for l=1,2,3,... while $\dot{h_l}$ for l=1,2... is equal to zero and $\dot{h_0} = v_x(t_0)$.

8.2.2 Non-intrusive PCE

As explained before, intrusive methods are inefficient in certain cases and thus non-intrusive procedures are developed. In [9] and [10] different techniques are implemented. One of these non intrusive methods is the Linear regression, which is the one that has been considered in the project.

$$\Phi \cdot a = R \tag{8.11}$$

Linear regression approach is one non-intrusive PCE method that calculates coefficients h_i by solving a system using the least square method. This system's expression gets introduced in Equation (8.11). This procedure just approximates the real value of coefficients h_i, though realistic results are obtained.

Where Φ is a matrix with the orthogonal polynomials, "a" is the matrix whose rows are the coefficients $h_0, h_1, ..., h_p$ and finally, R is the matrix with the values of the parameter that is approximated by the expansion

(in this project this parameter is r_x).

In order to obtain R-matrix, it is necessary to mix Monte-Carlo method (to generate with the initial sample final values of the parameter) and PCE. However, it has been proved that the initial sample can be much smaller (around 100 points) than the one that is used in MC procedure (around 1000 initial points) and because of that, this non-intrusive method is more efficient than Monte Carlo.

Finally, the expected value of the parameters and the standard deviation are calculated following Equations (8.8) and (8.9), which are the same expressions both for intrusive and non-intrusive PCE.

8.3 Results

As presented in the previous section, PCE can be implemented as an intrusive or non-intrusive method. In spite of the fact that both mathematical implementations have been previously introduced, only non-intrusive PCE's results are shown.

The reasons that support this decision is explained next:

1. **Efficiency**. It is not possible to directly obtain an expression for the coefficients h_i from the motion equation. Due to this reason, the property of orthogonal polynomials that has been introduced in Equation (8.1) should be directly applied in the terms of the equations to calculate these h_i. It makes the method completely inefficient. This fact is easily noticed for the multivariate case, as the following duration shows:
   - Initial uncertainty in position $(r_x(t_0))$. t = 3.255578 s
   - Uncertainty in density (ρ). t = 2.352361 s
   - Multivariate case. Initial uncertainty in position $(r_x(t_0))$ and ρ. t = 995.942439 s = 16.6 min
2. **Accuracy**. If the intrusive PCE results are compared with the ones obtained using Monte Carlo, one can notice that in the first procedure huge dissimilarities with the second technique are presented. For instance, the expected value of r_x when initial uncertainty in position is considered is -3909.7 km for intrusive PCE, whereas it is -3533.0 km for Monte Carlo. This difference of around 400 km cannot be accepted for the sake of precision.

Curiously, although GPC has thousands of applications: business, medicine, statistics ... in orbital mechanics, because of the complexity of the motion equation, the intrusive approach is unsuitable for a proper and efficient analysis.

However, this idea is developed in [18], where the term of non-intrusive polynomial chaos, as well as Gaussian mixture models and other techniques combined with PCE are introduced. These procedures are required because of the inefficiency of intrusive PCE to propagate uncertainty in orbital mechanics.

Due to these facts, only non-intrusive polynomial chaos' results are presented in the project.

Table 8.2 Initial orbital elements.

a	e	i	ω	Ω	M
6878.14 km	0.01	40º	90º	45º	0º

8.3.1 Uncertainty in initial position

In this test case, an initial uncertainty in r_x has been considered. This parameter initially follows an uniform distribution, whose mean is the one calculated by using the orbital elements introduced in Table 8.2 and the σ is equal to 0.5 km.

The expected values of the position vector's components and the standard deviation's values are presented in Table 8.3. Simulation's duration was 4,72 hours (3 revolutions of the satellite).

Table 8.3 Non-intrusive PCE. Uncertainty in position.

Caso a estudiar	E_x	E_y	E_z	σ_x	σ_y	σ_z	tiempo
GPC $r_x(t_0)$	-3533.5 km	3837.5 km	4376.2 km	66.4293	0	0	2.198687

On the other hand, the coefficient's oscillations over time are displayed in Figure 8.1. As expected, the coefficients converge, which means that h_i becomes smaller as "i" increases.

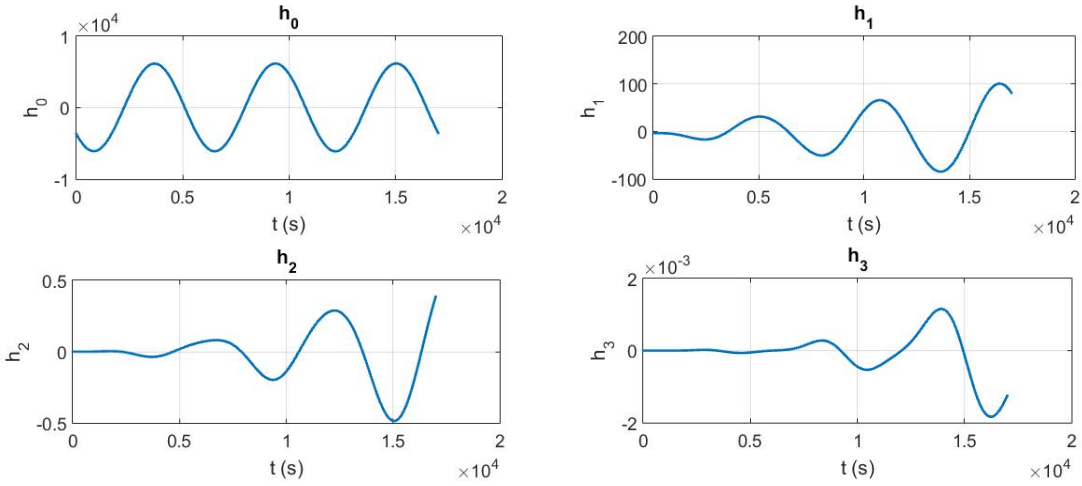

Figure 8.1 PCE uncertainty in initial position.

8.3.2 Uncertainty in density

The case of uncertainty in density is considered as well. Analogously to previous chapters, ρ follows an uniform distribution whose $\rho_0 = 1.585 \cdot 10^{-12} kg/m^3$ and standard deviation (σ) is equal to $1 \cdot 10^{-12} kg/m^3$. The simulation's duration is 4,72 hours again, whereas the initial orbital elements are shown in Table 8.2.

The expected values of r_x, r_y and r_z, as well as the standard deviation's values are presented in Table 8.4. Results are quite similar to the ones obtained in the previous subsection.

Table 8.4 Non-intrusive PCE. Uncertainty in density.

Caso a estudiar	E_x	E_y	E_z	σ_x	σ_y	σ_z	tiempo
GPC ρ (h=200km)	-3381.1 km	3668.7 km	4185.7 km	0.0558	0	0	10.850457

The coefficients $h_i(t)$ are shown again in Figure 8.2. They converge quickly, as it was shown before. However, as the propagation of uncertainty in ρ for altitudes over 300 km is not relevant compared with the previous test case of uncertainty in initial position, the coefficients tend faster to zero, than they did when the uncertainty was initially considered in position. These facts can easily be noticed if Figures 8.1 and 8.2 are compared.

8.3.3 Multivariate case. Uncertainty in position and density

Finally, the multivariate case is presented. As pointed before, non-intrusive PCE offers realistic results and an efficient implementation when the multivariate case is considered. As it is shown in Table 8.5, the MATLAB program finished after 55 seconds, which obviously is less time that the 16 minutes that the multivariate case needed for the intrusive PCE test case.

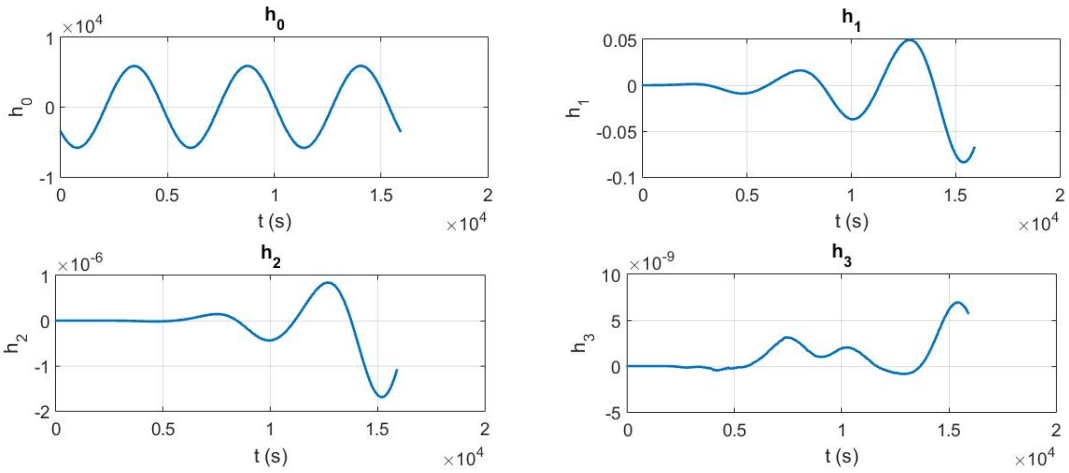

Figure 8.2 PCE uncertainty in density.

In this situation, initial uncertainty is considered in r_x and ρ. The initial r_x, as well as the density has been modelled using an uniform distribution. Simulation's duration is 4,72 hours. The expected values of position vector's components and σ are displayed in Table 8.5.

Table 8.5 Non-intrusive PCE. Multivariate case. Uncertainty in position and density.

Caso a estudiar	E_x	E_y	E_z	σ_x	σ_y	σ_z	tiempo
GPC 2 parameters	-3533.5 km	3837.5 km	4376.2 km	93.7112	0	0	55.009528 seg

As explained before, in the multivariate case, instead of 4 coefficients, it is necessary to calculate 16. They are displayed in Figure 8.3. Analogously to previous test cases, they converge quickly.

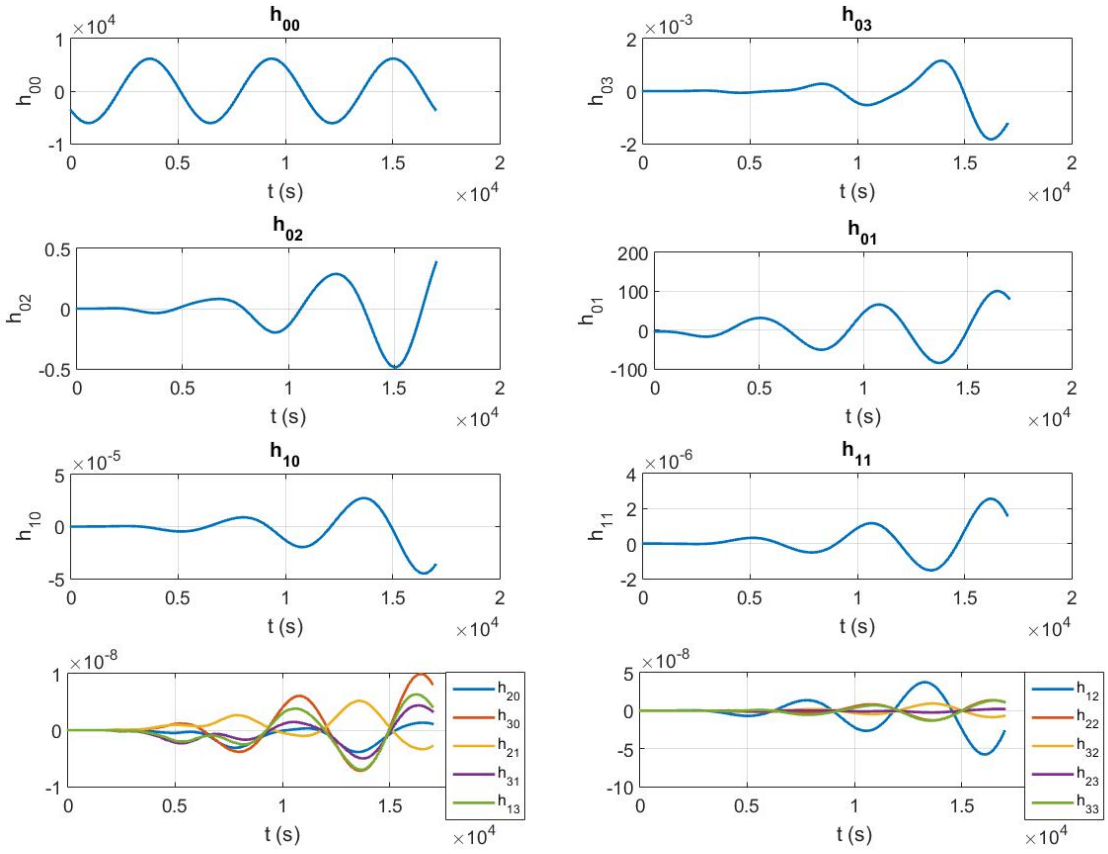

Figure 8.3 PCE multivariate case.

9 Comparison between different methods

The aim of the project is to explore and compare several uncertainty propagation methods and analyse their strengths and weaknesses.

In the previous chapters all of these methods have been developed and similar cases have been displayed. However, to properly compare all techniques, it is necessary to simulate the same test cases, so the efficiency and accuracy can be determined. The initial orbital elements are presented in Table 9.1. Initial altitude is $h = 500km$, with an integration step of 100 seconds and simulation's time equal to 4,72 hours (3 revolutions of the satellite).

Table 9.1 Initial orbital elements.

a	e	i	ω	Ω	M
6878.14 km	0.01	40º	9 0º	45º	0º

Two cases are shown in this chapter: uncertainty in density and initial position.

First at all, in Table 9.2 the expected values of r_x, r_y and r_z, their standard deviations in the final moment of the simulation, as well as compilation's time, are displayed. In this test case, uncertainty in ρ has been supposed. Density has been initially assumed to follow an uniform distribution whose mean is $1.585 * 10^{-12} \frac{kg}{m^3}$ and $\sigma = 1 * 10^{-12} \frac{kg}{m^3}$. This model has been obtained from reference [27].

Table 9.2 Initial uncertainty in density.

Method	$E[r_x]$	$E[r_y]$	$E[r_z]$	σ_{r_x}	σ_{r_y}	σ_{r_z}	time
MC	-3364.9 km	3686.0 km	4183.5 km	$3.01 \cdot 10^{-6}$	$2.93 \cdot 10^{-6}$	$4.5 \cdot 10^{-8}$	107.225336 s
DA	-3381.7 km	3668.1 km	4185.6 km	12.4643	12.4906	0.3541	2.873764 s
LinCov	-3381.0 km	3668.8 km	4185.7 km	0.246	0.272	0.2141	1.405359 s
PTM	-3364.7 km	3686.2 km	4183.5 km	0.0162	0.0158	$2.25 * 10^{-4}$	4.734055 s
PCE	-3381.1 km	3668.7 km	4185.7 km	0.0558	0	0	10.850457

On the other hand, in Table 9.3, results for the case of uncertainty in initial position are presented. Initial position has been supposed to follow an uniform distribution with initial deviation of 0.5 km.

Once results have been shown, several conclusion related to the comparison of these results are shown:

1. As developed in chapters 2 and 3, the model that has been implemented along the project shows results that are verified in the real world. According to [19], it means that Monte Carlo method shows realistic results. Taking into consideration this idea and looking at Tables 9.3 and 9.2, most accurate methods are Monte Carlo, PTM and PCE. In addition to this fact, standard deviations' values in DA and linearized

Table 9.3 Initial uncertainty in position.

Method	$E[r_x]$	$E[r_y]$	$E[r_z]$	σ_{r_x}	σ_{r_y}	σ_{r_z}	time
MC	-3533.0 km	3838.2 km	4376.3 km	30.1371	28.8689	0.5585	157.814438 s
DA	-3589.8 km	3784.5 km	4376.9 km	11.5597	11.7448	0.0714	1.460421 s
LinCov	-3525.6 km	3845.7 km	4376.2 km	836.7091	772.1654	0.2602	0.453542 s
PTM	-3529.0 km	3843.6 km	4374.7 km	29.2228	29.5048	0.6528	9.749841 s
PCE	-3533.5 km	3837.5 km	4376.2 km	66.4293	0	0	2.198687

covariance are much higher than the ones obtained in the other techniques.

2. However, As showed in Tables 9.3 and 9.2, Monte Carlo is the procedure that requires most time to complete the simulation. Due to this reason, it is the most inefficient technique that has been developed in the project and hence differential Algebra and linearized covariance are introduced. Although they are the less realistic than the other techniques, they actually are the faster. As explained in chapter 4, MC method is extremely conservative when the uncertainty is supposed to follow a normal distribution. On the other hand, DA works with an interval, as well as LinCov with an initial covariance matrix and does not require to simulate a huge sample of cases. These two last methods are more efficient due to this reason. Finally, PTM and PCE's efficiency depends on the amount of points of the initial sample.

3. As one can notice from the previous ideas, the higher precision, the less efficiency and back.

4. Moreover, results depend not only on the method that has been implemented, but also on the initial PDF that has been supposed. As showed in the previous chapter, normal distribution models quite well cases when different random parameters are considered. On the other hand, uniform distribution models really well the case when uncertainty in ρ is considered, as well as the gamma distribution function when the uncertainty is considered in one of the position's components.

5. Moreover, although the precision of the method, as well as its efficiency, have been considered, flexibility is contemplated as well. It is related to the idea of using all of these techniques in more areas of the science. As expected, these procedures can be implemented in a vast variety of sciences: business, medicine, biology, physics, chemistry, psychology ... These ideas have been commented before. It is one great strength that this project has.

10 Conclusions and future work

Uncertainty propagation is an extremely important topic nowadays, as it is shown in [28]. Companies are investing huge amounts of money to develop realistic uncertainty propagation methods. There are not only economic interests, but also political.

Such propagators are nowadays being developed by space agencies. For instance NASA uses SGP4 propagator. In such procedure, results are combined with last satellite's position in order to obtain the expected one after a certain time.

In this project, several uncertainty propagation methods have been considered, as well as different PDF to model the unknown parameters. This analysis has been focused on comparing such different techniques and evaluate their strengths and weaknesses.

To achieve this goal, a perturbation analysis has been required. As explained in the third chapter, for LEOs, J2 and atmospheric drag are the most important perturbations, whereas third body's effect and solar radiation pressure can be neglected.

Monte Carlo technique, as results have shown, is the most realistic but inefficient method. On the other hand, differential algebra, which is a common method in orbital mechanics, is high computationally efficient. It is often used as a first approximation to more complicated problems when long periods of time are considered.

Linearized covariance has been developed as well. It allows us to compare results with the ones obtained using the previous procedures, as well as to develop a faster technique. Furthermore, the importance of uncertainty in the initial velocity has been proved.

Finally, a deep analysis of PTM and PCE has been developed. In PTM both one parameter and two parameters cases have been studied. This method enables us to quickly determine which PDF models better each parameter, as well as to calculate the expected value of position and σ. On the other hand both intrusive and non intrusive PCE have been considered. However, only non-intrusive case results are presented as a result of the complicated implementation of the intrusive case and its extremely high inefficiency (it took 16 minute to compile a 4 hours simulation). Due to this reason it has been concluded that intrusive methods are not enough proper for orbital mechanics. Both PTM and PCE offer realistic results with high efficient methods.

To sum up, although all methods are coherent and offer interesting results, Monte Carlo, PTM and non-intrusive PCE are the best techniques to develop uncertainty propagation in Low Earth Orbits. It is concluded as a consequence of their accuracy, that has been constantly proved along the project. In addition to this fact, as the LEO satellite's position gets refreshed every 3-5 hours, which was shown in the real example, simulations are made in short-term periods of time and these three methods are high efficient in this case.

The project compiles and summarizes five techniques that are used not only in orbital mechanics, but also in the whole science. As a result of that, a great variety of future works can be proposed. The most important ones are presented:

- A deeper perturbation analysis should be considered in future projects. In this analysis different satellites can be considered (LEOs, GEOs ...) as well. It is not only engaging because of the importance of perturbations, but it can also be used in other future projects. On the other hand, solar radiation's effect is nowadays attractive, as it can be used to control the object's position, saving at the same time fuel.

- The consideration of Gaussian Mixture Models combined with polynomial chaos should be analysed as well. Several references indicated that these methods offer high accuracy and are not high computationally intensive. Moreover, they are quite common in orbital mechanics.

- Unknown initial velocity has been proved to be crucial in the satellite's behaviour, and thus, a deeper analysis of this subject should be considered.

Bibliography

[1] Dr. T.S. Kelso. Landsat 7's orbital elements. Searched in March 2019, URL: http://celestrak.com/norad/archives/ .

[2] William M. Adams and Ward F. Hodge, *Influence of solar radiation pressure on orbital eccentricity lenticular satellite of a gravity-gradient-oriented*, (1965).

[3] Francisco Javier Camacho Amaro, *Estudio del tiempo de vida de satélites en órbita baja mediante el método ptm*, (2016).

[4] Roberto Armellin, Pierluigi Di Lizia, Alexander Wittig, Alessandro Morselli, and Monica Valli, *Uncertainty propagation using differential algebra*, (2015).

[5] Vincent Azzopardi, *Uncertainties management for orbit propagation using taylor differential algebra*.

[6] Lei Chen, Xian-Zong, BaiYan-Gang, and LiangKe-Bo Li, *Orbital prediction error propagation of space objects*, 2016.

[7] Ondiz. MATLAB code file for the representation of a cube in 3D. Searched in March 2019, URL: https://ondahostil.wordpress.com/2018/10/05/lo-que-he-aprendido-dibujar-cubos-en-matlab/.

[8] Rubén García Díaz, *Estudio del efecto de incertidumbres en la trayectoria de una aeronave*, 2016.

[9] Bert J. Debusschere, Habib N. Najm, Philippe P. Pébay, Omar M. Knio, Roger G. Ghanem, and Olivier P. Le Ma'itre, *Numerical challenges in the use of polynomial chaos representations for stochastic processes*, 2004.

[10] M. S. Eldred and J. Burkardt, *Comparison of non-intrusive polynomial chaos and stochastic collocation methods for uncertainty quantification*, (2009).

[11] Giovanni Falsone and Rossella Laudani, *A probability transformationmethod (ptm) for the dynamic-stochastic response of structureswith non-gaussian excitations*, 1978.

[12] United Nations Office for Outer Space Affairs. Number of satellites in Low Earth Orbits. Searched in January 2019, URL: http://www.unoosa.org/oosa/en/ourwork/topics/space-debris/index.html.

[13] Pablo García, Diego Escobar, Alberto Águeda, and Francisco Martínez, *Covariance determination, propagation and interpolation techniques for space surveillance*, (2011).

[14] Capt Jesse Ross Gossner, *An analytic method of propagating a covariance matrix to a maneuver condition for linear covariance analysis during rendezvous*, 1991.

[15] Engineering Statistics handbook. Covariance matrix calculation. Searched in February 2019, URL: https://www.itl.nist.gov/div898/handbook/pmc/section5/pmc541.htm.

[16] John H. Hubbard and Benjamin Lundell, *A first look at differential algebra*.

[17] Ahmed K. Izzet, *Solar radiation pressure effects on the orbital elements of artificial earth satellite*, (2015).

[18] Brandon A. Jones, Alireza Doostan, and George H. Born, *Nonlinear propagation of orbit uncertainty using non-intrusive polynomial chaos*, (2012).

[19] Jan Krej‘cí, *Uncertainty propagation for tracking of moving objects*, (2018).

[20] Sergiu Lupu and Eugen Zaharescu, *Effects of direct and indirect solar radiation pressure in orbital parameters of gps satelittes*, (2014).

[21] Manuel Ángel Zapata Habas, *Análisis de trayectorias de crucero de aviones comerciales sujetas a incertidumbre en los datos*, (2015).

[22] Union of concerned scientists. Number of satellites in Low Earth Orbits. Searched in February 2019, URL: https://www.ucsusa.org/nuclear-weapons/space-weapons/satellite-database.XGBqDFxKjIV.

[23] Sebastián Orihuela, *Notas sobre propagación de incertidumbres y la elipse de error*, 2015.

[24] Eulalia Hernández Romero, *Probabilistic aircraft conflict detection using transformation of random variables*, 2016.

[25] Rafael Vázquez Valenzuela, *Mecánica orbital y vehículos espaciales; apuntes de la asignatura.*

[26] Rafael Vázquez Valenzuela and Francisco Gavilán Jiménez, *Fundamentos de navegación aérea; tema 8: Sistema de navegación autónomo. navegación inercial. errores.*

[27] David A. Vallado, *Fundamentals of astrodynamics and applications*, 3 ed., Space Technology Library, 2007.

[28] Massimiliano Vasile, *Uncertainty quantification in orbital mechanics*.

[29] Vivek Vittaldev, *Uncertainty propagation and conjunction assessment for resident space objects*, (2015).

[30] Vivek Vittaldev, Ryan P. Russell, and Richard Linares, *Spacecraft uncertainty propagation using gaussian mixture models and polynomial chaos expansions*, (2016).

[31] Rafael Vázquez and Damián Rivas, *Propagation of initial mass uncertainty in aircraft cruise flight*.

[32] Dongbin Xiu and George Em Karniadakis, *Modeling uncertainty in steady state diffusion problems via generalized polynomial chaos*, 2002.